Saurashtra University
Re – Accredited Grade 'B' by NAAC
(CGPA 2.93)

Jani, Yogesh N., 2001, *"Study of winds, tides and waves in the middle atmosphere"*, thesis PhD, Saurashtra University

http://etheses.saurashtrauniversity.edu/id/eprint/351

Ph. D. THESIS

STUDY OF WINDS, TIDES AND WAVES IN THE MIDDLE ATMOSPHERE
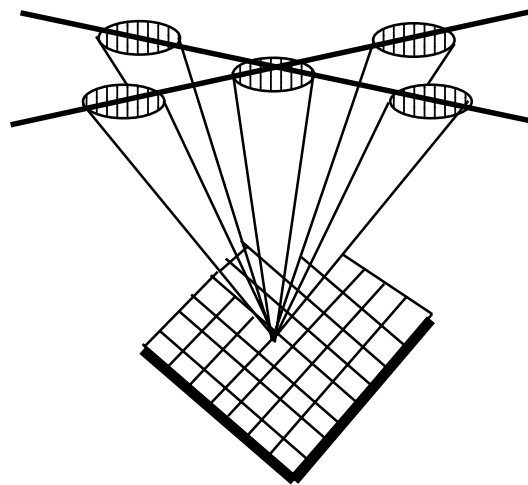
YOGESH N. JANI

**Department of Electronics,
Saurashtra University,
Rajkot - 360 005
INDIA**

May - 2001

SAURASHTRA UNIVERSITY

University Road,
RAJKOT - 360 005.

Dr. H.P. JOSHI

M.Sc., Ph. D.

Reader

Department of Electronics

Saurashtra University

Rajkot

No.   Dt. :- 24 / 05 / 2001

Statement under O. Ph. D. 7 of Saurashtra University

The work included in the thesis is my own work under the supervision of **Dr.H.P. Joshi** and leads to some contribution in Physics subsidised by a number of references.

Date : 24- 05 - 2001   **(Yogesh Jani)**

Place : Rajkot

This is to certify that the present work submitted for the Ph. D. Degree of Saurashtra University by *Yogesh Jani* is his own work and leads to the advancement in the knowledge of Physics. The thesis has been prepared under my supervision.

Date :   24- 05 - 2001

Place : Rajkot   **Dr. H.P. Joshi**

                             Reader,

                             Department of Electronics

                             Saurashtra University

                             RAJKOT

Dedicated
to
My beloved Family...

Acknowledgments

Abstract

The present thesis deals with the dynamics of the troposphere and lower stratosphere which form part of the middle atmosphere. Thesis presents the results of the studies of various mechanism like, tidal oscillations and equatorial waves (contributing to the middle atmospheric dynamics through momentum flux transport) using Indian MST (Mesosphere, Stratosphere, Troposphere) radar located near Tirupati. The detailed outline of the thesis is as follows.

The thesis contains five chapters :

Chapter 1 describes the thermal and chemical structure and dynamics of the middle atmosphere. The region between 10 to 100 km is called the middle atmosphere. This region contains mainly three layers i.e. troposphere, stratosphere and mesosphere. The atmospheric structure in this region is characterized by variations of longer time scales-annual, semi-annual, quasibiennial etc. eventhough shorter time scale changes are possible due to dynamical causes. This is the region where dynamics and energetics are strongly coupled..

The lower parts of the troposphere is highly prone to turbulence and is of great interest form the point of view of atmospheric dynamics. Instabilities can generate wave motions which can propagate both horizontally and vertically and the upward propagation of these waves has significance to middle atmospheric phenomena. In recent years there is great interest in determining long term trend in stratopause temperature as consequence of stratospheric ozone depletion. Solar activity effect in stratosphere is a topic of current research and quantitatively reliable estimates are not yet available.

Chapter 2 describes the MST Radar at Gandanki used in this study and its specifications. The MST radar situated near Tirupati (13.47°N 79.1°E) provides an excellent opportunity to study the lower and middle atmospheric dynamics particularly in the Indian sector.

Chapter 3 describes results of tidal oscillation particularly Non-migrating tidal oscillation. Many efforts were made in theoretical studies and numerical modelling of Non-migrating tides in the atmosphere. The role of the nonmigrating tides in transporting momentum and energy from near the ground to lower stratosphere seems to be an important research subject. To study the Non-migrating tidal oscillation diurnal cycles of Indian MST radar observations in different seasons are utilsed and results are presented in this chapter.

Chapter 4 describes the results on Momentum flux study, in the troposphere and upper stratosphere. The internal gravity waves as well as other, long period waves play an essential role in transporting momentum flux from the lower atmosphere upward into the mesosphere. It is generally regarded that atmospheric zonal motion are composed of a longitudinally averaged part (zonal mean) plus deviation from the average (perturbations) superimposed on the zonal mean. The divergence of momentum flux as well as heat flux associated with the perturbations is important sources for the mean zonal flow.

The waves efficiently transfer energy and momentum between different regions of the atmosphere and are important sources of turbulence. MST radar provide a unique opportunity to measure momentum flux, with excellent time and height resolutions. To study the momentum flux diurnal cycles of Indian MST radar observations in different seasons are utilized and results presented in this chapter.

Chapter 5 describes the characteristics of equatorial waves. Considerable amount of energy transported is takes place through waves and hence coupling processes, especially through waves has become important subject of study. The waves which are primary importance, because of their role in middle atmospheric dynamics, are forced internal modes which are excited by various processes in the troposphere and propagate vertically in to the middle atmosphere. The most significant forced vertically propagating extra tropical wave modes are the quasi-stationary Rossby waves, while the most significant forced vertically propagating trapped equatorial modes are the Kelvin and Mixed Rossby Gravity waves.

From the physics point of view, the most significant features of the equatorial middle atmosphere are quasibiennial and semi-annual oscillations produced by the equatorial waves. This chapter describes the characteristics of the equatorial waves with periods ranging   from 4 to 64 days (i.e. MRG waves, Kelvin waves and long period waves) in different seasons. The zonal and meridional winds using Indian MST radar located at Gadanki (13.47^{o}N, 79.1^{o}E) shows that in different seasons this tropical region is dominated by equatorial waves of different periods.

List of of Research papers published or presented at Workshops/Seminars

1.   *Indian MST Radar measurements of Momentum flux and Turbulence parameters in the Upper Troposphere and Lower Stratosphere*
Porc. MST Radar user scientist's workshop, Feb 6-7, 1997, Tirupati
R.D.Jivrajani, Y.N.Jani, H.P.Joshi & K.N.Iyer

2.   *Observation of Tides and Waves in the middle Atmosphere using Indian   MST Radar*
Porc. MST Radar user scientist's workshop, Feb 6-7, 1997, Tirupati
R.D.Jivrajani, Y.N.Jani, H.P.Joshi & K.N.Iyer

3.   *Study of tides and waves in the tropical atmosphere using Indian MST radar in ST mode.*
Paper presented at VIII Scientific Assembly of IAGA 97 held at Uppsala,
Sweden during 4-15, August,1997
H.P.Joshi, K.N.Iyer, Y.N.Jani and R.D.Jivrajani

4.   *Seasonal differences of Non-migrating tides in the troposphere and lower stratosphere over Gadanki (13.5^oN, 79.2^oE)*
Indian Journal of Radio and Space Physics,
Vol.29, August 2000, pp.210-221.
Y. N. Jani, H. P. Joshi and K. N. Iyer

5.   *Observation of Upper Tropospheric and Lower Stratospheric Equatorial Waves over Gadanki (13.5^oN, 79.2^oE) using Indian MST Radar*
Porc. MST Radar user scientist's workshop, Mar 10-11, 2001, Tirupati
Y. N. Jani, H. P. Joshi and K. N. Iyer

INDEX

1.1 INTRODUCTION

Weather has affected man in most of his activities. In every part of the world the weather patterns have determined the traditional patterns of food, clothing, housing, agriculture, social festivals etc. Even in the absence of recorded history, we can safely state that ever since man started walking on this earth, he has always attempted to understand and to forecast the weather of tomorrow. Instrumentation, observation and experimentation in the laboratories and in the free atmosphere led to the deeper understanding and discovery of the physical laws of nature operating in the atmosphere. The air thermometer was invented by Galileo and barometer by Torricelli, which are used to measure the temperature and pressure variation in the atmosphere. Towards the close of the nineteenth century and in the beginning of the twentieth century, the networks of surface observations increased all over the world, a few pilot balloon observations were started and even a few meteorograph measurements were initiated.

Balloons filled with hydrogen would rise up due to buoyancy and be drifted horizontally by winds of varying speed and direction. Their visual tracking by telescopes would give a measure of horizontal winds at various levels. The sensitive barographs and thermographs attached to these balloons would trace curves of pressure and temperatures. In 1920, pilot balloon observations with visual telescope (theodolites) were started on a routine basis in several countries. In 1930, the occasional pressure and temperature observations in the free atmosphere with meteorographs gradually gave place to routine measurements with radiosonde instruments which telemetred the observations while the balloon was rising with its instrumented package. In mid forties Radars and Satellites were invented and also utilized for the study of atmosphere. A major advance has been made in the radar probing of the atmosphere with realization in early seventies that it is possible to explore atmospheric dynamics up to a height of about 100 km by means of a high power VHF backscatter radar. It led to the concept of MST (mesosphere-stratosphere-troposphere) radar and this class of radar have come to dominate the atmospheric radar scene since seventies.

The atmosphere is conventionally divided into layers based on the vertical structure of the temperature field. These layers, the troposphere, stratosphere, mesosphere, and thermosphere, are separated by the tropopause, the strotopause, and the mesopause. In the past, meteorologists often designated the entire region above the tropopause as the "upper atmosphere". Only fairly recently has the term "middle atmosphere" become popular in referring to the region from the tropopause (10-16) km to the homopause (at ~ 110 km). In this region of the atmosphere eddy processes keep the constituents well mixed and ionization plays only a minor role. However the name "middle atmosphere" has eventually become the standard term for describing the layers of the atmosphere between about 10 to 100 km.

1.2 COMPOSITION OF AIR

The atmosphere is usually divided into three height regions : lower, middle and upper atmosphere (table 1.1). About 90 % of the mass of the total atmosphere is concentrated within the lower, atmosphere, while only 10^{-3} % of the total mass is found in the upper atmosphere.

Table - 1.1 Nomenclature of atmospheric region		
Region	Subdivision	Height (km)
Upper atmosphere	exosphere	> 400
	thermopause	@ 400
	thermosphere	85 - 400
Middle atmosphere	mesopause	@ 85
	mesosphere	50 - 85
	stratopause	@ 50
	stratosphere	15 - 50
Lower atmosphere	tropopause	@ 15
	troposphere	0 - 15

This division was made according to two minima of the mean temperature profile near 15 and 85 km height. The atmospheric waves, of course, are impervious to this arbitrary division and propagate through the whole atmosphere more or less undisturbed, thereby preferring an upward propagation into regions of decrease density.

The lower atmosphere behaves like an unstable nonlinear oscillator system in which the observed broad spectrum of more or less irregular 'noisy' wave structure is generated. These waves propagates into the middle atmosphere and cause instabilities due to wave-wave and wave-mean flow interaction. In spite of a constant external energy input (solar constant), stable conditions are not expected on a short term scale.

In the earth's atmosphere, the region which is roughly between the altitude 10 km and 100 km which separates the upper atmosphere, where solar energetic radiation input, ionization phenomena, and electric and magnetic fields dominate the processes, from the lower most 8-10 km region near the earth's surface, where the weather related phenomena and biospheric inputs dominate the processes, is generally called the Middle Atmosphere. In the lower and middle atmospheres, mixing by fluid motions on all scales tends to produce uniform mixing ratios for all gaseous constituents of the atmosphere.

The air near the ground, and even up to heights of 50 km or more, is remarkably uniform in composition apart from a few special gases such as water vapour and ozone. Table 1.2 gives the proportions of the non-varying gases.

Table 1.2 Proportions of gases in the atmosphere		
Gas	Proportion by volume	Relative thickness
Total	100 per cent	8.0 km
Nitrogen	78.1 per cent	6.25 km
Oxygen	20.9 per cent	1.68 km
Argon	0.9 per cent	74 m
Carbon Dioxide	0.033 per cent	2.6 m
Neon	18 parts per million	15 cm
Helium	5 parts per million	4 cm
Methane	2 parts per million	1.6 cm
Krypton+Zenon	1 part per million	8 mm
Hydrogen	0.5 part per million	4 mm
Nitrous Oxide	0.5 part per million	4 mm

Since it is difficult to appreciate figures such as those given in column 2, column 3 has been added to show the proportions in another way, which can be explained as follows : if all the air in the atmosphere were contained in a uniform layer of constant density at all heights and equal to the normal density at ground level, then the atmosphere would have a sharp top at a height of 8 km. For the purpose of Table 1.2, the gases of the atmosphere are supposed to be separated out into their different layers, each layer containing only nitrogen, only oxygen, only argon etc., so that the total thickness of all the layers makes up the 8 km referred to above.

Table 1.2 gives the composition of the air near the ground. If the atmosphere were entirely quiescent and stagnant, the heavier gases would concentrate under gravity in the lower levels while the lighter gases would be more uniformly distributed in height. There would, therefore, be a change in the composition with height. In the actual atmosphere, however, there is so much mixing that no certain evidence of an increase in the proportion of lighter gases has ever been obtained below 100 km. Some years ago it was thought that the stratosphere would be stagnant enough for separation of the heavy and light gases to take place, but it is now known that the proportions are constant up to much greater heights.

The primary constituents in the lower and middle atmosphere are diatomic nitrogen and oxygen, which together account for 98.65 % of the total mass of the dry atmosphere. <u>Nitrogen</u> : This is much the most abundant gas in the atmosphere but, for the most part, it is chemically inactive and takes no important part in the chemical activities of the atmosphere. At the present time very large amounts of nitrogenous fertilizers are made by artificial methods from the nitrogen of the air, but the total amount of nitrogen in the atmosphere is so enormous that the amount used for fertilizers is a very small fraction of the whole, and when plants and animals decay, much of the nitrogen that they contain goes back into the atmosphere.

<u>Oxygen</u> : Earth is exceptional among the planets in having an appreciable amount of oxygen in its atmosphere. Both nitrogen and oxygen are nearly transparent to the incoming radiation from the sun and also to the outgoing radiation from the Earth and atmosphere. However oxygen does absorb extremely short-wave, ultra-violet and X-ray radiation from the Sun at a high level in the atmosphere and this is partly responsible for the formation of an electrically conducting layer- the ionosphere. Absorption by oxygen of longer ultra-violet solar radiation splits the two atoms associated in a molecule of oxygen into single atoms. These single atoms may combine with an oxygen molecule to give a molecule of ozone. It is in this way that the ozone in the upper atmosphere is formed. The primary constituents have no significant sources or sinks in the stratosphere or mesosphere, so that their mass fractions are nearly constant in height.

The radiatively active trace species carbon dioxide, water vapour and ozone are species of major importance for middle atmosphere dynamics. <u>Carbon Dioxide</u>: Though this gas is only present to the extent of three parts in ten thousand, it is of great importance. It is estimated that, on the average, any molecule of carbon dioxide in the atmosphere is taken up by a plant, and given off again when the plant decays, once in every ten to thirty years. Carbon Dioxide is fairly transparent to most of the solar radiation passing downwards through the atmosphere to the ground, but it strongly absorbs some of the radiation passing outwards from the Earth to space and is important in determining the temperature of some of the layers of the upper atmosphere. It is clear that there have been changes in the proportion of carbon dioxide in the atmosphere within geological time, but at the present time the amount is rather constant, both with time and with place. Though forest fires and the combustion of coal adds large amount of carbon dioxide to the atmosphere, the variations are usually not more than 5 per cent.

Some extensive measurements made during the International Geophysical Year have indicated that in the northern hemisphere there is a fairly regular annual variation in the amount of atmospheric carbon dioxide of about five parts in a million, the maximum being in spring and the minimum in autumn. No such annual variation was found in the southern hemisphere.

It has been suggested that the variation is due to the action of plants in taking up carbon dioxide during the growing season. Normal carbon (atomic weight 12) is a stable element, but there is another isotope of carbon (atomic weight 14) usually called 'radio-carbon', which is radio active. When cosmic radiation enters the upper atmosphere from outer space it produces neutrons, and if one of these neutrons strikes an atom of nitrogen (atomic weight 14) in the atmosphere it may enter its nucleus and if so a proton (with one positive charge) is immediately ejected from the nucleus. Thus while the mass of the nucleus remains unchanged, its positive charge is reduced by one unit and the nitrogen atom is changed into a carbon atom, with all the chemical properties of a normal carbon atom, but having an atomic weight of 14. Since this new type of carbon atom is radio-active, after existing for some time as a carbon atom, it suddenly ejects an electron, thus increasing the positive charge on the nucleus by one unit and the atom again becomes a normal atom of nitrogen. The average life time of the radio-active carbon atom is 5700 years. The radio-carbon formed in the upper atmosphere becomes radio-carbon dioxide and is gradually mixed throughout the whole atmosphere. Thus radio-carbon dioxide is always being slowly formed and is also slowly disintegrating, and after a sufficient time the amount in the atmosphere will be in equilibrium, when the rate of formation will be equal to the rate of disintegration.

Water vapour : The dry air from the upper troposphere is continually descending into the lower layers, water is all the time evaporating from the ground, thus supplying water vapour to lower air. This damp air is then mixed with air higher up by small-scale turbulence caused by winds, but the amount of this mixing depends very much on the rate fall of temperature with height. The variability of water vapour in the lower atmosphere is due entirely to the processes of evaporation, condensation, and sublimation that occur as part of hydrological cycle. Although water vapour in the troposphere may have mixing ratios as high as 0.03 by volume, the stratosphere is observed to be extremely arid with mixing ratios in the range of 2-6 ppmv (parts per million by volume). The dryness of the stratosphere can be qualitatively accounted for if it is assumed that all air entering from the troposphere into the stratosphere passes through the extremely cold tropical tropopause (Fig.1.1), where most of the remaining water content is frozen out. This "freeze-dry" model for the aridity of the stratosphere places important constraints on the nature of the mass exchange between the lower and middle atmosphere. The extremely low water concentration in the middle atmosphere make accurate measurement of the water vapour distribution very difficult.

Ozone : It is the most significant trace species in the middle atmosphere. The absorption of solar ultraviolet insolation by ozone is the major radiative heat input for the middle atmosphere.
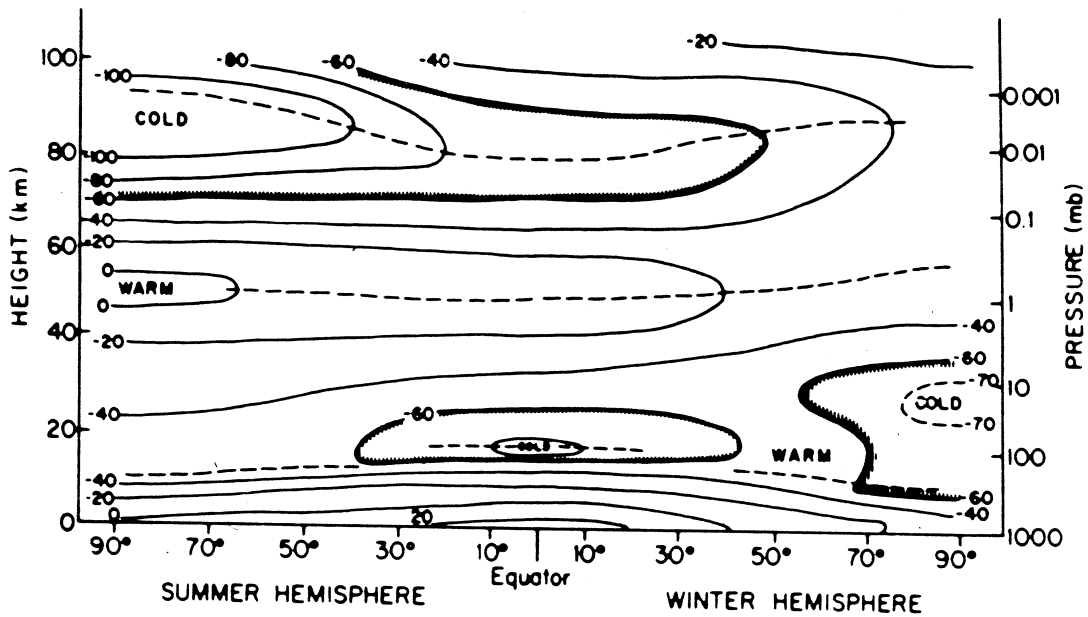
Fig.1.1 : Schematic latitude-height section of zonal temperature (°C)
for solstice conditions. Dashed lines indicate tropopause
stratopause and mesopause levels (after R.J.Reed)

By depleting the solar ultraviolet flux this absorption protects the biosphere from damaging effects of ultraviolet radiation. The budget of atmospheric ozone, which involves very complex photochemical cycles depending on many trace species, both natural and man-made, is thus a major environmental concern. The observed spatial and temporal variability of many of the species involved in ozone photochemistry implies that transport and mixing by atmospheric motions are crucial aspects of the ozone problem. To a large extent it is the threat posed to the ozone layer by anthropogenic perturbations in atmospheric composition that has accounted for the rapid pace of middle atmospheric research in the past decade. The complex coupling among photochemical, radiative, and dynamical processes that ultimately controls the distribution of ozone still provides a major challenge for middle atmospheric research.

In addition to the three major radiatively active trace species, there are a large number of trace species present in sufficient concentrations to play significant roles in the chemistry of the middle atmosphere. Of special significance for meteorological studies are the so-called "long-lived" trace species such as nitrous oxide (N_2O), methane (CH_4), and the chlorofluoromethanes (CF_2Cl_2 and $CFCl_3$). These species all have sources at the ground that are primarily natural for N_2O and CH_4 and entirely man-made for $CFCl_3$ and CF_2Cl_2. They are well mixed in the vertical in the troposphere and are destroyed in the stratosphere by oxidation and / or photodissociation. Thus, they all have vertical profiles in which mixing ratios decay with altitude in the middle atmosphere.

The absorption of solar radiation spectrum by different trace species at different levels in the atmosphere is highly variable and important for the energetics, radiation balance, structure and dynamics of the atmosphere at altitude region above 90 km and in ionization phenomena.

1.3 SOLAR RADIATION SPECTRUM

Solar radiation controls the entire structure and the energetics of the earth's atmosphere and has a dominant influence on the chemical and dynamical processes taking place in it. However, different parts of the solar electromagnetic spectrum play different roles, have different influences and at different levels in the atmosphere. Figure 1.2 illustrates the distribution of energy in the solar electromagnetic spectrum received at the top of the atmosphere. The solar flux is variable on a large variety of time scales and the degree of variability is wave length dependent, the eleven year period associated with the sunspot cycle being the most dominant feature. Reliable quantitative estimates of the eleven year, 22 year and longer period variations in the solar constant is not yet possible. For most of the studies in the middle and upper atmosphere this flux is treated as constant.
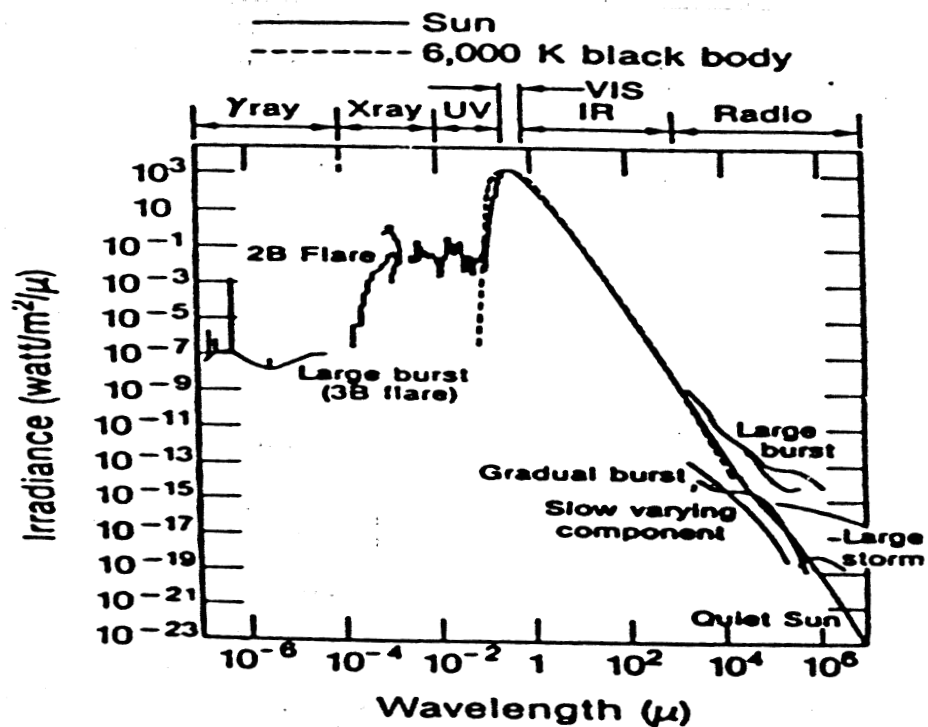
Fig.1.2: Solar electromagnetic spectrum (after Nicolson 1982)

The energetic radiation at shorter wavelength in the UV, EUV and X-rays are emitted from different regions of the sun, e.g. the chromosphere and the corona where the temperatures are higher and these radiations exhibit significant short term and long term variation. Eventhough this part of solar spectrum constitutes less than 1% of the total solar flux, it has great significance for atmospheric phenomena.

The most important variations are those related to the eleven year period. These are given in Table 1.3. These changes in solar flux do have an impact on the structure and energetics of the middle atmosphere (e.g. Breasseur et al., 1978, Hood 1978).

Table 1.3 Variability of the solar radiation flux from solar minimum to solar maximum.	
Spectral Region	Variability
Visible and the infra red $l > 4000$ A°	Extremely small. Negligible for most purpose
Ultraviolet to near visible 3000 A° $< l < 4000$ A°	Very small, fraction of a percent.
Ultraviolet 2000 A° $< l < 3000$ A°	1-2 % from solar minimum to solar maximum
Ultraviolet 1000 A° $< l < 2000$ A°	A few percent to about 10 percent from solar minimum to solar maximum
Lyman-alpha (1216A°)	Factor of 2 from solar minimum to solar maximum
EUV and X-rays $l < 1000$ A°	Highly variable. Orders of magnitude variations from solar minimum to solar maximum to flare conditions, especially in the X-ray region.

1.4 ABSORPTION OF SOLAR RADIATION IN THE EARTH'S ATMOSPHERE

The absorption of solar radiation spectrum in different regions of the earth's atmosphere is detailed in Table 1.4. Most of the radiation in the visible and the infra red (which constitutes 90 % of the total solar flux) is relatively unabsorbed by the atmosphere and reaches the earth's surface. It is responsible for warming the earth's surface as well as the lowermost regions of the atmosphere. However, the wavelength region in the infrared $l > 7000$ A° is not completely free from absorption. Water vapour, carbon dioxide and to some extent ozone have a number of absorption features in this wavelength region (Fig.1.3).

The ultra violet part of the solar spectrum especially at wavelengths less than 3000 A° gets almost completely absorbed in the atmosphere. Radiation with wavelength $l < 1000$ A° gets completely absorbed at altitude above 90 km and is responsible for the formation of ionosphere. However, from the point of view of the middle atmosphere it is the radiation of wavelength 1000 A° - 3000 A° which is more important. The two major feature of this wavelength region are :

Table - 1.4
Absorption of solar radiation in the earth's atmosphere

Wavelength region	Fraction of solar energy	Altitude level at which it is absorbed	Primary absorbing mechanism	Percentage of energy absorbed
$\lambda < 1000$ A°	3 parts in a million	90-200 km	Ionization of atmospheric species	100%
1000 A° $< \lambda < 2000$ A°	100 parts in a million	50-100 km	Photodissoation of oxygen molecule	100 %
Lyman-alpha (1216 A°)	a few parts per million	60-90 km	Ionization of nitric oxide	100 %
2000 A° $< \lambda < 3100$ A°	1.75 %	30-60 km	Photodissoation of O_3	More than 95 %
31000 A° $< \lambda < 7000$ A°	48 %	---	---	very little
$\lambda > 7000$ A°	50 %	0-10 km	Absorption by water vapour	10-15 %
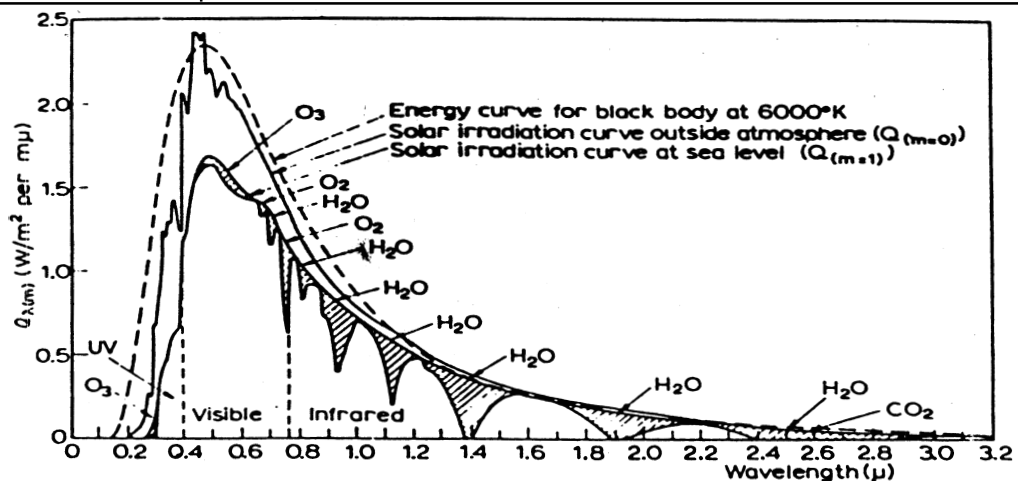
Fig.1.3: Absorption features due to water vapour, CO_2 and O_3 in the visible and infrared part of the solar spectrum (after Robinson 1966)

1.4.1 Absorption by molecular oxygen

This is specially significant in the wavelength region 1000 A° - 2000 A° (except for a few window regions, such as hydrogen Lyman-alpha (1216 A°) where the absorption cross section is smaller) causing photodissociation of molecular oxygen. This results in ionization and chemistry of the atmosphere. Photodissociation threshold is 5.1 eV ($\lambda = 2424$ A°).

$$O_2 + h\upsilon \,(\lambda < 2424 \text{ A}^\circ) \longrightarrow O + O \underline{\quad\quad} (1)$$
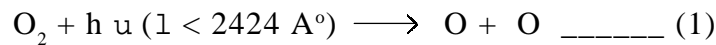
Eventhough this occurs almost throughout the atmosphere down to about 50 km, it is more important at altitudes above 90 km where absorption takes place at wavelength less than 1760 A°.

$$O_2 + h\upsilon \,(\lambda < 1760 \text{ A}^\circ) \longrightarrow O^3P + O^1D \underline{\quad\quad} (2)$$
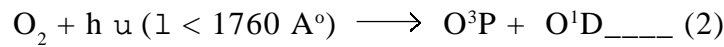
This produce atomic oxygen in the ^1D state which plays an important role in photochemical and radiative processes. Atomic oxygen so produced is lost by

    1. Recombination

$$O + O + M \longrightarrow O_2 + M \underline{\quad\quad}(3)$$
$$K = 5 \times 10^{-34}\, T^{1/2}\,(\text{cm}^6/\text{sec})$$

and $\quad\quad O + O \longrightarrow O_2 + M \underline{\quad\quad}(4)$
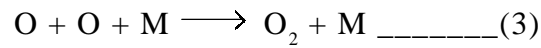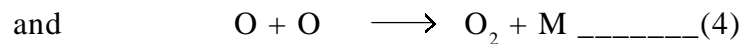
Radiative recombination (Eq.4) is not important at altitudes below about 110 km.

    2. Formation of Ozone
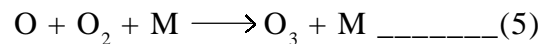
$$O + O_2 + M \longrightarrow O_3 + M \underline{\quad\quad}(5)$$
$$K = 1.1 \times 10^{-34}\, e^{510/T}\,(\text{cm}^6/\text{sec})$$

or $\quad\quad O + O + O \longrightarrow O_3 \underline{\quad\quad\quad} (6)$
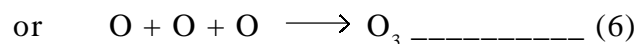
Eq. (6) is not important at altitudes below 90 km.

Eventhough photodissociation of O_2 occurs during daytime only, the atomic oxygen concentrations in the atmosphere remain practically constant from day to night altitude about 80 km. The photochemical time constants of atomic oxygen at some typical altitudes in the atmosphere are :

Altitude	Time constant
60 km	~ 1 hour
80 km	~ 1 day
100 km	~ 1 month

O_2 is completely dissociated at higher altitudes in the atmosphere. Transition from O_2 to O occurs around 110 km.

1.4.2 Absorption by Ozone

Ozone plays an important role in middle atmospheric chemistry and radiation balance. It is produced in the atmosphere by reactions as mentioned earlier by Eq's (1), (5) and (6). It is lost by photodissociation, and recombination reactions involving atomic oxygen

$$O_3 + O \longrightarrow 2O_2 \underline{\quad\quad}(7)$$
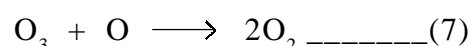
and a number of catalytic reactions of the type

$$O_3 + X \longrightarrow O_2 + XO$$
$$XO + O \longrightarrow O_2 + X \underline{\quad\quad}(8)$$
$$\text{Net} \quad O_3 + O \longrightarrow 2O_2$$
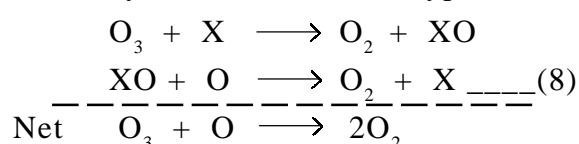
Where X belongs to the family of hydroxyl radical, NO or a halogen related radical, e.g. chlorine.

The total overhead ozone may be getting slowly depleted with time due to the catalytic reaction and that most of these arise out of long-lived chemicals which are released into the atmosphere by anthropogenic activities. The photodissociation threshold for ozone is very low 1.1 eV (corresponding to 11,800 A°) and in principle the entire visible and near infra red parts of the spectrum can dissociate an ozone molecule.

$$O_3 + h\nu\, (\lambda < 11{,}800\ A°) \longrightarrow O_2 + O \underline{\hspace{2cm}} (9)$$
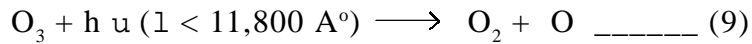
But the absorption cross section is strongly wavelength dependent and absorption by ozone is dominant in the wavelength region of 2000-3000 A°. The absorption spectrum of ozone maximizes around 2500 A° and almost the entire solar flux of 2800 A° is absorbed at altitudes above about 20 km. This gives rise to heating of the ambient medium and produces the so called stratosphere with a temperature maximum around 50 km, a unique feature of the earth's atmosphere. At wavelength less than 3100 A° the dissociation produces the oxygen atom in the ^1D state.

$$O_3 + h\nu\, (\lambda < 3100\ A°) \longrightarrow O_2{}^1D\,g + O^1D \underline{\hspace{1.5cm}}(10)$$
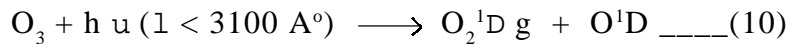
Since some part of this radiation reaches down to ground level, there is a small population of O^1D even at lower levels of the atmosphere. This plays a very significant role by oxidation of methane and production of the OH radical which plays an important role in tropospheric chemistry. Above about 60 km there is very little direct absorption of solar radiation (and consequent heating) in the atmosphere until the altitude 90 km where photodissociation of O_2 begins in a significant way. The only radiation absorbed in this region in the Schumann Runge bands $(1700A° < \lambda < 1950\ A°)$ by O_2.

1.5 TEMPERATURE STRUCTURE OF THE ATMOSPHERE

The region above about 90 km where the solar EUV and x-ray absorption gives rise to atmospheric heating as well as ionization is called the Thermosphere. The temperatures at first rises rapidly at the base of the thermosphere upto about 150 km with a gradient of 6 to 8° K/km and above this altitude the gradient is relatively smaller. At higher altitude in the thermosphere, i.e. above about 250 km, the temperature is nearly constant with altitudes. There is very little direct absorption of solar radiation, and the temperature structure is being controlled mostly by conduction from lower regions where the bulk of the solar EUV and X-ray energy is absorbed. The entire structure and composition of the thermosphere is controlled by the level of solar EUV and X-ray flux - solar activity. The temperature structure in the atmosphere is shown in Figure.1.4.

The altitude region 20 km to about 60 km is called the stratosphere. It is formed due to heating by solar UV absorption of ozone. The maximum temperature is attained in the 45-50 km region, the so called stratopause.
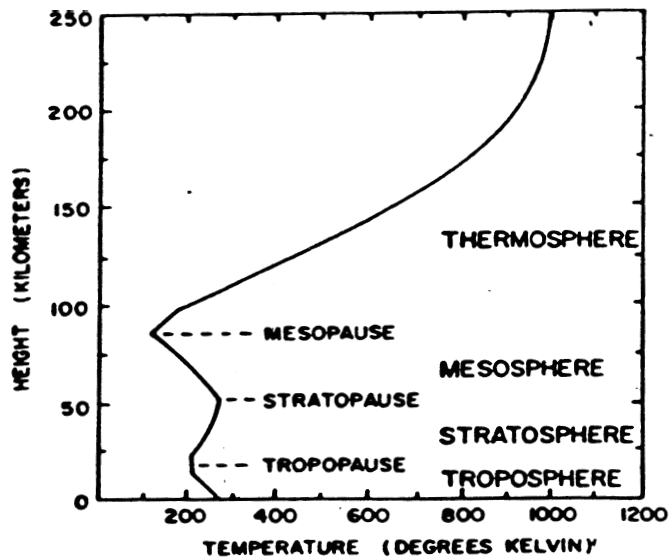
Fig.1.4 : Temperature structure of the atmosphere
(after chamberlain 1978)

The atmospheric structure in this region is characterized by variations of longer time scales, annual, semi-annual etc. eventhough shorter time scale changes are possible due to dynamical causes. In recent years there is great interest in determining long term trend in stratopause temperatures as consequence of ozone depletion.

The temperature structure below the stratosphere, i.e. at altitude below about 20 km is not directly controlled by absorption of solar radiation. In this region, called troposphere, the temperature decreases with increasing altitude until a temperature minimum is reached. This level is called the tropopause and above the tropopause the effect of ozone absorption sets in giving rise to the increase in temperature in the stratosphere. The decreasing temperature structure of the troposphere is governed by the fact that absorption of solar visible and infra red radiation gives rise to a warming of the earth's surface upto about 250° K and the earth's surface itself acts as a blackbody at this temperature and emits long wave radiation in the wavelength band 4 m to 100 m (Fig.1.5a). This long wavelength radiation emitted upwards into the atmosphere by the earth's surface is absorbed by several trace constituents of the atmosphere, the so called greenhouse gases (Fig.1.5b). Prominent among them are H_2O, CO_2, CH_4, N_2O and O_3. Recently a number of man-made chemicals, the CFCs which are being emitted into the atmosphere have also been found to play an important role in the greenhouse warming. The result is an enhanced warming of the earth's surface and the lower regions of the atmosphere. The troposphere therefore is a medium which is heated from below. Hence the decrease in temperature with increasing altitude. The temperature gradient in the troposphere, the so called lapse rate is of the order of 6°K/km.
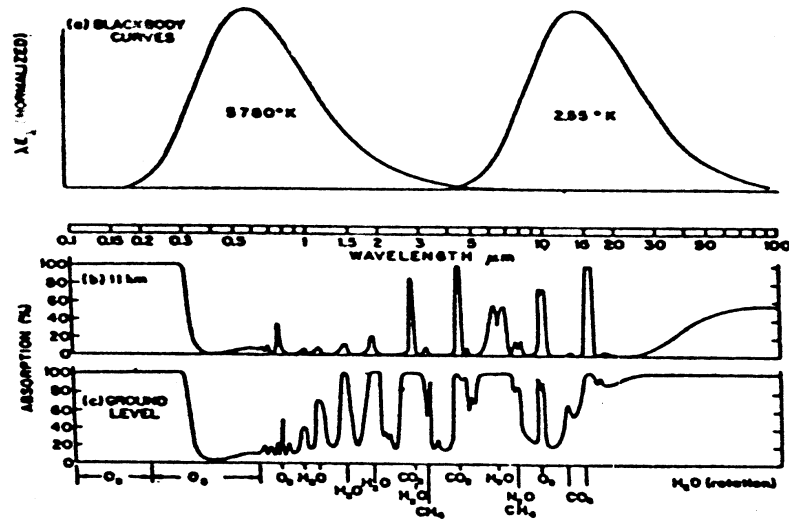
Fig.1.5(a) : Normalized blackbody spectrum for the sun (6000°K)
and the earth (245°K)

(b) : Atmospheric absorption of the long wave radiation

A negative temperature gradient i.e. a decrease in temperature with increase in altitude is in general conducive to the growth of instabilities in the atmosphere, if the lapse rate is greater than what is known as the adiabatic lapse rate (Iribane and Cho 1981) which is given by $L_A = g/C_p$ (9.8°K/km for a dry atmosphere). If the lapse rate becomes greater than this value, the atmosphere becomes unstable against convection (Fig.1.6). Convective instability grows and the medium becomes turbulent. The resulting dissipation of energy heats up the atmosphere to bring the temperature profile back to a stable condition.
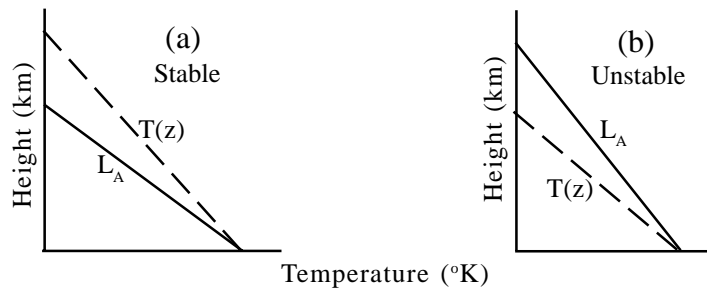
Fig.1.6 : Convective instability in the troposphere. Full line corresponds to the adiabatic lapse rate. An observed temperature profile similar to the dashed line in (a) corresponds to stable conditions and that in (b) corresponds to unstable conditions.

Hence in the lower parts of the troposphere, i.e. upto about 10-12 km convective transport dominates over radiation in the energetics. This part of the atmosphere is highly prone to turbulence and is of great interest from the point of view of atmospheric dynamics. Instabilities can generate wave motions which can propagate both horizontally and vertically and the upward propagation of these waves has significance to middle atmospheric phenomena.

1.6 IMPORTANCE OF WAVES AND TIDES IN THE STRUCTURE AND ENERGETICS OF THE ATMOSPHERE

The atmosphere between the ground and exosphere at about 400 km altitude is a huge wave guide in which large-scale waves (planetary waves) of various periods can be excited. The wave guide characteristics of the atmosphere allow only certain individual wave modes to exist. Some of these waves modes have sufficiently large horizontal and vertical scales to avoid destructive interference, so that they can be filtered out the meteorological noise (daily weather). Tidal waves with periods fixed by the geometry of the Sun-Moon-Earth system, planetary waves with periods around 2,5,16 and 40 days, and impulsive disturbances have now been identified. All have been theoretically interpreted in terms of Laplace's theory with varying degree of success.

The terrestrial atmosphere is set into motion by the persistent but spatially nonuniform solar heating and to a much lesser extent by lunar gravitional tidal forces and solar activity. The atmosphere, as a nonlinear oscillator system, reacts in a complicated manner to these primary forces. The atmospheric wave guide behaves like a resonance cavity for certain spectral ranges of atmospheric waves. Secondary driving forces result from the external primary forces through interactions with ocean currents, cryosphere, continents and biosphere or by latent heat, turbulence, coupling between atmospheric waves, and Joule heating. These additional complications make predictions of atmospheric motions difficult, even worse. The atmosphere, due to its nonlinearity, may behave like strange attractor with sensitive dependence on the initial conditions, which may long-range forecasting of atmospheric motions practically impossible.

The atmospheric motions, display a wave like structure on a global scale. Ultralong planetary waves with periods ranging from a few days to a few years and with horizontal scales of the order of Earth's diameter, as well as tidal waves with a basic period of one solar or lunar day, respectively, belong to this category.

Tidal waves are wave which are forced by regular external sources so that their periods and their horizontal structures are predictable. To this type of waves belong not only the diurnal tides and their higher harmonics, but also waves which are generated by solar differential heating during the course of one year. The so-called mean zonally averaged atmospheric circulation and its seasonal variations are tidal waves according to that definition, known as seasonal tides. Feed back between planetary waves and seasonal tides can cause sudden changes in the wave structure, in particular within the middle atmosphere.

The dynamical processes in the atmosphere are generally considered as being driven by thermal processes, waves can also be a means of energy and momentum transport as well as transport of longlived trace constituents in the atmosphere.

The large differences in the levels of energy absorbed in different regions of the atmosphere (table 1.5) makes transport of energy from one region to another, especially from lower to upper regions a significant source of perturbation in the energetics of that region.

Table - 1.5
Energetics of the different regions of the atmosphere

1.	Thermosphere/Upper atmosphere : > 90 km	
	Almost all energy short of 1750 A°	30 ergs/sec/cm² col.
	Schumann Runge 1750-1950 Lyman-Alpha and X -rays	100 ergs/sec/cm² col.
	Total energy absorbed	130 ergs/sec/cm² col.
2.	Middle atmosphere 20-90 km $\}$ Stratospheric Ozone absorption 30-60 km. 2000 - 3000 A°	~ 1.8×10^4 ergs/sec/cm² col.
3.	Lower atmosphere Visible Infrared and longwave	few times 10^6 ergs/sec/cm² col.

The ozone and water vapour absorption in the stratosphere and troposphere are the sources of atmospheric tides. Energy carried into the upper atmosphere by the tidal modes is in some cases much more than the solar radiation absorption at these higher levels (Chapman and Lindzen, 1970, Forbes, 1985). Shorter period waves generated in the troposphere and propagating upwards, the so called internal gravity waves carry with them considerable amount of energy. Waves also give rise to transport of energy from high latitudes to middle and low latitudes during disturbed conditions (Roble et al. 1978). These waves when they reach the mesosphere can become a significant source of energy especially in the mesopause region where direct solar radiation absorption is negligible. Under certain conditions some of these waves grow in amplitude and give rise to turbulence (Hocking 1985).

Atmospheric waves originating in the tropical troposphere are responsible for the Quasi-Biennial oscillation (QBO) in which most of the variance in the zonal wind is confined at equatorial latitudes in the lower stratosphere. The QBO is explained on the basis of wave-mean flow interaction. The theory is based on the vertical momentum fluxes carried by the eastward propagating Kelvin waves (~15 day period) carrying westerly momentum and the westward propagating mixed Rossby gravity (MRG) waves (4-5 day period) carrying easterly momentum to explain the downward propagation of alternating westerly and easterly wind regimes of the QBO.

The semi-Annual Oscillation (SAO) in the zonal wind is quite strong in the equatorial upper stratosphere and mesosphere. The westerlies of the SAO are due to the momentum deposition due to Kelvin waves of tropospheric region (with periods shorter than those responsible for westerly regime of QBO). The easterly phase of SAO is attributed to advection of the easterlies in the summer hemisphere by the meridional wind forced by solar heating and to planetary waves.

1.7 OBSERVATIONAL TECHNIQUES

The systematic observation of the middle atmosphere dates only from the International Geophysical Year (IGY) of 1957-58. Knowledge concerning the temperatures, winds, and composition of the middle atmosphere has increased dramatically in the years following the IGY.

During the 1960s the operational meteorological radiosonde network provided sufficiently frequent sounding of the lower stratosphere up to about the 10-mb level so that the climatology of the lower stratosphere gradually was established at least in the Northern Hemisphere. In the same period a meteorological rocket network was established that provided wind and temperature measurements in the upper stratosphere and lower mesosphere. Observation of the global stratosphere really only began in 1969 with the launching of the Nimbus - 3 satellite and subsequent research and operational satellites have provide more than a decade of global remote sounding of stratospheric temperatures and total ozone as well as limited measurements of profiles of ozone and a few other trace constituents. The Lidars are also designed to detect the Rayleigh back-scatter from air molecules can yield density profiles in the altitude range of 30-90 km. Lidar is similar to radar except that in lidar, the radiation is in the form of visible or infrared laser beams rather than microwaves. They are applied primarily to detect particles in the atmosphere- in smoke plumes, in the stratosphere, or even in the lower thermosphere. Doppler lasers can measure the velocities of the particles.

Direct velocity measurement in the middle atmosphere have been made by rocket sounding and remotely from the ground using several radar methods, operating in a variety of frequency ranges. These include the partial reflection drift method, meteor radars, and so called MST (mesosphere-stratosphere-troposphere) radars. The MST technique utilizes very high frequency (VHF) radars (wavelengths of the order of a few meters) in Doppler mode to determine the drift velocities of back-scattering elements whose nature depends on the region being scanned. The echoes received by such radars from the troposphere and lower stratosphere are caused by refractive-index variation due to density fluctuations associated with neutral atmosphere (clear air) turbulence. With MST radars technique it is possible to obtain three-dimensional velocity fields. MST radars have limited horizontal coverage but can produce data with high temporal and vertical resolution in a given

locality. They are thus particularly appropriate for studying high-frequency components of the motion field, such as waves and tides.

A number of radars of this kind have been established all over the world in recent years and extensive observations have been made of the wind fields in the middle atmosphere with excellent time and height resolutions. A major MST Radar has been installed as a national facility at Gadanki in Andhra Pradesh became available to the Scientific Community since 90's. The result reported in this thesis is from measurements using this MST Radar.

CHAPTER - 2

MST RADAR TECHNIQUE

2.1 INTRODUCTION

The name radar reflects the emphasis placed by the early experimenters on a device to detect the presence of a target and measure its range. Radar is a contraction of the words Radio Detection and Ranging. It was first developed as a detection device to warn of the approach of hostile aircraft weapons. Radar is an electromagnetic system for the detection and location of objects. It operates by transmitting a particular type of waveforms, a pulse-modulated sine wave for example, and detects the nature of the echo signal. Radar is used to extend the capability of one's senses for observing the environment, especially the sense of vision.

An elementary form of radar consists of a transmitting antenna emitting electromagnetic radiation generated by an oscillator of some sort, a receiving antenna and an energy detecting device, or receiver. A portion of the transmitted signal is intercepted by a reflecting object (target) and is reradiated in all directions. It is the energy reradiated in the back direction that is of prime interest to the radar. The receiving antenna collects the returned energy and delivers it to a receiver, where it is processed to detect the presence of the target and to extract its location and relative velocity. The distance to the target is determined by measuring the time taken for the radar signal to travel and back. The direction , or angular position, of the target may be determined from the direction of arrival of the reflected wave front. The usual method of measuring the direction of arrival is with narrow antenna beams. If relative motion exists between target and radar, the shift in the carrier frequency of the reflected wave (Doppler effect) is a measure of the target's relative (radial) velocity and may be used to distinguish moving targets from stationary objects. In radar which continuously track the movement of a target, a continuous indication of the rate of change of target position is also available.

The typical radar transmits a simple pulse-modulated waveform, there are a number of other suitable modulations that might be used. The pulse carrier might be frequency - or phase-modulated to permit the echo signals to be compressed in time after reception. This achieves the benefits of high resolution without the need to resort to a short pulse. The technique of using a long, modulated pulse to obtain the resolution of a short pulse, but with the energy of a long pulse, is known as pulse compression. Continuous waveforms (CW) also can be used by taking advantage of the Doppler frequency shift to separate the received echo from the transmitted signal and the echoes from the stationary clutter.

Radar systems are used for the study of atmospheric processes because of their simplicity, reliability and by virtue of the fact that a radar system provides a means of sampling the atmosphere at a rapid rate in a cost effective way. Initially microwave radar systems were used for the study of cloud coverage, precipitation, storm location, characterization of the intensity of storm clouds and for general day to day meteorological predictions.

A new generation of pulse Doppler Radar system has emerged for probing the atmosphere and studying the dynamics of the atmosphere using the backscattered signals from clear air turbulence. The tracer elements for such radar systems are variations in the atmospheric refractive index. Such radars have come to be known popularly as the MST, the ST and the T Radars depending upon the maximum effective height coverage of the radar corresponding to the three regions of the atmosphere viz., Mesosphere, Stratosphere and Troposphere.

2.2 THE RADAR EQUATION

The radar equation relates the range of a radar to the characteristics of the transmitter, receiver, antenna, target and environment. It is useful not just as a means for determining the maximum distance from the radar to the target, but it can serve both as a tool for understanding radar operation and as a basis for radar design. If the power of the radar transmitter is denoted by P_t, and if an isotropic antenna used (one which radiates uniformly in all directions), the power density (watts per unit area) at a distance R from the radar is equal to the transmitter power divided by the surface area $4pR^2$ of an imaginary sphere of radius R, or

$$\text{Power density from isotropic antenna} = \frac{P_t}{4pR^2} \underline{\hspace{1cm}} (1)$$

Radars employ directive antennas to channel, or direct, the radiated power P_t into some particular direction. The gain G of an antenna is a measure of the increased power radiated in the direction of the target as compared with the power that would have been radiated from an isotropic antenna. It may be defined as the ratio of the maximum radiation intensity from the subject antenna to the radiation intensity from a lossless, isotropic antenna with the same power input. (The radiation intensity is the power radiated per unit solid angle in a given direction) The power density at the target from an antenna with a transmitting gain G is

$$\text{Power density from directive antenna} = \frac{P_t G}{4pR^2} \underline{\hspace{1cm}} (2)$$

The target intercepts a portion of the incident power and reradiates it in various directions. The measure of the amount of incident power intercepted by the target and reradiated back in the direction of the radar is denoted as the radar cross section s, and is defined by the relation.

$$\text{Power density of echo signal at radar} = \frac{P_t G}{4pR^2} \frac{s}{4pR^2} \underline{\hspace{1cm}} (3)$$

The radar cross section s has units of area. It is a characteristic of the particular target and is a measure of its size as seen by the radar. The radar antenna captures a portion of the echo power. If the effective area of the receiving antenna is denoted A_e, the power P_r received by the radar is

$$P_r = \frac{P_t G}{4\pi R^2} \frac{s}{4\pi R^2} A_e = \frac{P_t G A_e s}{(4\pi)^2 R^4} \underline{\quad} (4)$$

The maximum radar range R_{max} is the distance beyond which the target cannot be detected. It occurs when the received echo signal power Pr just equals the minimum detectable signal S_{min}. Therefore

$$R_{max} = \left[\frac{P_t G A_e s}{(4\pi)^2 S_{min}} \right]^{1/4} \underline{\quad} (5)$$

Equation (5) is a fundamental form of the radar equation. Antenna theory gives the relationship between the transmitting gain and the receiving effective area of antenna as

$$G = \frac{4\pi A_e}{l^2} \underline{\hspace{3cm}} (6)$$

Since radars generally use the same antenna for both transmission and reception, Eq. (7) can be substituted in to Eq. (5), first for A_e then for G, to give two other forms of the radar equation

$$R_{max} = \left[\frac{P_t G^2 l^2 s}{(4\pi)^3 S_{min}} \right]^{1/4} \underline{\hspace{1.5cm}} (7)$$

$$R_{max} = \left[\frac{P_t A_e^2 s}{4\pi l^2 S_{min}} \right]^{1/4} \underline{\hspace{1.5cm}} (8)$$

These three forms (Equations 5,7 and 8) illustrate the need to be careful interpretation of the radar equation. For example, from equation (7) it might be thought that the range of a radar varies as $l^{1/2}$, but equation (8) indicates a $l^{-1/2}$ relationship, and equation (5) the range to be independent of l . The correct relationship depends on whether it is assumed the gain is constant or the effective area is constant with wavelength. Furthermore, the introduction of other constraints, such as the requirement to scan a specified volume in a given time, can yield a different wavelength dependence.

These simplified versions of the radar equation do not adequately describe the performance of practical radar. Many important factors that affect range are not explicitly included. In practice, the observed maximum radar ranges are usually much smaller than what would be predicted by the above equations, sometimes by as much as factor of two. Part of this discrepancy is due to the failure of equation (5) to explicitly include the various losses that can occur throughout the system and another important factor that must be considered in the radar equation is the statistical. The simple radar equation (Equation 5) will be extended to include most of the important factors that influence radar range performance.

2.3 THE MEASUREMENT TECHNIQUES

The radar technique makes use of the fundamental properties of an electromagnetic (radio) wave viz., its frequency, phase, amplitude and polarization. Atmospheric radars derive information on the dynamical atmospheric phenomenon by making use of the variations on the above four parameters of radio waves which are trasmitted from the radar system, backscattered by the atmosphere and received by the radar system again. Atmospheric radar differs from the communicational (military) radar in the sense that the echo in the former is obtained by volume backscatter from a soft target while in the later it is obtained by specular reflection from a hard target.   The pulsed Doppler radars emit either a single pulse or a train of pulse of electromagnetic radiation, and some of the energy is backscattered when variations in the refractive index structure of the atmosphere fluctuations at the scale of half the radar wavelength coherently backscatter the signal, thereby increasing the echo strength considerably. The simple block diagram of a pulse radar is shown in figure 2.1.
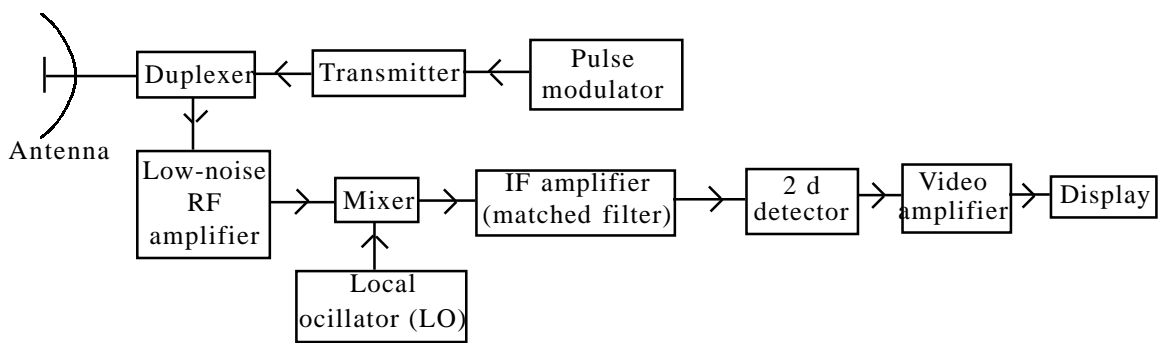
Fig.2.1 :   Block diagram of a pulsed radar

By measuring the frequency of the returned signal, the small change in frequency due to the motion of the scatterers can be determined. The Doppler shift in frequency can then be related directly to the line-of-sight velocity of the turbulent variations in the refractive index. If the turbulent variations are frozen in the medium during the time it takes to cross the radar beam (the Taylor hypothesis), the Doppler velocity is then a measure of the mean motion of the atmosphere over the volume that the radar illuminates. The general features of Doppler radar velocity measurements have been described by Wilson and Miller, 1972; Battan, 1973; Doviak et al., 1979.

The accuracy of the radar-deduced winds has been tested by comparisons of radar wind profiles and rawinsonde profiles from nearby stations (Balasley and Farley, 1976; Farely et al., 1979; Strauch, 1981). The agreement is usually good, but not perfect, and the differences are then attributed to variations over the spatial separation between the balloon ascent and the radar sampled air. The microwave radar makes wind measurements indirectly by measuring the velocity of precipitating particle.

The comparison were carried out under the appropriate conditions and good agreement was achieved. There are three methods in use for determining the vector winds. The first method is Velocity azimuth display (VAD): The technique in which a steerable antenna beam, pointed at some angle off zenith, is used to measure the line-of-sight velocity as a function of azimuth and height (Lhermitte and Atlas, 1963; Wilson and Miller, 1972). If winds donot vary over the cone traced out by the beam, and velocity is strictly horizontal, the velocity measured by the radar will vary sinusoidally as a function of the azimuth. A nonzero vertical velocity component will create an offset in the sinusoid. The main advantage of VAD technique is that in theory at least, variations of the winds over the sampling cone due to divergences or rotations in the wind field can also be resolved by this technique if more Fourier components than just the first order sinusoid are include in the fit. Inspite of this advantage, the information has not really been put to practical use in any of the experiments that are aware of. The major disadvantage of the VAD technique is that the need for a steerable dish antenna puts a practical limit on the antenna size.

The second method of determining the vector wind is to use a fixed dipole array (Woodman and Guillen, 1974). By phasing the signal fed to the various parts of the array, the transmitted beam can be moved off vertical. The vector wind can be determined uniquely by pointing beams in three different directions in what amounts to a simplified VAD technique. Usually one beam is pointed in the vertical direction and two in the off-vertical direction at an angle of 5° to 15°. The Poker Flat MST radar is operated in this configuration (Balsley et al., 1980). The main advantages of this type of system are that the antenna is easy to construct and relatively inexpensive. Also, antenna arrays with dimensions as large as 200 m ´ 200 m can be utilized, something that would be very difficult with a steerable dish system. The disadvantages are that for large antennas, considerable real estate is involved and there is no way to take into account variation in the wind field over the distance separating the beams. This method is adopted in Indian MST Radar.

The third technique is the spaced antenna (SA) measurement advocated by Rottger and Vincent (1978) and Vincent and Rottger (1980). The capabilities of the SA were compared to the two methods described above by Briggs (1980) and Rottger (1981). For this method one transmitter array and three spatially separated receiver arrays are used. The horizontal wind components are determined by a correlation analysis of the signals measured at the three receiver arrays. The method measures the temporal and spatial variations of the field pattern of the radar echoes with vertically beamed antennas. The vertical velocity is derived from the Doppler-shift of the radar echoes. Radars are particularly sensitive to temperature inversions and other stratified structures such as "fronts".

It has been determined that there is an enhanced reflectivity for radars operating at wavelengths of the order of meters when the radar beam is pointed vertically and that the returned power drops off very rapidly within a few degrees of vertical. Since the SA technique uses only vertically pointing beams, it is possible to detect echoes with a higher signal-to-noise ratio than those that could be detected with a system using an off vertical beam configuration. The disadvantage of the SA method are essentially the same as those of the fixed dipole array method. Perhaps the SA radar handles inhomogeneities in the sampling volume slightly better than the Doppler method since measurement, by its very nature, tends to average variations in the atmospheric structure between the two receiving antenna. Also, the vertical velocities can be measured in all three receiving beams simultaneously and this provides direct information on the spatial variations within the sampling volume.

2.4 MST RADAR TECHNIQUE

The origin of MST radars dates back to the early days of ionospheric back scatter observations which were carried out with a 41 MHz radar in Illionis (USA) by Bowles (1958). Strong echoes, observed at 79-90 km height, were interpreted as due to ionospheric scattering of the turbulence variety in the mesosphere. Subsequently, Flock and Balsley (1967) reported about VHF radar observations at Jicamarca(Peru) , which confirmed echoes from 75 km height and were also interpreted to be most likely caused by turbulence scattering in the presence of a gradient of electron density. Several years later Ronald F. Woodman with Alberto Guillen (1974) substantially improved the technique in order to measure velocities and they also reported the detection of stratospheric returns. They recognized the great potential of this technique for remote sounding of the middle atmosphere. Their studies triggered the evolution of a new generation of radars for atmospheric research, and VHF radars were started thereafter to be developed for the only purpose of lower and middle atmosphere observations. Although earlier expectations that the entire region of the Mesosphere, Stratosphere and Troposphere, which gave the name MST radar, could be monitored more or less continuously, have emerged to be an overestimate, their very unique applications to investigate the structure and dynamics of the middle atmosphere is widely accepted (Gage and Balsley, 1978; Walker, 1979; Balsley and Gage, 1980; Crane, 1980; Harper and Gordon, 1980; James , 1980; Rottger, 1980; Klostermeyer, 1981; Rastogi, 1981; Woodman, 1981; Larsen and Rottger, 1982; Larsen, 1983a). It has turned out that the MST radar technique is also very suitable for operational applications in meteorology (Lhermitte, 1979; Wilson et al.,1980; Gage and Balsley, 1980; Rottger, 1981a; Balsley and Gage, 1982; Hogg et al., 1983; Larsen, 1983b.).

MST radars make use of scattering and reflection from variations of humidity, temperature and electron density, induced by turbulence in the lower and middle atmosphere. Essentially, MST radars can observe: the 3-dimensional wind field, atmospheric reflectivity and stability, and morphology of turbulence and waves. The continuous measurements with MST radars offer very good quality and quantity middle atmosphere observations of wind velocities (Gage and Van Zandt, 1981). MST radars operate at frequencies around 50 MHz, and therefore are also called VHF radars. Higher frequency radars mostly cover only the troposphere and stratosphere. Typical peak powers of VHF radars are between 1 KW and 1 MW. Range resolutions down to about 100m and time resolutions down to some ten seconds are possible. The antenna arrays with typical dimensions of 100 m^2 to some 1000 m^2 point close to the zenith direction. Coherent detection, digital control and data acquisition are mandatory. An MST radar is a high power, coherent pulse Doppler radar. The power aperture is an important 'figure of merit' of a radar. Table 2.1 shows this parameter for different types of Radars.

Table - 2.1 Power aperture products for different types of radars		
Type	Peak power aperture product (Wm^2)	Frequency (MHz)
MST	10^7 to 10^{10}	41 to 55
ST	10^5 to 10^7	41 to 404
T	10^2 to 10^5	404 to 961
LT	10 to 10^2	915 to 3000
MST - Mesosphere-Stratosphere-Troposphere, ST - Stratosphere-Troposphere, T - Troposphere, LT - Lower Troposphere		

For determination of various atmospheric parameters the received radar signal is coherently integrated and spectrum analyzed and three order moments are obtained. The zeroth moment i.e. power under the spectrum gives the radar reflectively which is related to strength of turbulence. The first moment gives the Doppler shift of the medium along the line of sight of radar and second moment gives the random motion of the turbulence within the scattering volume. The scattering and reflection mechanisms responsible for MST Radar have been described by Balsley and Gage (1981) and Gage and Balsely (1980) and others. They are classified as :

(i) Back-scattering from turbulence

(ii) Fresnel (partial) reflection/scatter

(iii) Thermal (incoherent or Thomson) scatter.

2.5 INDIAN MST RADAR AND ITS SPECIFICATIONS

2.5.1 INTRODUCTION

Woodman and Guillen's studies of the middle atmosphere at 50 MHz triggered the evolution of a new generation of VHF radars for atmospheric research. Measurements of the Doppler spectrum of echoes from the troposphere and stratosphere were made, and it was shown that the mean Doppler shifts were highly correlated with radiosonde winds. Thereafter such radars were built at many place in the world.

In the Indian sector before nineties, for the study of lower and middle atmospheric dynamics, mostly rawinsonde (balloon) and rocket-borne chaff were used from the different stations. But during bad weather conditions, particularly during monsoon it is difficult to lunch rawinsonde or rockets and hence misses very important opportunity for the study of lower and middle atmospheric dynamics. Therefore to study the essential parameters of the atmosphere, such as three dimensional wind vector, clear air turbulence and atmospheric wave phenomena there is a need of, continuous reliable measurements with routine basis, regardless of the state of the weather. Thus, a major MST radar system has been established as a national facility at Gadanki near Tirupati (13.47^{o}N, 79.18^{o}E).

The radar has been developed in two phases. In the initial phase it was commissioned in ST mode using partial power aperture (average power aperture = 4.8 ´ 10^6 Wm^2). The ST mode operation, from Feb.1992 to July 1992, has helped in validation of various sub-systems of the radar and also for collection of some interesting observations on atmospheric turbulence, wind field in ST region and also on ionospheric irregularities (Rao et al.,1994.1995). This radar system became operational in full MST mode in March 1994 with average power aperture product of 7 ´ 10^8 Wm^2. This system has now completed first five years of operation in MST mode. In this period, radar has been used to study wide range of problems related to atmospheric structure, dynamics and coupling processes in the lower and middle atmosphere and ionospheric field-aligned irregularities. Important scientific results are obtained during the first five years of operations in MST mode. The study would give an idea of the potential of this modern facility for atmospheric research and the type of scientific programs that are currently in progress. It has also been possible to use Indian MST radar system in spatial domain interferometry (SDI) mode to study the ionospheric irregularities and meteor-trail-associated ionization irregularities.

2.5.2 RADAR AND ITS SPECIFICATIONS

The Indian MST radar is a highly sensitive, pulse coded, coherent VHF phased array radar, operating at 53 MHz with an average power-aperture product of 7×10^8 Wm². The basic system has been discussed in detail by Jain et al (1995), Rao et al. (1994,95). The system design specifications are presented in Table 2.2 and figure 2.2 shows functional block diagram of the Indian MST radar.

Table 2.2 - Main specifications of the Indian MST radar	
Parameter	: Specification
Location	: Gadanki (13.4°N, 79.18°E)
Frequency	: 53 MHz
Average Power aperture product	: 7×10^8 Wm²
Peak power	: 2.5 MW
Maximum duty ratio	: 2.5 %
Number of Yagi antennas	: 1024
Beam width	: 3°
Number of beams for automatic scan Pulse	: 7*
Pulse width	: 16 and 32 ms coded and 1-32 ms uncoded (in binary steps)
Pulse repetition frequency	: 62.5 Hz - 8 kHz(in binary step)
Maximum number of range bins:	: 256
Number of coherent integrations	: 4 to 512 (in binary steps)
Maximum number of FFT points	: 512
Radar controller	: PC\AT featuring programmable experimental specifications file
computer system	: 32-bit super mini with vector accelerator (Masscomp MC5600)
* Zenith in X and Y polarizations, ± 10° off-zenith in E-W and N-S plane, and 14.8° N looking transverse to *B* filed. This capability has now been enhanced to 18 beams which can be chosen from available 82 beams.	

The phased antenna array consists of 1024 crossed 3-element Yagi antennas occupying an area of 130 × 130 m. It generates a radiation pattern with a main beam of 3°, a gain of 36 dB and a sidelobe level -20 dB. The main beam can, in principle, be positioned at any look angle, but is currently programmed to position at six look angels, Zenith, ± 10° off zenith in east-west and north-south direction and 14° due north to look transverse to the earth's magnetic field over the magnetic equator.
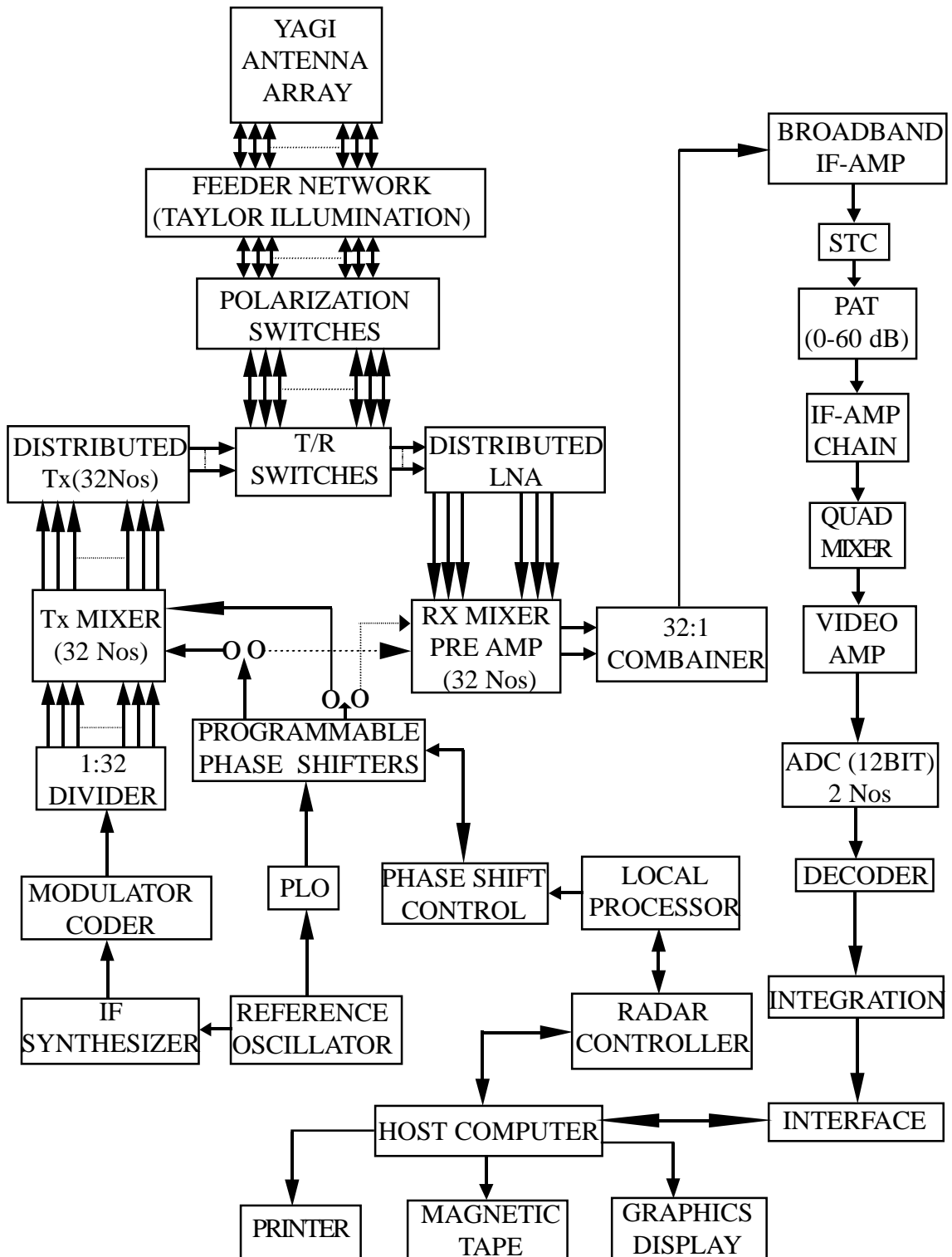
Fig.2.2 : A block diagram of Indian MST Radar system
(After Jain et al., 2000)

A total transmitted power of 2.5 MW (peak) is provided by 32 transmitters ranging in power from 20 KW to 120 KW each feeding a subarray of 32 Yagis. To achieve the desired low side lobe level to the radiation pattern, the power is tapered across the array according to a modified Taylor distribution. The required power taper is accomplished in one principal direction by differential powers of the transmitters and in the other direction by the series feed net work. Some of the important feature of the Indian MST radar are listed below :

(i) The 16 or 32 ms pulse can be coded using 16 or 32 baud bi-phase complementary pairs with a baud length of 1 ms, providing a range resolution of 150 m.
(ii) The radar system is rendered phase coherent by using a frequency synthesizer with a master oscillator of stability better than one part in 10^{10} (short term). The same provides transmitter carrier and modulation as well as receiver injection signals.
(iii) The radar receiver is a phase coherent receiver with two quadrature channels having an overall gain of 110 dB, a dynamic range of 70 dB, and a bandwidth matching the baud length of the coded pulse.
(iv) The quadrature outputs of the receiver are given to a signal preprocessor. The unit consist two identical channels of A/D convertor (ADC), decoder and coherent integrator. The ADC is of 12-bit resolution to match the dynamic range (70 dB) of the receiver.
(v) The radar preprocessor transfers data to the host computer for further processing. The host is a 32-bit super-minicomputer (Masscomp-MC 5600) which operates in a real-time unix environment.
(vi) The radar controller is a PC/AT which executes an experiment according to the data given in the form of an experiment specification file (ESF).

2.5.3 DATA PROCESSING

The MST radar is pulsed Doppler radar to support the atmospheric research. Normally radar target will be a hard target having better reflection co-efficient. Without much signal processing technique, the extraction of signal is possible. In the case of atmospheric radar the target is soft target and it is buried 40 to 50 dB below the back ground noise/clutter and sophisticated signal processing technique is required to extract the signal.

The purpose of radar signal processing is to extract desired signal from radar returns. The desired data usually concerns the detection of a target of interest, the location of the target in space. The accuracy of the data available from a radar is limited by the thermal (known as clutter), and externally generated interferences. As a result radar signal processing is also used to enhance signals and to suppress clutter and externally generated signals (noise).

The radar output can either be taken in raw data format, i.e. the time series samples of two quadrature channels (I&Q) after coherent integration, or in the form of Doppler power spectra, after on-line FFT for each range bin of the selected range window. The parametrization of the Doppler power spectrum is carried out off-line. The scheme involves (i) removal of d.c., (ii) estimation of the average noise level, (iii) removal of the interference, if any, (iv) incoherent integration and (v) computation of three low order moments as described by Jain et al. (1995) and Rao et al. (1995). The three moments represent the signal strength, the weighted mean Doppler shift and half-power width of the spectrum.

The received signal power could be used to compute the volume reflectivity (h). The mean Doppler shift provides a direct measure of the radial velocity of the scattering irregularities acting as tracer of the background wind. Three (u,v,w) components of wind are obtained from a minimum of three non-coplanar beam positions. When observations are made at more than three look angles (Table 2.1), the wind vector can be determined using the method of least-square. The spectral width provides the variance of the velocity fluctuations from which various turbulence parameter can be determined (Hocking, 1985).

After maximizing a peak Signal to Noise Ratio (SNR) in the IF amplifier, the IF signal is detected by a quadrature detector which produces a time series of sine and cosine components (I & Q) of the received signal. This will essentially reduce the sampling time of analog signal to half and helps to do complex spectrum analysis. The maximum bandwidth on each channel is 0.85 MHz. The detected signal is finally converted to a digital signal by an analogue to digital converter (ADC). The signal processing is implemented in hardware with the point of view to do it in real time. The hardware implemented processing steps includes decoding of the coded signals, and coherent integration. The received signal may include phase modulation due to a pulse compression technique, which is decoded after digitization. The decoding of the signal is essential to get back the original signal from its coded nature. This is nothing but a correlation operation on received signal with its original coded waveform used for transmitting the signal. This essentially would not increase any process gain. The block diagram (Fig.2.3) shows the basic processing steps involved in the extraction and estimation of atmospheric parameters.

2.5.4 RECENT DEVELOPMENTS

Some limitations were experienced during the operation of the Indian MST radar in support of user scientists experiments. This has resulted in further technical developments of the system which are summarized below :
(i) Minimum coherent integration can now be set at 1 instead of 4 (see table 2.1). This allows large Doppler window of observations as required for observation of field-aligned plasma irregularities at ionospheric heights.

```
        ┌──────────────────────────┐
        │  DECODED INPUT (I & Q)   │
        └──────────────────────────┘
                    │
        ┌──────────────────────────┐
        │        COHERENT          │
        │      INTEGRATION         │
        └──────────────────────────┘
                    │
        ┌──────────────────────────┐
        │      NORMALIZATION        │
        └──────────────────────────┘
                    │
        ┌──────────────────────────┐
        │        WINDOWING          │
        └──────────────────────────┘
                    │
        ┌──────────────────────────┐
        │     FOURIER ANALYSIS      │
        └──────────────────────────┘
                    │
        ┌──────────────────────────┐
        │     POWER SPECTRUM        │
        └──────────────────────────┘
                    │
        ┌──────────────────────────┐
        │       INCOHERENT          │
        │       AVERAGING           │
        └──────────────────────────┘
                    │
        ┌──────────────────────────┐
        │     POWER SPECTRUM        │
        │       CLEANING            │
        └──────────────────────────┘
                    │
        ┌──────────────────────────┐
        │  NOISE LEVEL ESTIMATION   │
        └──────────────────────────┘
                    │
        ┌──────────────────────────┐
        │   MOMENTS  ESTIMATION     │
        └──────────────────────────┘
                    │
        ┌──────────────────────────┐
        │     UVW COMPUTATION       │
        └──────────────────────────┘
```
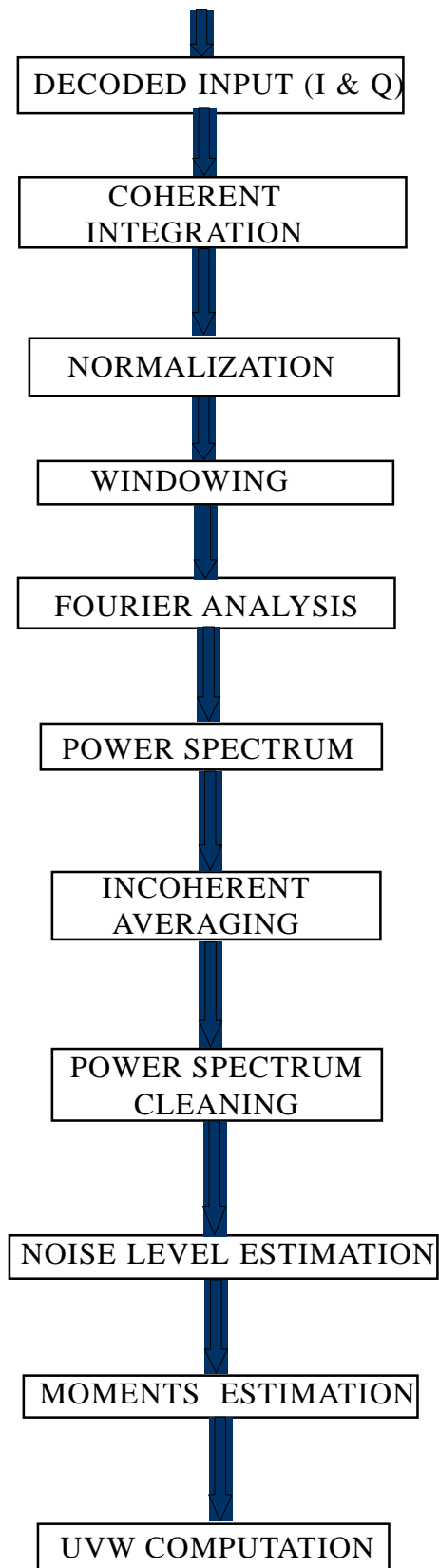
Fig.2.3 : (After Anandan (ADP, Technical and user Reference Manual))

(ii) the number of beams that can be operated in auto-mode has been increased to 18 instead of 6 (see table 2.1). These 18 beams could be selected out of the available 82 beams between zenith angle of ± 20°, at an interval of 1°, in two planes, i.e., east-west and north-south of antenna array. This available flexibility has made it feasible to conduct special experiments on (i) radar echo aspect sensitivity to understand the nature of atmospheric structure and dynamics during the tropical convection events.

(iii) Two experimental specification files (ESFs) can be operated sequentially in auto-mode. These two ESF can be totally independent of each other. This has provided considerable flexibility in radar operation and optimal utilization of radar time.

(iv) A new software called Atmospheric Data Processor (ADP) has been developed. This software makes use of adaptive method of signal tracing as described by Anandan (1997). This has resulted in better signal tracing and thus makes it feasible to retrieve low-order moments of radar signal spectrum over large height range.

(v) It has been possible to use Indian MST radar in spatial domain interferometry (SDI) mode. This technique has been applied to echo arising due to backscatter from a (a) ionospheric irregularities and (b) meteor trails.

2.6 DETECTION OF TROPICAL WAVES AND TIDES

The ability of the VHF radars to measure vertical velocities on a routine basis also can have important consequences for tropical meteorology. Radars operating at meter wavelengths can measure both the vertical velocities within clouds and the centimeter per second velocities associated with the waves. Fukao et al. (1978) analysed a full day of stratospheric wind measurements from the Jicamraca radar(12°S) for diurnal and semidiurnal wind components. They inferred a diurnal wind oscillation with characteristics similar to those inferred from the averaged rawinsonde data. Fukao et al. (1980) have used the Arecibo radar to study the dynamics of the diurnal and semidiurnal tidal components. The phase progression indicates that the source of energy for the diurnal tide is in the troposphere and is in agreement with the result of Wallace and Tadd (1974), whose investigation based on radiosonde data showed that the strong diurnal component seen in the troposphere at low latitudes is not the classical tidal component.

It was possible to resolve the wave structure because radars with high spatial resolution had been used to track the rawinsondes launched during the experiment. With the radars it will be possible to observe the waves on a more routine basis. The transport and deposition of energy and momentum by gravity waves in the lower stratosphere, which can be measured with ST radar (Fukao et al.,1988: Tsuda et al.,1990), is believed to have an impact on the mean stratospheric circulation.

The evident capabilities of MST radars to investigate and monitor waves and turbulence and their mutual coupling with the mean flow of the general circulation pattern as well as the impact on vertical transport is recognized and accepted (e.g.,Gage and Clark, 1978; Gage, 1979; Klostermeyer, 1981; Lindzen, 1981; Woodman et al.,1981; Larsen et al., 1982). A large international MST system is planned for operation close to the equator especially to allow the measurements of (vertical) velocities through almost the entire middle atmosphere. Wind measurements made at the Arecibo Observatory by Sato and Woodman (1982) using the 430 MHz radar always show perturbations in the vertical profile with a scale size of ~ 1 km. The perturbations usually only undergo one complete oscillation in the vertical direction, so it is difficult to speak of a wave train. There is very little vertical phase progression, but on a scale of several days. It was determined that the period of the wave likely to be four or five days. Fukao et al. (1981) have observed the same kind of wave at Jicamarca, Peru, during a 48 hours observation period and estimated period of the wave to be between four and five days.

The period and the wavelength are characteristics of a mixed Rossby-gravity wave, which is an important part ot the dynamics at low latitudes (Holton 1975). Since the period is of the order of days, the high time resolution of the radars is not really necessary to observe the wave, but the high spatial resolution is, since the vertical wave length is so small. Cadet and Teitelbaum (1979) detected the mixed Rossby-gravity wave in data taken during the GATE experiment.

The Indian MST radar high resolution wind measurements are also used to study the equatorial waves such as Rossby-Gravity (RG) waves and Kelvin waves. Iyer et al.(1994) detected atmospheric waves and tides first time using Indian MST radar wind field data in ST mode. The observations using the Indian MST radar at Gadanki are used to look for the presence of tidal oscillations and equatorial waves in the data of zonal and meridional winds over the altitude range 4-18 km (Jivrajani et al.,1997). Sasi et al., (1998) observed characteristics of diurnal nonmigrating tides in the troposphere and lower stratospheric winds over Gadanki (13.5°N, 79.2°E) during an equinox season. Seasonal differences of non-migrating tides in the troposphere and sratosphere over Gadanki (13.5°N, 79.2°E) is observed by Jani et al.,(2000) using diurnal cycles of different seasons derived from the Indian MST radar wind data. Sasi et al (1999) estimated the equatorial wave momentum fluxes using MST radar winds observed at Gadanki. The preliminary results of the study of equatorial waves (i.e Kelvin and Mixed Rossby Gravity waves) with periods ranging 4 to 32 days using Indian MST radar wind data are discussed and presented in the chapter-v.

CHAPTER - 3

STUDY OF TIDAL OSCILLATION

3.1 INTRODUCTION

Both the sun and the moon exert periodic forces upon the earth's atmosphere. In the case of moon these forces are wholly gravitational, except for the minute heating effect from the reflected radiation at the full moon. The sun, however exerts a strong thermal effect as well as a much weaker gravitational effect. The earth's atmosphere will respond to these forces in a manner analogous to forced mechanical vibrations. It is possible to analyse the forcing term into harmonic components, the steady-state response of the atmosphere to these forces are known as atmospheric tides. They will have periods that are submultiples of the solar or lunar day.

The absorption of solar radiation at the ground and in the earth's atmosphere sets up a thermal forcing which can drive atmospheric oscillations with periods which are integral fraction of a day . Tides in the middle atmosphere are generated by heating due to the absorption of solar infrared radiation by water vapour in the troposphere and ultraviolet radiation by Ozone in the stratosphere and mesosphere. They, along with gravity waves, are believed to be responsible for generation of turbulence in the mesosphere/lower thermosphere and play a vital role in thermospheric mean circulation and thermal structure by contributing to the momentum and energy budget of that region. Atmospheric pressure, temperature, density and winds are all subject to variation with 24-hour (diurnal) and 12-hour (semi-diurnal) periods. Tidal oscillations in the middle atmosphere can, to first order, be viewed as the superposition of several quasi-modes each with somewhat distinguishable and identifiable horizontal structures and vertical wavelengths. There are mainly two types (i) migrating and (ii) non-migrating tidal oscillations observed in the atmosphere.

(i) <u>Migrating tides</u> - The heating has a strong altitude variation and latitude variation as well. The heating generates pressure changes with particular patterns of variation with latitude, longitude and height. In particular, the maximum heating rate and associated pressure change at any given altitude travel with the sub-solar point in the atmosphere and for this reason the tides generated by solar heating are known as 'migrating tides'. The classical theory of tides by Chapman and Lindzen assumed a zonally symmetric distribution of water vapour and O_3 so that the diurnal tide generated by the solar heating is migrating in nature. The migrating zonal and meridional pressure gradients generate acceleration of air parcels, which are subject to Coriolis torque's as they move.

(ii) <u>Non-migrating tides</u> - Asymmetry in the distribution of water vapour and ozone will generate tides that are not migrating in nature with the Sun and is called non-migrating tides. Non-migrating tides may also be generated by other zonally isolated sources such as in the Planetary Boundary Layer (PBL) and latent heat released by deep convective clouds in the tropics. The cumulus convection which could cause excitation of atmospheric tides is dominant in the equatorial

.

region. However, such heat sources are localized in their horizontal extent, which is largely affected by the land-sea distribution. So they may not generate a global (migrating) tide but may instead excite non-migrating tides which consist of higher order modes with small vertical scales. Classical tidal theory has been mainly used to study non-migrating tides in the atmosphere. The role of the non-migrating tides in transporting momentum and energy from near the ground to lower stratosphere seems to be an important research subject.

3.2 THEORY OF TIDAL OSCILLATION
3.2.1 INTRODUCTION

Towards the end of seventeenth century when barometric observations were taken in the tropics, it show something very exciting, quite different from what it had seen in the middle latitudes; that there is a very regular 24-hours oscillation of pressure in the tropics. During the eighteenth century, Newton' theory of gravitation was successfully applied to the oceans for explaining some features of the oceanic tides. Laplace was able to treat mathematically the problem of the oscillation of an ocean of uniform depth on a rotating globe under the action of gravitational tide-generating forces. He also showed that the tidal oscillations of an isothermal atmosphere undergoing isothermal changes were analogous to the tidal oscillations of an homogeneous incompressible fluid having equivalent depth. This equivalent depth was the height of an hypothetical atmosphere having the same hydrostatic pressure at the bottom as the isothermal atmosphere and a uniform density in the vertical equal to the density of the isothermal atmosphere at the bottom.

Laplace felt that there was a difficulty in deducing that the observed atmospheric pressure wave was of gravitational forcing. He observed that 24-hour oscillation had the harmonics pertaining to 24,12,8,6,... hours. Out of these, the 12-hour oscillation had the largest amplitude and was very regular both in amplitude and phase. The other sub harmonics were present but had very small amplitudes. The causes of the 24-hour (diurnal) and the 12-hour (semidiurnal) pressure waves could be two-fold: gravitational and/or thermal. If the cause was mainly gravitational, then the lunar gravitational potential which was greater than the solar gravitational potential should generate greater lunar tidal wave than the solar tidal wave.

But observations showed that pressure wave corresponding to the lunar day was hardly perceptible while the pressure wave corresponding to the solar day was so prominent. If the cause was mainly thermal, then the 24-hour wave should be more dominant than the 12-hour wave because the temperature has a dominant 24-hour wave rather than the 12-hour wave. Infact the dominant pressure wave is the 12-hour wave. Hence neither simple gravitational forcing nor the simple thermal forcing could provide answer for the observed pressure wave.

In the year 1882 Kelvin gave 'resonance' theory. According to him the atmosphere as a whole oscillated like an ocean and that its period of free oscillation was 12 hours. In such a case, the regularly recurring 12-hourly solar gravitational tidal potential would enhance about 100-fold through resonance. When the mean annual 12-hourly component was examined in greater detail, it was found that near the poles, the maxima and minima did not occur at the same local time as they did in tropical and middle latitudes, but instead tended to occur at the same Greenwich mean time, like a standing oscillation. Pressure rising at the poles and falling in the lower latitudes at one and the same time and vice versa. In 1890 Schmidt suggested that the solar 12-hourly oscillation consisted of two components, one travelling with the sun having maximum amplitude at the equator and nearly zero amplitude at the poles; the other standing oscillation having maximum amplitude at the poles and zero amplitude at the latitude of about 35^0N and 35^0S. Lamb(1910) showed that adiabatic atmosphere undergoing adiabatic changes should have the same equivalent depth as Laplace's isothermal atmosphere undergoing isothermal changes. In 1926 Jeffreys gave the formula for equivalent depth that is

$$\text{Equivalent Depth} = \int_{z=0}^{\infty} \left(\frac{p}{p_o} \right) dz$$

This method of deriving the analogy between the atmosphere and the ocean had a discrepancy of dimensions. The remedy for this was suggested by Bartels (1927) and gave an alternative formula:

$$\text{Equivalent Depth} = \int_{z=0}^{\infty} \left(\frac{p}{p_o} \right)^{1/\varsigma} dz$$

According to resonance theory, the tidal maxima should occur at mid-day and mid-night but these actually occur two hours ahead of mid-day and mid-night at least near the ground. To reconcile this fact of observation with the tidal theory Chapman had suggested that the thermal excitation would have its maxima considerably earlier than mid-day and mid-night so that under the joint influence of gravitational and thermal excitations, the actual maxima occurred a couple of hours earlier than the mid-day and the mid-night. However, this explanation also get into difficulties. On the basis of this hypothesis, it would be expected that on clear days, the semi-diurnal pressure wave should show its maxima earlier than on cloudy days. But Spar's (1952) analysis of surface observations (New-York) showed that on clear days, the maxima occurred about half an hour later than on cloudy days. Sen and White (1955) took the vertical distribution of temperature as given in NASA Atmosphere and found that the resonant amplification of the gravitational tidal wave would not be adequate to give the observed magnitude of the semi-diurnal pressure wave and that thermal excitations have to be invoked. Haurwitz and Moller (1955) analysed the semidiurnal variations of the surface temperature separately for the standing and for the migratory temperature waves.

They argued that solar tidal potential has no term corresponding to the observed standing semi-diurnal pressure oscillation of the atmosphere. Hence its cause must lie in some temperature oscillation of the earth's atmosphere. This oscillation would come from solar heating. They even suggested that this phenomenon of standing semi-diurnal pressure oscillation was in further support for the resonance theory. Chapman and Lindzen (1970) have considered thermal forcing to be all important and gravitational forcing to be of no great significance.

According to them, thermal forcing arises out of radiation absorption by water vapour and ozone. For the forcing, one has to specify the period, phase, amplitude, vertical distribution and horizontal distribution. In respect of the horizontal distribution, no account is taken of land-sea contrasts or orography. Hence the forcing is symmetrical along a latitude circle. Therefore, for horizontal distribution, it is enough to specify the distribution with respect to latitude only. Chapman and Lindzen specify different forcing for the 24-hour and the 12-hour periods. Vertical distribution of thermal forcing is considered to be the same both for 24-hour and 12-hour oscillations, although different for water vapour and ozone (Fig.3.1).
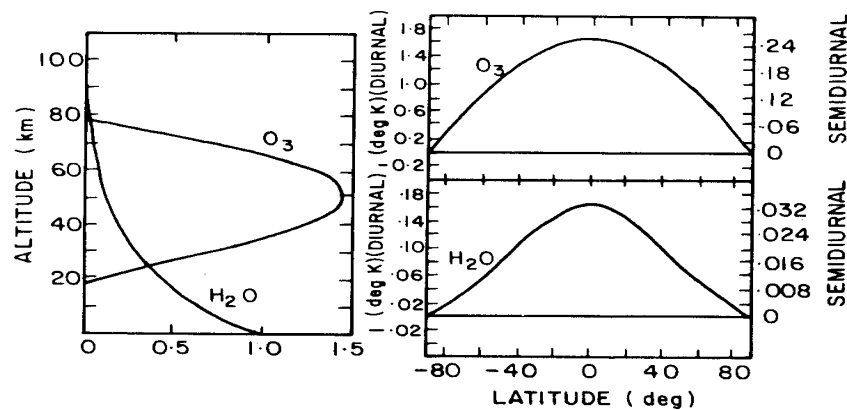
Fig.3.1 : Vertical and latitudinal distribution of thermal excitation due to water vapor (H_2O) and Ozone(O3) (after Lindzen 1968).

Latitudinal distribution is also considered to be the same for 24h and 12h oscillation, although amplitudes and phases are different. Chapman and Lindzen made broad assumptions to explain various processes in their theory. Hong and Lindzen (1976) developed a three-dimensional model to study the characteristics of the semi-diurnal tide in the thermosphere. In this model, they included viscosity, thermal conductivity and ion drag. Lindzen (1978) suggested that the additional source of heating lay in the release of latent heat of a semi-diurnal oscillation in tropical rainfall. He also showed that this semi-diurnal precipitation could not be released simply by the horizontal velocity convergence of tidal horizontal winds. The tidal motions might act to trigger squall line instabilities which might produce the required precipitation. In the last decade, the availability of good ozone data made it possible to compute the heating rates more realistically and to generate the heating rates for different seasons and for different tidal modes.

3.2.2 MATHEMATICAL TREATMENT OF ATMOSPHERIC TIDES

Atmospheric tides are treated mathematically with the use of three basic equations which describe the relevant physical processes in the atmosphere.

The equation of motion (force balance equation)

$$\frac{D\overline{W}}{Dt} + 2(\overline{w} \times \overline{W}) = -\frac{1}{r}\tilde{N}p + \overline{g} + \overline{F} \underline{\hspace{1cm}} (1)$$

Where, $\overline{W}$ = Wind, $\overline{w}$ = Earth's angular velocity or rotation, $\overline{g}$ = acceleration due to gravity, r = atmospheric density, p = atmospheric pressure, $\tilde{N}p$ = pressure gradient force, $\overline{F}$ = sum all forces driving or decelerating the wind W

Thermodynamic energy equation (Energy conservation equation)

$$Q = C_V \frac{DT}{Dt} + \frac{D}{DT}\left(\frac{1}{|}\right) \underline{\hspace{1cm}} (2)$$

Where Q = rate of input or loss per unit mass (in unit time), C_V = Specific heat at constant volume, T = Temperature. The continuity equation,

$$\frac{D|}{DT} + | \ div \ \overline{W} = 0 \underline{\hspace{1cm}} (3)$$

In addition, the perfect gas law, $p = nkT = rRT \underline{\hspace{1cm}} (4)$

Where n = number density, (r = nm), R = Universal gas constant k = Boltzmann constant. The hydrostatic equation

$$-\frac{\P P_o}{\P z} = |_o \ g \underline{\hspace{1cm}} (5)$$

Equation (5) results from (1) with $\overline{W}$ = 0 and $\overline{F}$ = 0. In the above equations (1), (2), and (3)

$$\frac{D}{DT} = \frac{\P}{\P t} + \overline{W.\tilde{N}} \underline{\hspace{1cm}} (6)$$

denotes the Lagrangian (total) derivative following the motion of a given air parcel. It gives the time variation of the parameter due to (a) the change of parameter with time plus (b) the change of the parameter with location because of spatial gradients.

$$\overline{W.\tilde{N}} = U\frac{\P}{\P x} + V\frac{\P}{\P y} + W\frac{\P}{\P z} \underline{\hspace{1cm}} (7)$$

for x, y, and z co-ordinate system. In spherical co-ordinates, f (longitude), q (co-latitude) and r (radial distance), than equation. (7) becomes

$$\overline{W.\tilde{N}} = U\frac{1}{a \ sinq}\frac{\P}{\P f} + V\frac{1}{a}\frac{\P}{\P q} + W\frac{\P}{\P z} \underline{\hspace{1cm}} (8)$$

Where U, V and W are eastward, norhward and upward components of $\overline{W}$.

For winds ($\overline{W}$) which vary with time scale of half- a day or one day and which have spatial changes only on a global scale, the $\overline{W.\tilde{N}}$) term, represents the advection with W, can be neglected in comparison with the inertial term ($\P / \P t$). This approximation is commonly used in tidal theory. The atmosphere has a basic state characterized by W_o, r_o , P_o, T_o. The tide-generating forces generate perturbations in the above parameters. These perturbations can be considered as small compared to W_o, P_o, T_o and they are represented by

$$\frac{\left|\overline{W_1}\right|}{\left|\overline{W_o}\right|}, \quad \frac{p_1}{p_o}, \quad \frac{\rho_1}{\rho_o}, \quad \frac{T_1}{T_o} \quad << 1 \underline{\hspace{3cm}} (9)$$

In equations (1), (2) and (3) $\overline{W}$, p , r, and T can be considered to consist of the basic state values plus the perturbations, i.e.

$\overline{W} = \overline{W_o} + \overline{W_1}$, $\quad p = po + p1$, $\quad r = r_o + r_1$ and $\quad T = To + T1$ \underline{\hspace{1.5cm}}(10)

Substituting the above values for $\overline{W}$, p, r, and T in the equations (1) to (4), and neglecting all terms which are second order, obtain the following equations for the perturbations. Using $\overline{W_1} = iu + jv + kw$; $\overline{W_o} = iU_o + jV_o + kW_o$

$$\frac{\partial u}{\partial t} - 2W\,v\,\cos q = -\frac{1}{a\,\sin q}\,\frac{\partial}{\partial f}\left(\frac{p_1}{p_o} + p\right) \underline{\hspace{2cm}} (11)$$

$$\frac{\partial v}{\partial t} - 2W\,u\,\cos q = -\frac{1}{a}\,\frac{\partial}{\partial q}\left(\frac{p_1}{p_o} + p\right) \underline{\hspace{2cm}} (12)$$

$$\frac{\partial w}{\partial t} + \rho_1 g = -\frac{\partial p_1}{\partial z} \underline{\hspace{3cm}} (13)$$

$$\frac{\partial \rho_1}{\partial t} + w\frac{\partial \rho_o}{\partial z} + \rho_o c = 0 \underline{\hspace{3cm}} (14)$$

$$\frac{\partial p_1}{\partial t} - \rho_o\,g\,w + \rho_o\,C^2\,c - (v-1)Q\,\rho_o = 0 \underline{\hspace{2cm}}(15)$$

Where p = gravitational tide potential, and $c = \operatorname{div}\overline{w_1}$. In the above equation $c = \operatorname{div}\overline{w_1}$ the horizontal component ($W\,\sin q$) W of has been neglected as making no contribution to atmospheric motions, while the vertical component $W\,\cos q$ has been retained, a = the radius of the Earth. In equations (11) to (15) for the tidal perturbations, there are six perturbations parameters : u , v , w , p_1, r_1 and T_1

However, p_1, r_1 , and T_1 are not independent of each other, because they are related by the equation, based on perfect gas law equation (4)

$$\frac{p_1}{p_o} = \frac{\rho_1}{\rho_o} + \frac{T_1}{T_o} \underline{\hspace{3cm}} (16)$$

There fore, the six equations (11) to (16) can be used to solve for the above six unknown parameters of tidal perturbation, if the pressure gradient forces in (11),(12) and the heat input rate Q in (15) are known. The tidal perturbations in any parameter is assumed to have sinusoidal variations in time with fundamental period of 24 hours or 12 hours, and sinusoidal variations with longitude (f), with longitude wave numbers   m = 0, 1, 2, ...

$$\therefore \ u, v, w, p_1, r_1, T_1 \ \mu \ e^{i\,(wt + mf)} \underline{\hspace{1.5cm}} (17)$$

Where $w = 2\pi/T_w$, T_w = tidal wave period of one solar day or one lunar day m = 0 represents a standing zonal wave, m=1 represents a migrating diurnal wave, m = 2 represents semi-diurnal wave. With the above assumption, equation (17) and from the equations (11) to (15),

$$\frac{\partial}{\partial t} = i\,w \quad \text{and} \quad \frac{\partial}{\partial \phi} = i\,m \qquad (18)$$

With above substitutions equations (11) to (15) reduce to linear equations in the six variables u, v, w, p_1, r_1, and T_1 with height gradient terms ($\partial/\partial q^2$) and latitude gradient term ($\partial/\partial q$) remaining in the equations. However, in equations (11) and (12) for horizontal velocity components u, v there is no dependence on height gradient. Using equation (18) and the identity $f \circ W/2W$, the equation's (11) and (12) can be written as

$$u\,(w,\,m) = \frac{-\,w}{4\ aW^2\ (f^2 - \cos^2 q)}\ \left[\frac{\cos q}{f}\frac{\partial}{\partial q} + \frac{m}{\sin q}\right]\ \left(\frac{p_1\,(w,\,m)}{r_o} + p\,(w,\,m)\right) \qquad (19)$$

$$v\,(w,\,m) = \frac{-\,i\,w}{4\ aW^2\ (f^2 - \cos^2 q)}\ \left[\frac{\partial}{\partial q} + \frac{\cot q}{f}\cdot m\right]\ \left(\frac{p_1\,(w,\,m)}{r_o} + p\,(w,\,m)\right) \qquad (20)$$

In order to get the tidal perturbations from the differential equations (11) to (15) and the perfect gas law (16) the following methodology is used. First the five differential equations (11) to (15) along with (16), can be used to eliminate five unknowns and thus obtain a differential equation for single variable. For this purpose of obtaining a differential equation for a single parameter, it is found that the most convenient parameters to deal with is :

$$G \circ \frac{1}{g\,p_o} = \frac{Dp}{Dt} = \frac{1}{r_o C^2}\frac{Dp}{Dt} \qquad (21)$$

G is related to wind divergence $c \circ \operatorname{div} \overline{W}_1$, as $\quad G \circ c - \dfrac{Q}{C_p\,T_o} \qquad (22)$

The differential equations for G, as obtained from equations (13) to (16) and (19)-(20) is :

$$H\frac{\partial^2 G}{\partial z^2} + \left[\frac{\partial H}{\partial z} - 1\right]\frac{\partial G}{\partial z} - \frac{iw}{g}\frac{\partial^2 p}{\partial z^2} = \frac{g}{4\ a^2 W^2}F\left[\left(\frac{\partial H}{\partial z} + e\right)G - \frac{eQ}{g\,gH}\right] \qquad (23)$$

the scale of z- variation for the tidal potential p is the moon-earth or sun-earth distance, and hence third term on L.H.S., involving $\partial^2 p/\partial z^2$), can be ignored then the equation

$$H\frac{\partial^2 G}{\partial z^2} + \left[\frac{\partial H}{\partial z} - 1\right]\frac{\partial G}{\partial z} = \frac{g}{4\ a^2 W^2}F\left[\left(\frac{\partial H}{\partial z} + e\right)G - \frac{eQ}{C^2}\right] \qquad (24)$$

involves the derivative of G with height and latitude, and the derivatives of Q with latitude. Q is also a function of height. F is the differential operator (for latitude variation) and is given as:

$$F = \frac{1}{\sin q}\frac{\partial}{\partial q}\left[\frac{\sin q}{f^2 - \cos^2 q}\frac{\partial}{\partial q}\right] - \frac{1}{f^2 - \cos^2 q}\left[\frac{m}{f}\frac{f^2 + \cos^2 q}{f^2 - \cos^2 q} + \frac{m^2}{\sin^2 q}\right] \qquad (25)$$

It may also be noted that G includes the latitude derivatives of pressure perturbation p_1 (resulting from solar heating) and of the gravitational potential p, because the substitution of (19) and (20) into the equation

$$c \circ \tilde{\tilde{N}}.\overline{W}_1 = \frac{1}{a \sin q}\frac{\partial}{\partial q}\,(v\,\sin q) + \frac{1}{a \sin q}\frac{\partial u}{\partial \phi} + \frac{\partial w}{\partial z} \qquad (26)$$

which leads to

$$c - \frac{\partial w}{\partial z} = \frac{iw}{4\,a^2\,W^2}\,F\,\left[\frac{p_1}{r_o} + p^{w,n}\right] \underline{\hspace{3cm}} (27)$$

If the variation of G and Q in equation (24) above are assumed to be independent of each other, then equation (24) can be solved by the method of variables, using appropriate boundary conditions. The amplitude of G with regard to its dependence on latitude and height may be represented as

$$G^{w,m} = \sum_n L_n(z)\,Q_m(q) \underline{\hspace{2.5cm}} (28)$$

Where G = is the altitude structure function of particular mode which is (by implication) the same as at all latitudes, $Q_m(q)$ = the latitude structure function of a particular latitudinal mode which is (by implication) the same at all heights. The above equation also implies that a particular tidal oscillation with a given set of w, m can have different modes of latitude structure, each mode having a different height structure compared others. The height and latitude variations of the amplitude of a given tidal oscillation, with a frequency w and zonal wavenumber m, are given by the summation of $L_n(z)$ and $Q_n(q)$ for all n, at any given z and q. The total amplitude of G (w) with a given period of oscillation (24-hour, for example) is obtained by a further summing up of G (w,m) in equation (27) for all m values (m = 0, 1, 2, ...)

The problem now is to find out the terms of the height structure function L_n (z) and the latitude structure function $Q_n(q)$. It turns out that [$Q_n(q)$] for all n is a complete set for $0 £ q £ P$ and can be represented by an expansion in associated Legendre Polynomials. Moreover, the heating rate Q (w, m) can also be represented, for its height and latitude variations, in terms of similar function as in (27) :

$$Q^{w,m} = \sum_n Q_n(z) \cdot Q_n(q) \underline{\hspace{3cm}} (29)$$

Substitution of (27) and (23) into (24) results in two equations, one involving only latitude variation and another involving only the height variation :

$$F\,(Q_n^{w,m}) + \frac{4\,a^2\,W^2}{gh_n\,(w,m)}\,Q_n^{w,m} = 0 \underline{\hspace{2.5cm}} (30)$$

$$H\,\frac{\partial L_n^2}{\partial z^2} + \left[\frac{\partial z}{\partial H} - 1\right]\frac{\partial L_n}{\partial z} + \frac{1}{h_n}\left[\frac{\partial H}{\partial z} + e\right]L_n = \frac{e}{C^2\,h_n}\,Q_n \underline{\hspace{1cm}} (31)$$

Equation (30) is a homogeneous equation involving no forcing term and it represents the d.c. term for free oscillation of an ocean of depth h_n. This is the (h_n) well known "Laplace Tidal Equation" which was solved for w (contained in the differential operator F) as an eigen value problem of finding the frequencies of the surface oscillations of an ocean of depth h. The same equation can be used for dealing with oscillations of the atmosphere with the diurnal (24-hour) and semi-diurnal (12-hour) periods.

3.2.3 SOURCES OF EXCITATION

The atmosphere is set into motion by the various external and internal energy and momentum sources. The transformation of these sources into heat and momentum of the atmospheric gas is a complicated process that depends on the physical and chemical conditions of the atmosphere.

(1) <u>Gravitational Excitation</u> : This is primarily due to the gravitational potential of the moon and secondarily to that of the sun.

(2) <u>Thermal excitation due to exchange of heat with the ground</u> : Of all the solar radiation incident on the earth and its atmosphere system, most is absorbed by the ground and sea. The daily variation produced in the ground temperature   are conveyed to the adjacent atmosphere by turbulence and infrared radiative transfer.

(3) <u>Thermal excitation due to direct atmospheric absorption of insolation :</u>
Although most insolation is absorbed at the ground, a significant amount is absorbed by the atmosphere by water vapor and Ozone (and by O_2 to a lesser extent). The daily, variation in heating due to this absorption is distributed throughout the bulk of the atmosphere, and is the most important of the tidal and thermotidal excitation.

3.3   OBSERVATIONS AND NUMERICAL MODELS

The detection and study of actual tidal oscillation at the ground consists of a long series of reading of recordings of meteorological data particularly of pressure, but also of wind and temperature made at numerous observatories widely distributed over the globe. Pressure reading are used so often in tidal analysis because they are least subject to local geographic variations but reflect tidal nature most clearly. From an analysis of global surface pressure data, Haurwitz (1965) came to the conclusion that diurnal non-migrating tides have large amplitude on land than over ocean. There is strong evidence from rawinsonde data that the wind oscillation of period 24 h that occurs at tropospheric and stratospheric heights at low to mid-latitudes is not wave number 1 tide (i.e. migrating tide) predicated by classical tidal theory (Chapman and Lindzen, 1970; Forbes and Garrett, 1979) and apparently observed in the upper mesosphere, but rather an oscillation linked to local, regional or continental topography (Wallace and Hartranft, 1969).   Kato et al. (1982) investigate the generation and propagation of tides due to geographically localized sources of excitation and explained many characteristics of the observed structures, which are apparently nonmigrating tidal components. Many efforts were made in theoretical studies and numerical modelling of non-migrating tides in the atmosphere. Numerical model of McKenzie (1968) had simplified latitudinal and logitudinal structures of the heat source model and could successfully account for the large diurnal and wind amplitudes below 30 km. Forbes and Groves (1987), have studied the effect of non-migrating tides on the longitudinal structure of diurnal tides.

Tsuda and Kato (1989) have developed a numerical model of diurnal non-migrating tides excited by upward heat flux within the PBL localized only on land, which has been found as the major excitation source of the diurnal non-migrating tides by Tokioka and Yagai (1987).

The tidal theory suggests that the vertically propagating modes of diurnal tides have larger amplitudes in the latitude range equatorward of 30°; therefore, non-migrating diurnal tides are expected to be significant in the equatorial region. As a matter of fact, a numerical model predicted that non-migrating diurnal tides could have been larger amplitudes than the migrating component in the equatorial region. Both theoretical and experimental works reported in the literature reveal significant seasonal variations in the diurnal and semidiurnal wind components (Natstrom and Belmont 1976; Vial 1986).

The numerical study by Williams (1994) has stressed the importance of constructive and destructive interference of higher order nonmigrating modes with the migrating modes in interpreting simultaneous tidal observations in the tropical troposphere over different stations separated in longitude. Non-migrating tidal oscillation in the atmospheric winds was detected by Wallace and Tadd (1974) from radiosonde data. Tsuda et al., (1994) also detected diurnal oscillation in winds measured by radiosondes over Indonesia below 25 km characterized by amplitudes of 1-1.5 ms^{-1} and interpreted as manifestation of non-migrating tides. Similar short-vertical wavelength diurnal oscillations were detected in the tropical lower stratosphere in rocket-measured winds, also by Groves, (1980), Sasi and Krishna Murthy, (1990,1993). Using radiosonde data Tsuda et al.,(1992) found that the diurnal cycle of the cumulus convection which could cause excitation of atmospheric tides was dominant in the equatorial region.

The observations with high power VHF radars at Jicamarca and other locations have given very valuable information on tidal winds in the mesosphere and lower stratosphere (Fukao et al.,1978). Only a few observational studies have been carried out in the Indian low latitude region by conventional techniques (Sasi and Krishnamurthy, 1990, 1993). Iyer et al., (1994) detected atmospheric waves and tides first time using Indian MST radar wind data in ST mode. The observations using the Indian MST radar at Gadanki are used to look for the presence of tidal oscillations and equatorial waves in the data of zonal and meridional winds over the altitude range 4-18 km (Jivrajani et al.,1997). Sasi et al., (1998) observed characteristics of diurnal nonmigrating tides in the troposphere and lower stratospheric winds over Gadanki (13.5^{o}N, 79.2^{o}E) during an equinox season. Seasonal differences of non-migrating tides in the troposphere and sratosphere over Gadanki (13.5^{o}N, 79.2^{o}E) is observed by Jani et al.,(2000) using diurnal cycles of different seasons derived from the Indian MST radar wind data. Though there is a paucity of observations for troposphere and stratosphere at equatorial latitudes.

3.4   DATA AND ANALYSIS

The diurnal cycles derived from Indian MST radar (Gadanki) wind data in the height range of 4-20 km for the winter, summer, monsoon and equinox seasons are utilized to study the tidal oscillation . The details of diurnal cycles used are given in the table -1.

Table -1			
Sr. No	Diurnal cycle	Season	Altitude range
1. 2. 3.	16-17 Jan.1996 31Jan.1Feb.1996 15-16 Feb.1996	*Winter*	
4.	10-11 June1996	*Summer*	4-20 Km
5. 6. 7. 8. 9.	22-23 July1997 6-7 August1996 3-4 Sept.1996 13-14 Sept.1995 18-19 Sept.1996	*Monsoon*	
10. 11.	3-4 Oct.1996 31Oct.1Nov.1996	*Equinox*	

For this study Doppler spectra are obtained in the height range 4-20 km at 150 m intervals using successively six beams (two vertical and four oblique beams10° off zenith in the east, west, north, and south directions) of the radar every 1 hour for 24 hours. The measurements lasted for ~10 min period every 1 hour, obtaining four samples of the spectra corresponding to each beam. These four spectra were incoherently averaged to obtain a single spectra in every range bin. This incoherent averaging improves the detectability of the true Doppler peak by a factor of 2. The noise level in each range bin was objectively determined adopting the method developed by Hildebrand and Sekhon (1974). Then the largest spectral peak in each range bin was determined and taken as the true Doppler peak corresponding to the atmospheric motion. The height profiles of line-of-sight (LOS) velocities from these Doppler peaks corresponding to each beam were constructed. Then the hourly vector wind components, namely, westerly (u), southerly (v) and vertical (w), were obtained in each range bin from the six LOS velocities using a least squares method. Thus the time series of u, v and w were obtained for the 24 hour period with a time resolution of 1 hour and height resolution of 150 m.

Once the vertical profiles (resolution 150 m) of u,v and w are obtained, these are subjected to a 5 point running mean in height with weights 0.125, 0.125, 0.5, 0.125 and 0.125 (Sasi et al. 1997). This smoothing procedure eliminates large scale wind fluctuations with height which may be due to random fluctuations or real atmospheric phenomena. Then the time series in each range bin was examined for the presence of any wild point which may be a true outlier or produced by short-period large amplitude gravity waves. This was achieved by calculating the mean and the standard deviation (s) in each range bin and the wind value was considered an outlier if it exceeded 1.7 s from the mean. These outlier were replaced by interpolated values from adjacent hourly bins. In practice, occurrence of such outliers were absent below about 13 km height and were 1 or 2 at about ~ 16-18 km. These time series of the smoothed u, v and w in each range bin of diurnal cycles were subjected to harmonic analysis to bring out the diurnal tidal and semidiurnal components of the horizontal winds. Total 11 diurnal cycles of different seasons have been utilized in this study of tidal oscillations.

3.5 RESULT AND DISCUSSION

In this section some interesting features of the observed temporal variation of the amplitudes and phases of the diurnal and semidiurnal tides and height structure of the amplitude and phase of the diurnal tides in the horizontal wind components over Gadanki are pointed out and possible physical processes responsible for them are discussed. The zonal and meridional wind components after subtracting the mean for representative days in the three seasons at selected heights shows existence of diurnal periodicity in both the components. Figure 3.2 shows daily variation in the zonal winds (after removing mean) at 8.1 and 16.05 km during 16-17 January1996.
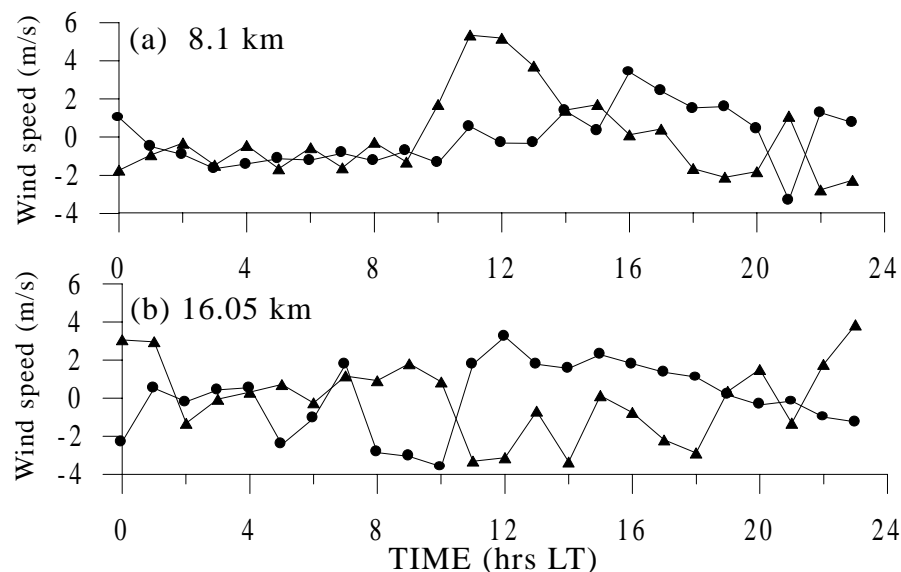
Fig.3.2 : Time variations (after removing the mean) of zonal (circles) and meridional (triangles) components of the horizontal winds at Gadanki (13.5°N, 79.18°E) during 16-17 January1996 : (a) at 8.1 km and (b) at 16.05 km.
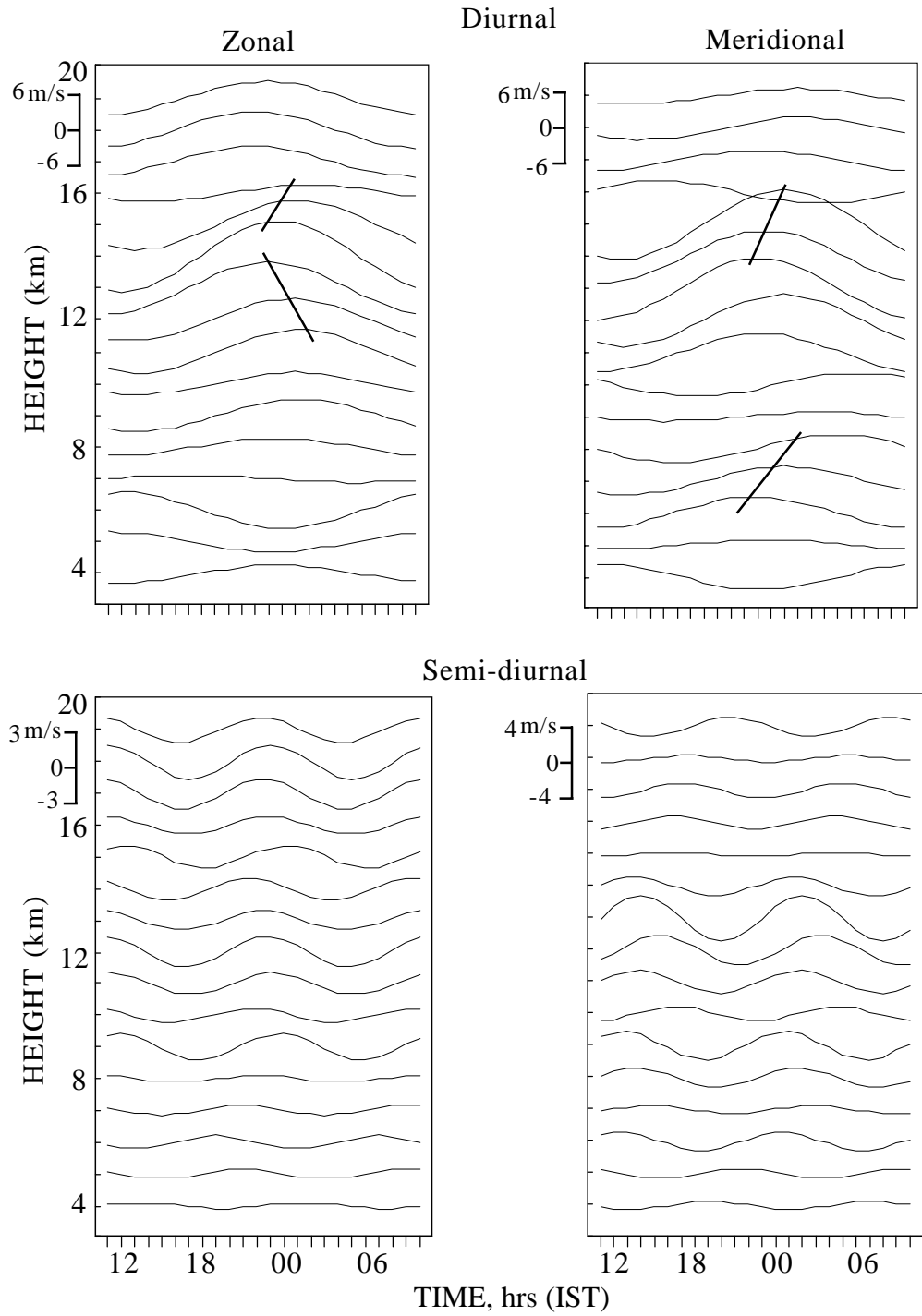
The diurnal and semidiurnal oscillations in zonal and meridional winds is seen. At the higher altitude (16.05 km) short period fluctuations with a period of 3-4 hours can be easily seen which may be a manifestation of short period gravity waves. However, the study is confined to the diurnal tides. The time series of the smoothed u and v in each range bin during given data set were subjected to Fourier analysis to bring out the diurnal tidal components of the horizontal wind. It may be mentioned here that the diurnal amplitudes and phases could be possibly affected by the presence of inertia gravity waves (IGW) with periods around 24 hours. Since local inertial period at a latitude of 13.5^{o}N is ~ 51.4 hours, the effect of these waves on the diurnal amplitudes and phases determined from hourly data is small as this will appear as random errors because of their relative temporal incoherence for a period of 24 hours when compared to the coherent diurnal tidal oscillations.

Figure 3.3 shows, the diurnal and semi-diurnal components of the temporal variation in the zonal and meridional wind velocity obtained after harmonic analysis of 24 hours data set on 16-17 January1996 (winter). The amplitude of the diurnal components in zonal and meridional winds, ranging $\pm$ 6 ms^{-1} . For semidiurnal component it ranges $\pm$ 3 ms^{-1} for zonal , and $\pm$ 4 ms^{-1} for meridional wind at different heights. In zonal wind (Fig.3.3), below 8 km, the amplitude of oscillation becomes very small and phase reversals are observed between 4 and 8 km for diurnal component, and between 8 and 10 km for semidiurnal component. Again at ~ 15 km phase reversal is seen for semidiurnal component. The phase progression is not very obvious below 10 km for diurnal and semidiurnal components. While for meridional wind phase reversals are observed at ~ 16 km for diurnal component and between 8 and 12 km for semidiurnal component.

Figure 3.4 shows the diurnal and semi-diurnal components of the temporal variation in zonal and meridional winds, obtained after harmonic analysis of 24 hours data set on 31January 1February 1996 (winter). The amplitude of the diurnal component ranging $\pm$ 3-4 ms^{-1} and for semidiurnal component it ranges $\pm$ 2 ms^{-1} at different heights for the both wind velocity, below 8 km, the amplitude of oscillation becomes very less. Temporal variation of harmonic amplitudes (diurnal and semidiurnal component) in zonal and meridional winds observed during 15-16 February 1996, is shown in Figure 3.5. The amplitude of the diurnal component ranging $\pm$ 5-7 ms^{-1} and for semidiurnal component it ranges $\pm$ 2-4 ms^{-1} at different heights in the zonal and meridional wind . Phase reversals are observed between 4 and 8 km for diurnal and semidiurnal components in the meridional wind oscillation.

The amplitudes and phases of the diurnal oscillation in zonal and meridional winds during 16-17 January, 31January 1February and 15-16 February 1996 (winter) obtained after harmonic analysis are shown in Figures 3.6 and 3.7 and 3.8. Amplitude and phases are plotted at 150 m height intervals.

16-17 January 1996

Diurnal

Zonal

Meridional
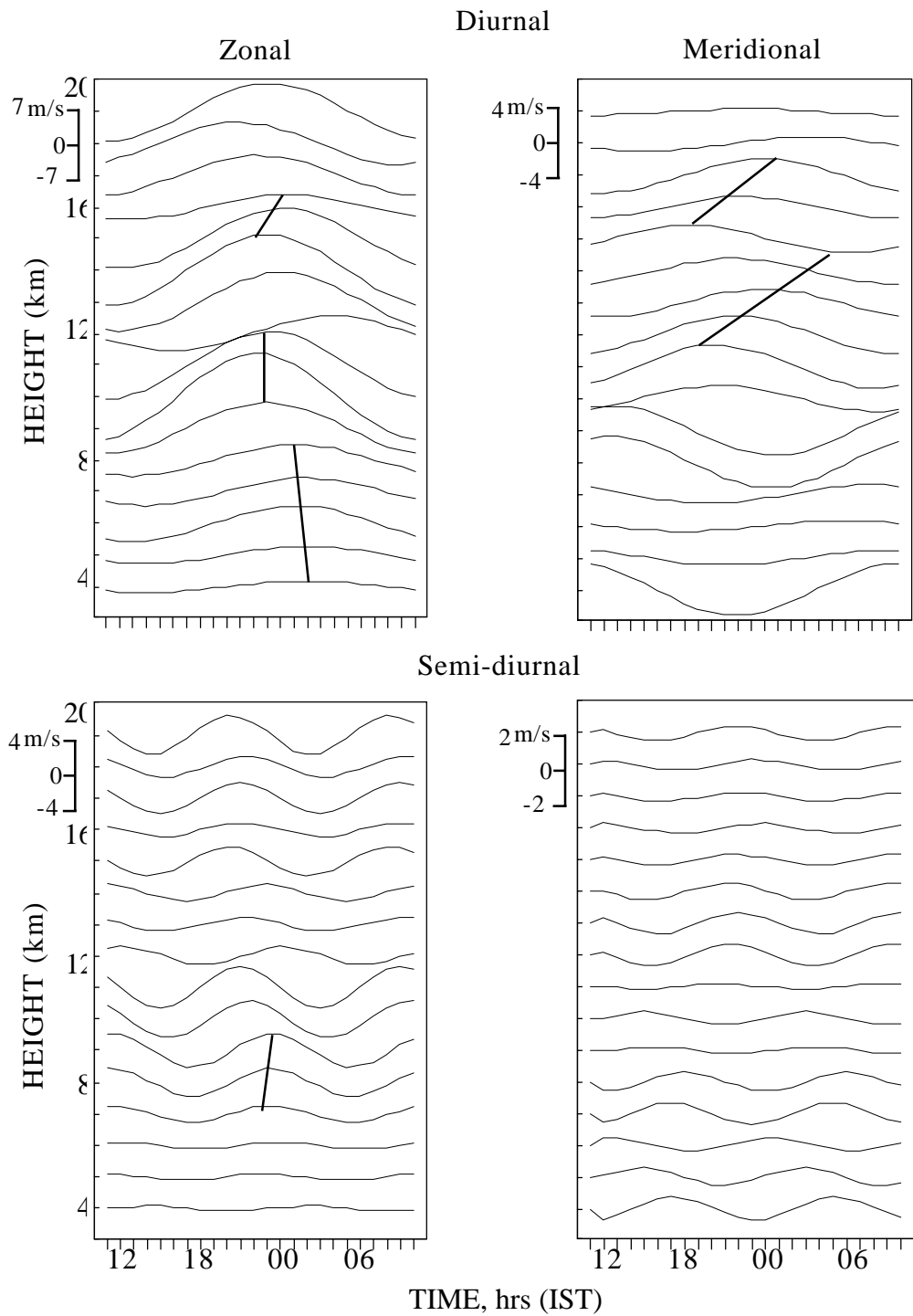

Semi-diurnal

TIME, hrs (IST)

Fig.3.3 : Temporal variation of harmonic components(diurnal and semidiurnal) of the tidal oscillations observed in the zonal and meridional winds.

31January 1February 1996

Diurnal

Zonal

Meridional

Semi-diurnal

TIME, hrs (IST)
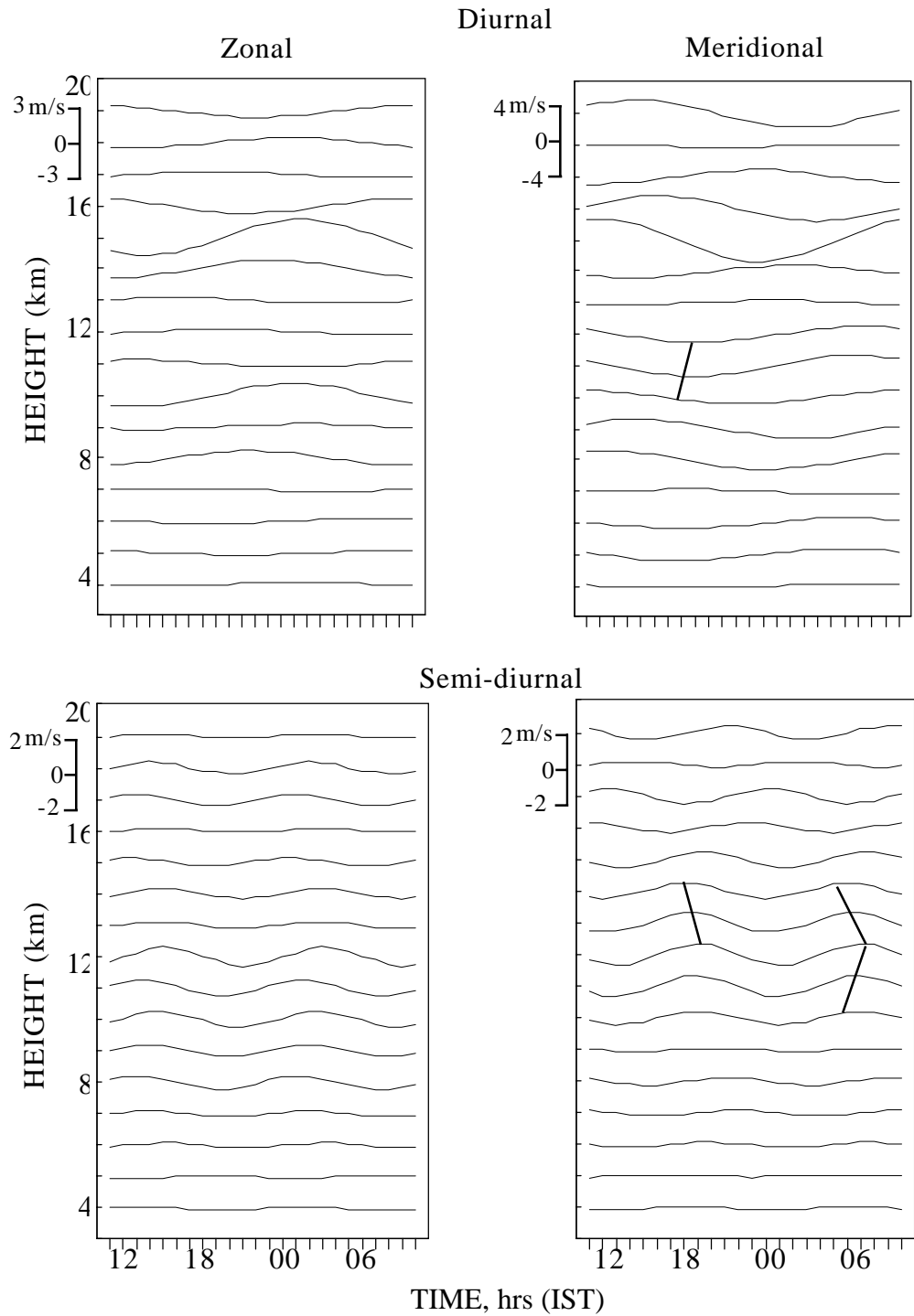
Fig.3.4 : Temporal variation of harmonic components(diurnal and
semidiurnal) of the tidal oscillations observed in the
zonal and meridional winds.

15-16 February 1996

Fig.3.5 : Temporal variation of harmonic components(diurnal and semidiurnal) of the tidal oscillations observed in the zonal and meridional winds.

16-17 January 1996

Zonal

Meridional

Amplitude (m/s)

Phase (degree)
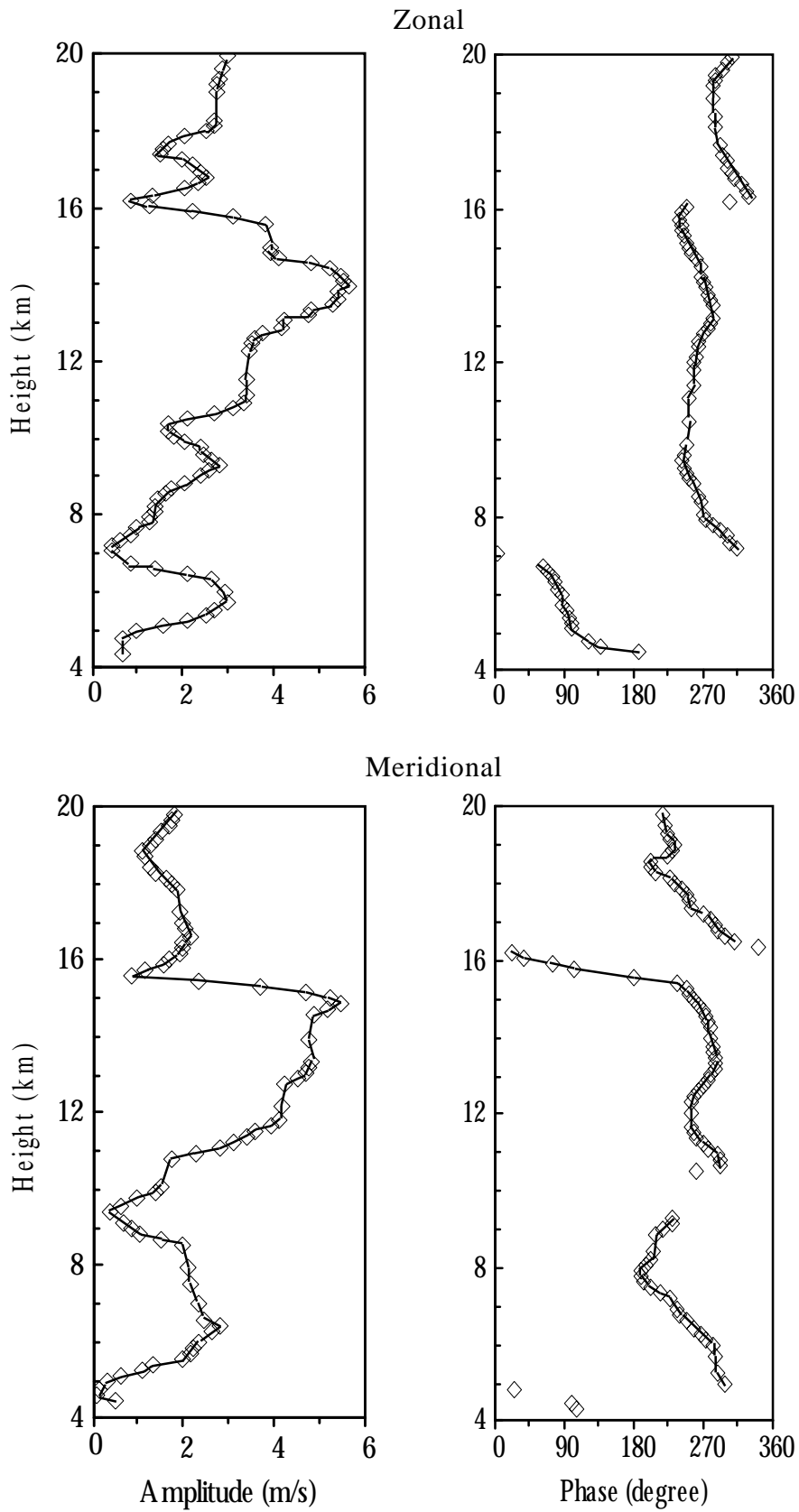
Fig. 3.6 : Amplitude and phase profiles of diurnal oscillations in the zonal and meridional winds at Gadanki.

31January 1February 1996
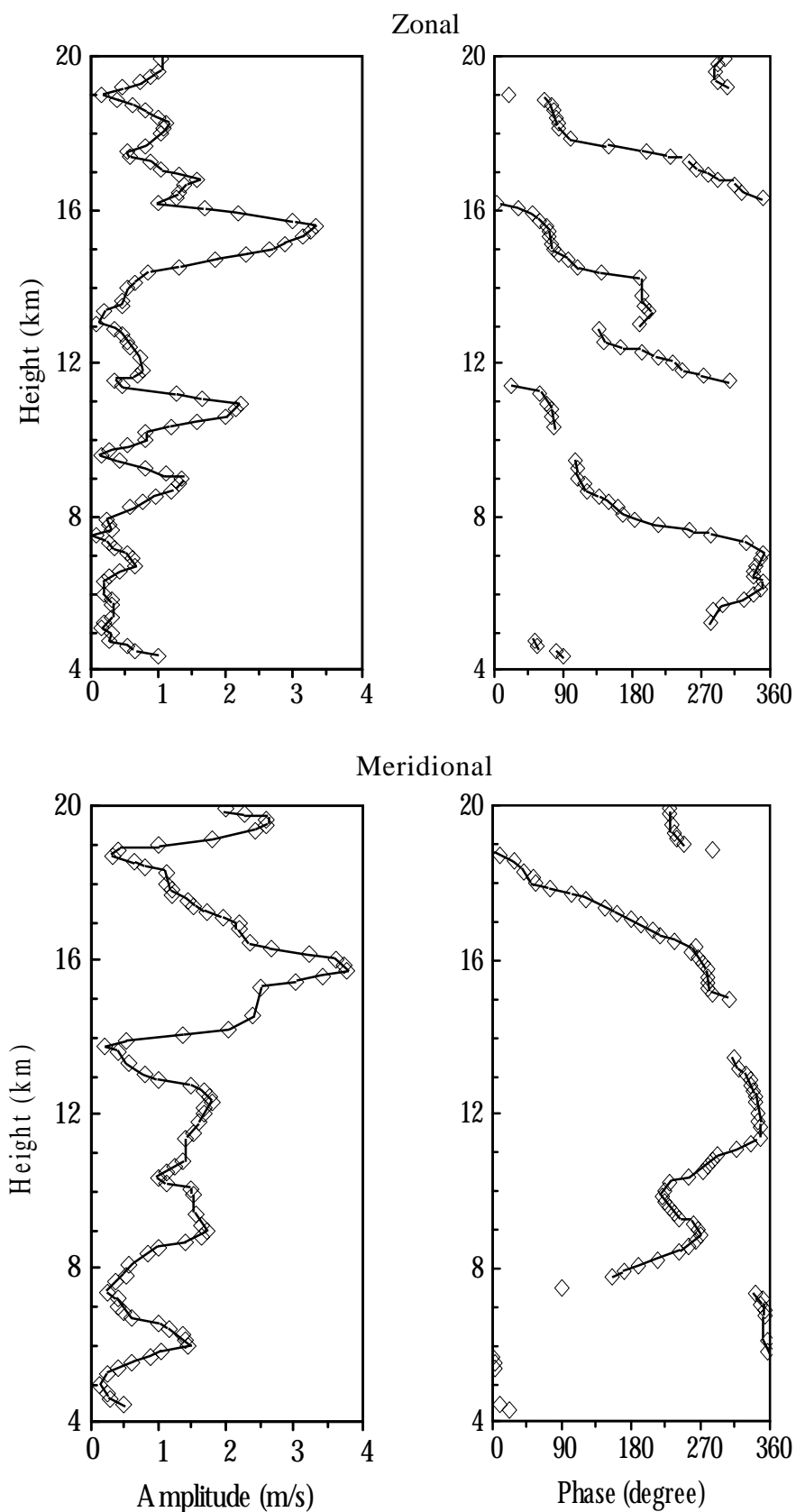
Zonal

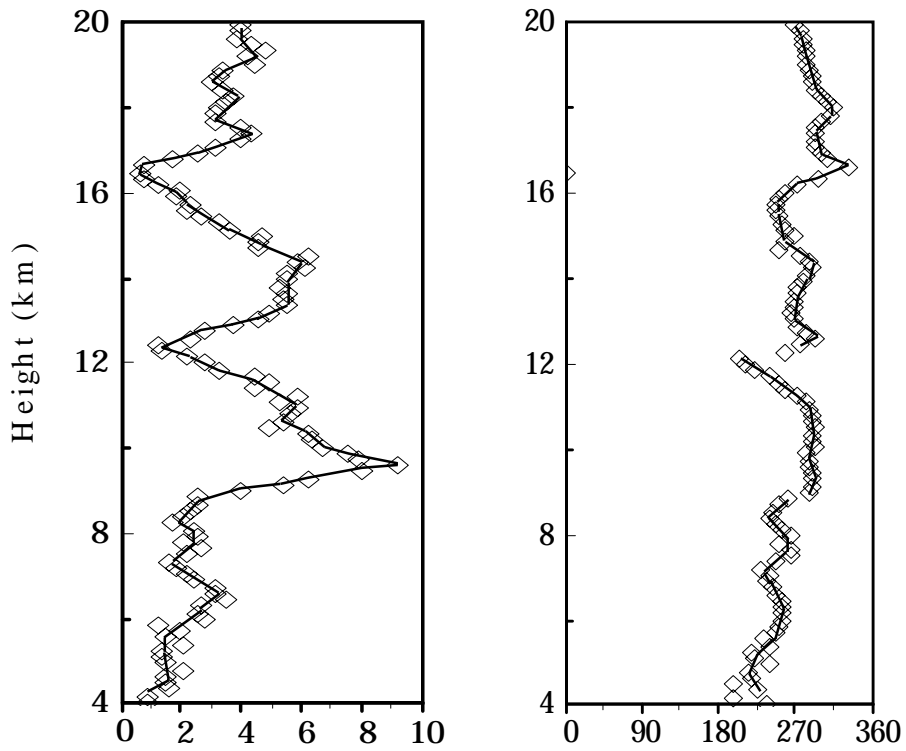

Meridional

Amplitude (m/s)

Phase (degree)

Fig. 3.7 : Amplitude and phase profiles of diurnal oscillations in the zonal and meridional winds at Gadanki.

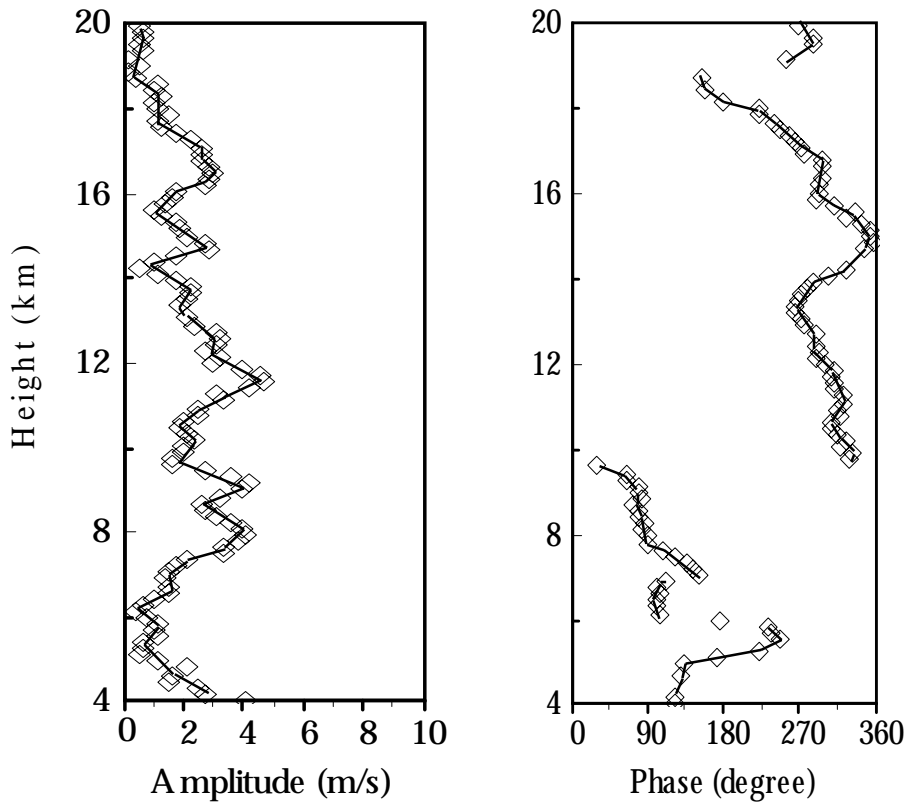**Fig. 3.8 :** Amplitude and phase profiles of diurnal oscillations in the zonal and meridional winds at Gadanki.

It is seen from the height profiles of amplitudes, that diurnal oscillations attain large amplitude (4-6 ms^{-1}) during winter, in the upper troposphere (i.e. at ~14-16 km), except it reaches significantly high value of ~ 10 ms^{-1} at ~ 10 km on 15-16 February in zonal wind and having less value (2-4 ms^{-1}) in meridional wind. The peaks in amplitude and inversion in phase at specific altitude separated by about 3-4 km clearly seen in the zonal component are indicative of the vertical wavelengths of tides. The phases are almost constant in both zonal as well as meridional components, particularly in height region between 10 to 16 km. It suggests a standing wave pattern created by (a) the upward propagation of tidal waves from a ground source and (b) the downward propagation of these waves probably from another source at 14-16 km (below the troposphere). It is seen from Figures 3.6, 3.7 and 3.8 that diurnal amplitude in the zonal, as well as meridional wind attain large amplitude of 4-5 ms^{-1} both in the troposphere and lower stratosphere during winter. A detailed examination of Figures 3.7 and 3.8 shows that the diurnal amplitudes in the zonal and meridional winds fluctuate with height creating complex height structure. The vertical separation between the observed successive amplitude maxima or successive minima can be taken as the vertical wavelength of the stronger non-migrating tidal mode. From Figures 3.7 and 3.8 it is seen that in zonal wind, the successive amplitude maxima are separated by 2-3 km below 10 km and 5-6 km above 10 km, suggesting the vertical wavelength below 10 km is 2-3 km and 5-6 km above 10 km.

The successive maxima and minima in the amplitudes profile may be indication of interference between the weak migrating tides and strong non-migrating tides (Sasi at al., 1998). The vertical wavelength calculated from the rate of phase propagation is found to be consistent with those inferred from the vertical separation between the amplitude peaks. The height profiles of amplitude and phase of diurnal tidal oscillation in zonal wind show very similar relationship between the amplitude and phase fluctuations with height (Fig.3.7). For example, the vertical wavelength inferred from the vertical separation between successive maxima \ minima of amplitude values in the 10-15 km region is ~ 5 km. The vertical wavelength calculated from the rate of phase propagation is ~ 4 km. Below 10 km in both zonal and meridional winds (Fig. 3.7), particularly in the 6-10 km region vertical wavelength of ~ 3 km is inferred from the amplitude peaks and also from phase propagation.

Figure 3.9 shows the temporal variation of diurnal and semi-diurnal components in zonal and meridional winds obtained after harmonic analysis of 24 hours data set on 10-11 June1996 (summer). The amplitude of the diurnal component ranging ± 4 ms^{-1} and for semidiurnal component it ranges ± 3 ms^{-1} at different heights in both the wind oscillations. Phase reversal are seen near 8 km in the zonal wind, and between 16 and 20 km in the meridional wind for diurnal component.
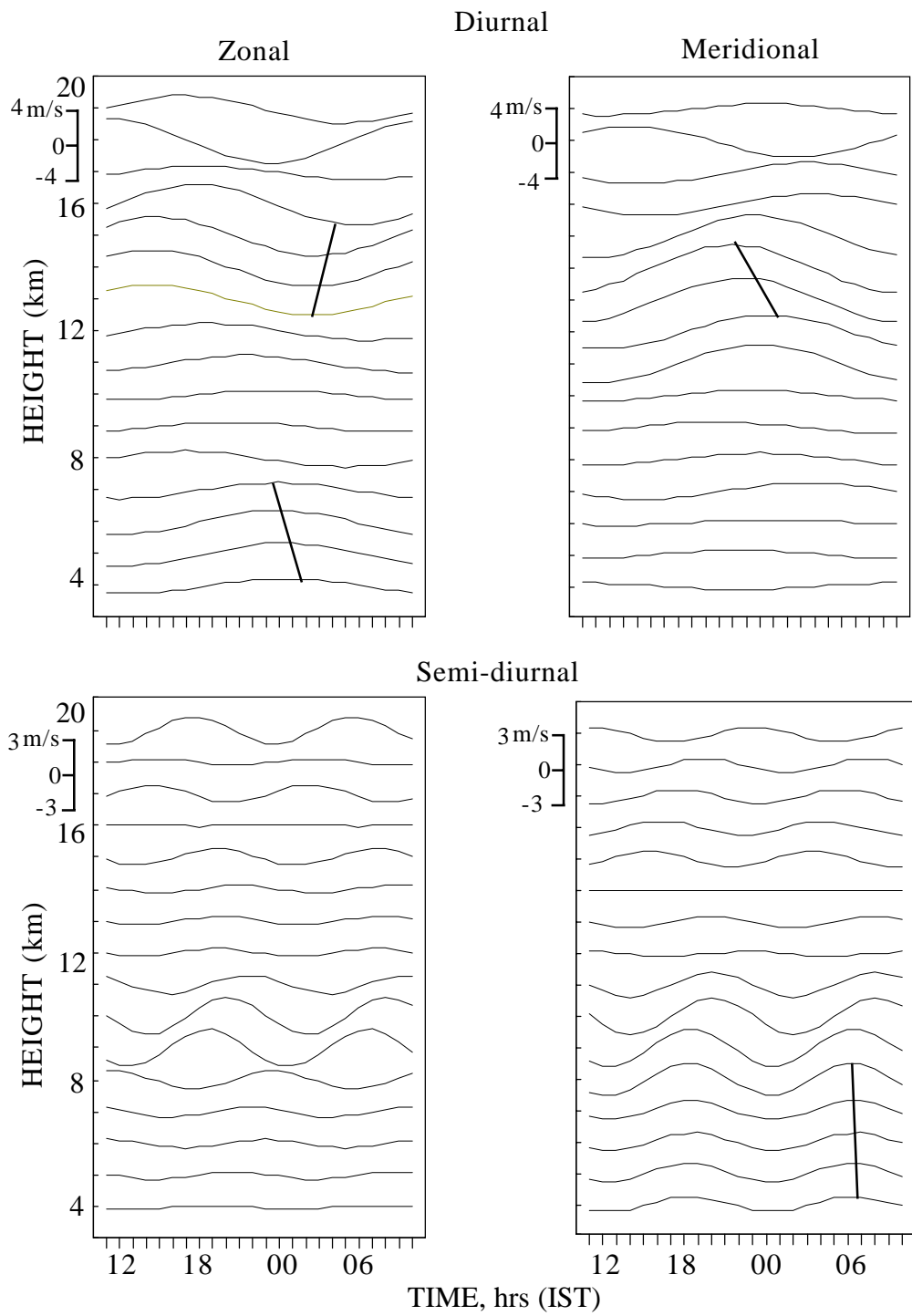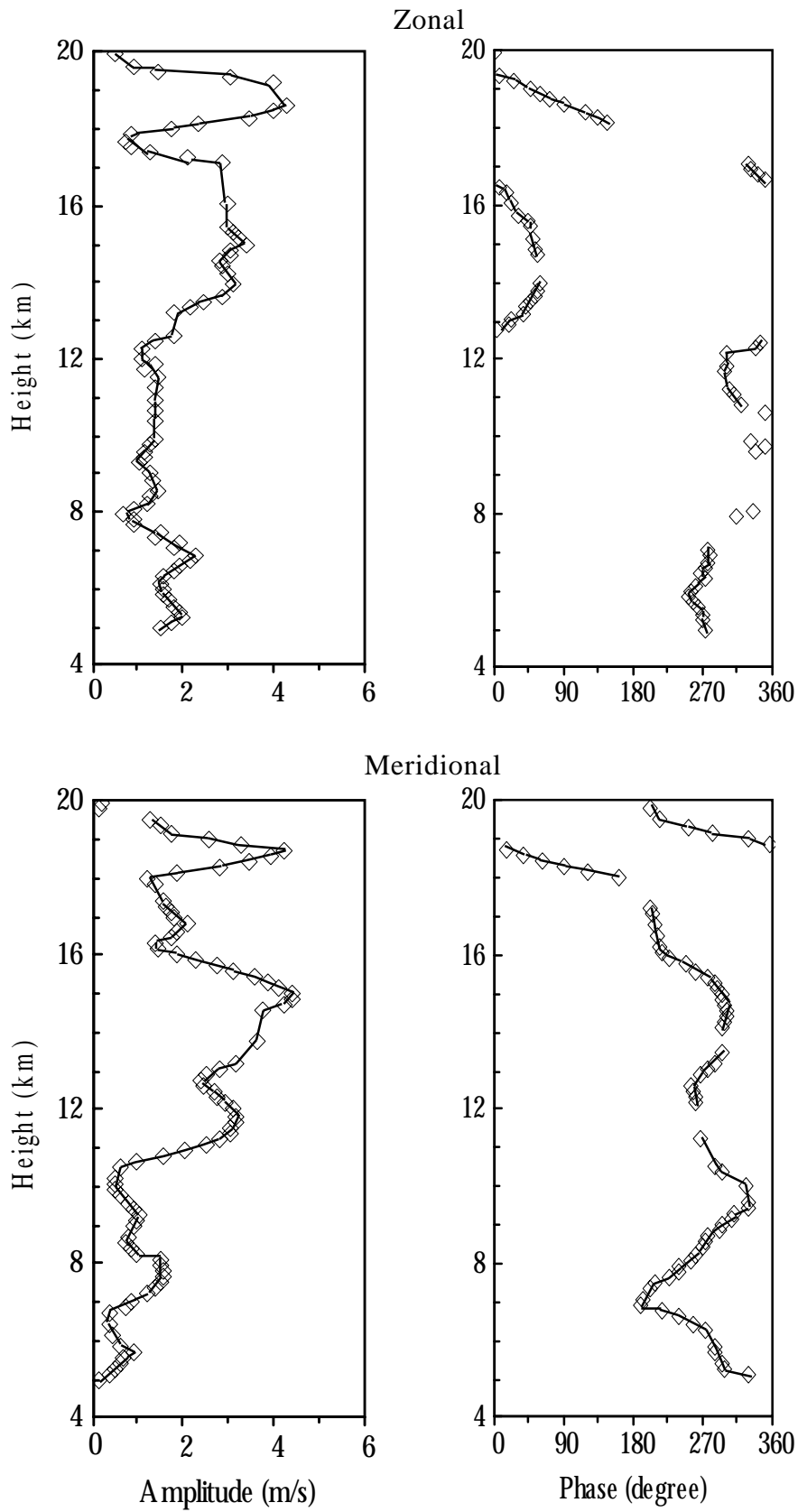
Fig.3.9 : Temporal variation of harmonic components(diurnal and semidiurnal) of the tidal oscillations observed in the zonal and meridional winds.

Phase reversal are seen near 8 km in the zonal wind, and between 16 and 20 km in the meridional wind for diurnal component. The amplitudes and phases of the diurnal oscillation in the zonal and meridional winds observed during 10-11 June1996 is shown in Figure 3.10. In the zonal wind diurnal component attains large value of   4 ms^{-1} at ~18 km, while in meridional wind two large amplitude peaks are seen at ~ 15 km and ~18 km.

The vertical separation between these two peaks and rate of phase propagation at that particular region (14 to 19 km) again suggest the vertical wavelength is ~ 4 km above 10 km (at upper tropospheric \ lower stratospheric height). Below 10 km two or three smaller amplitude peaks are seen, especially in the meridional wind component and vertical separation between these peaks shows the vertical wavelength is ~ 2-3 km. The height profiles of phases shows downward phase propagation between 15 to 20 km and suggests vertical wavelength of about 3-4 km. Figure 3.11 shows that the amplitude of the diurnal component ranging ± 5-6ms^{-1} and for semidiurnal component it ranges ± 2-3 ms^{-1} at different heights in both the wind oscillations on 22-23 July 1997 (monsoon). Phase reversal are seen between 6 and 10 km for diurnal component and between 4 and 8 km for semidiurnal component in both the wind oscillations. The amplitudes and phases observed during 22-23 July is shown in Figure 3.12.   The amplitudes attains large value of about 6ms^{-1} at ~ 13 km in zonal wind, while in meridional wind two peaks are seen at 8 and 17 km. The phase is fluctuating below 10 km and more or less steady above 12 km in the zonal wind. The standing wave pattern is seen between 10 and 16 km which is quite similar as seen on 16-17 January (Fig.3.6). For meridional wind phase progression is not clear for given height range.
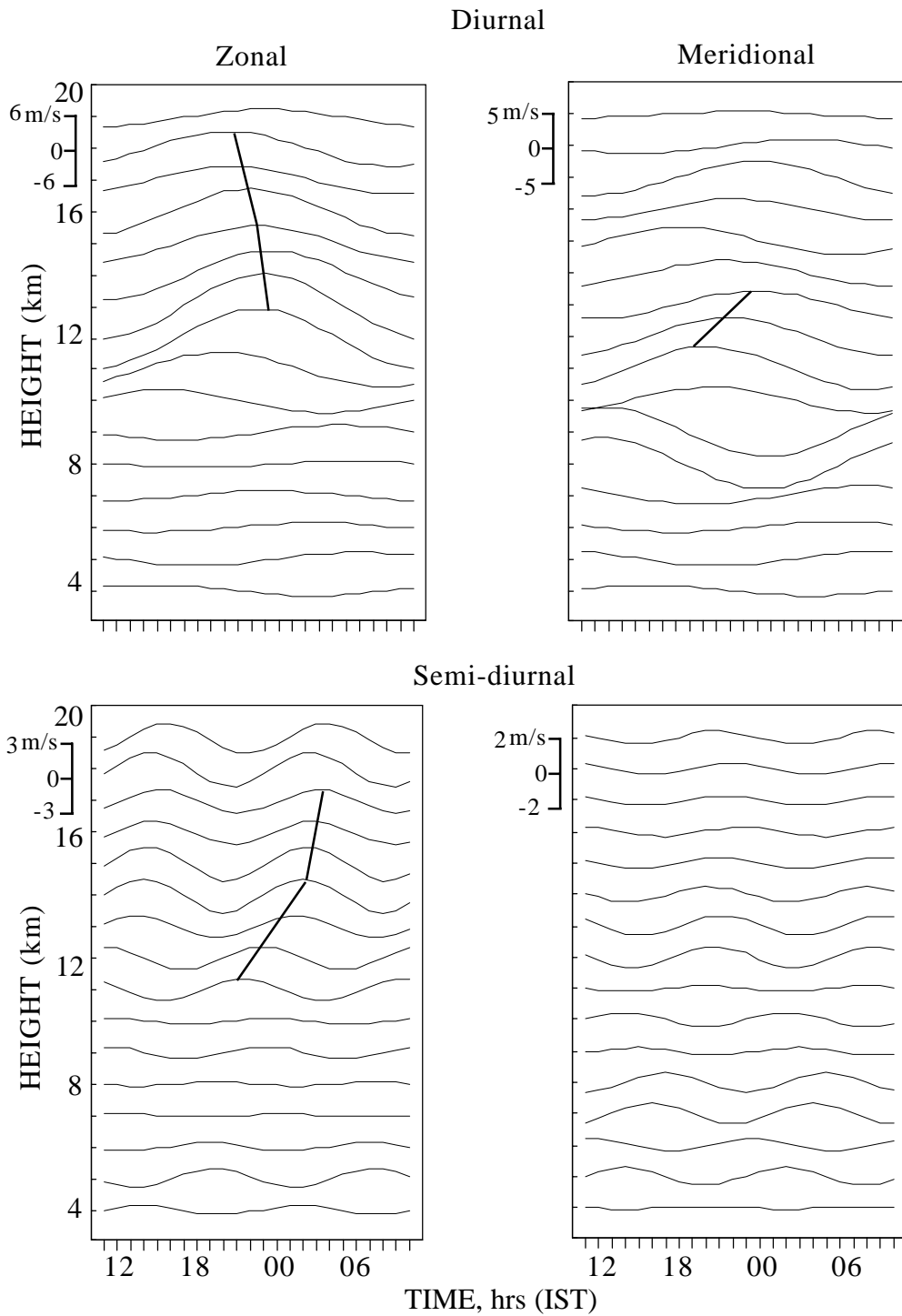
The temporal variation of diurnal and semidiurnal components in the zonal and meridional winds on 6-7 August 1996 (monsoon) is shown in Figure 3.13. The amplitude of the diurnal component ranges ±11ms^{-1} in zonal wind and ± 4 ms^{-1} in meridional wind. While it ranges ± 4 ms^{-1} for both the winds for semidiurnal component. Phase reversals are observed between 16 km and 20 km for semidiurnal in both the wind oscillation. Figure 3.14 shows that the observed diurnal amplitudes during 6-7 August are not increasing monotonically with height. In the zonal component diurnal amplitude attain significantly high value of ~ 9 to 11 ms^{-1} at ~ 16 km, which is lager compare to any other seasons. The diurnal amplitudes of meridional component fluctuate with height creating a complex height structure and also attain larger value at ~ 16 km. The height profile of phase for zonal winds shows that the phase is constant in the height region between 10 to 16 km and with down ward phase (upward energy) propagation between 7 and 9 km. This again (previously observed on 16-17 Jan.(Fig.3.6) and on 22-23 July (Fig.3.12)) indicates the standing wave pattern between upward and downward propagating waves above 8 km and upward propagating from the ground source below 8 km.

10-11 June 1996

Zonal

Meridional

Amplitude (m/s)

Phase (degree)

Height (km)

Fig. 3.10 : Amplitude and phase profiles of diurnal oscillations in the zonal and meridional winds at Gadanki.

Fig.3.11: Temporal variation of harmonic components(diurnal and semidiurnal) of the tidal oscillations observed in the zonal and meridional winds.

22-23 July 1997

Zonal

Meridional

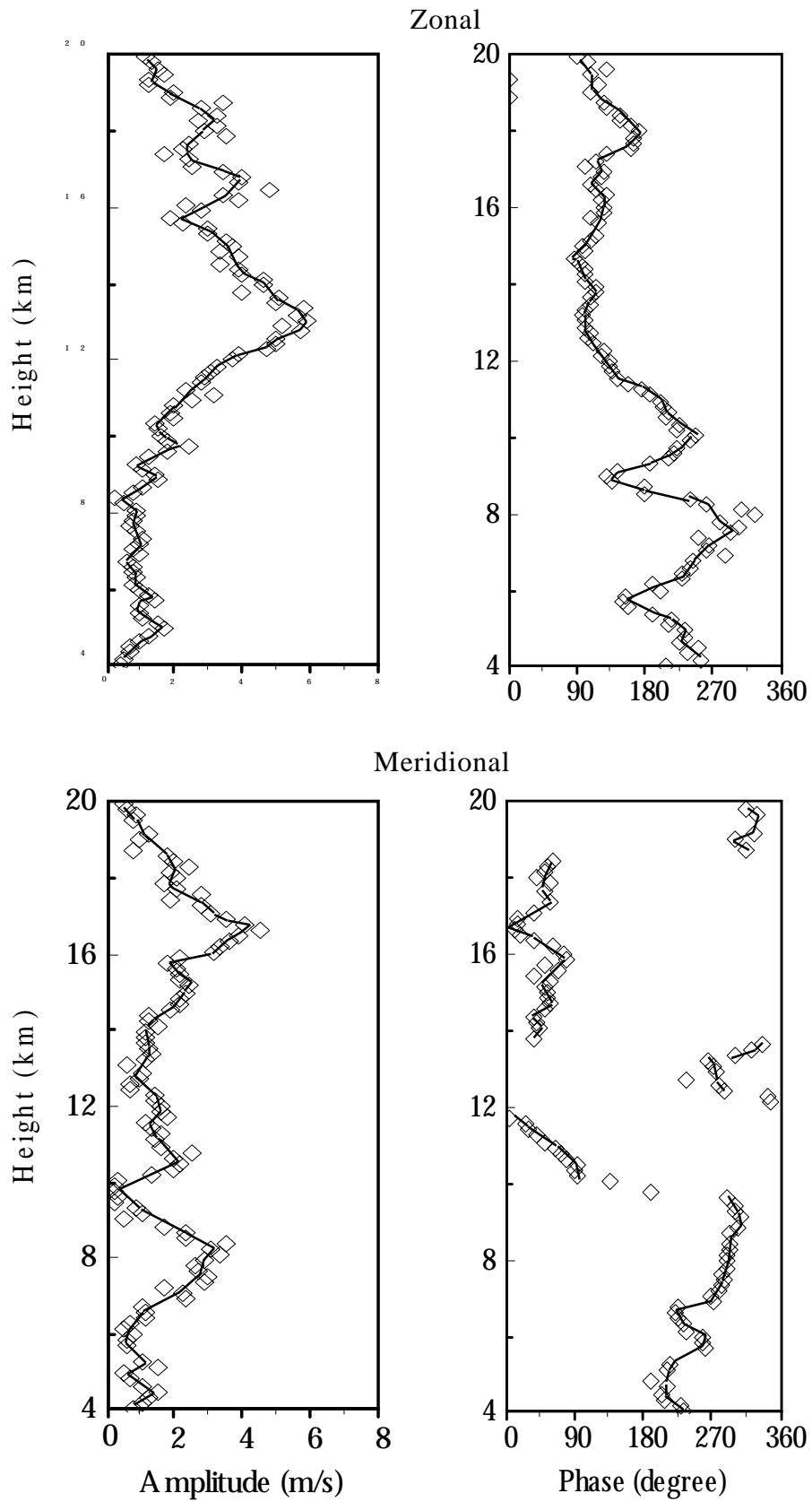**Fig. 3.12 :** Amplitude and phase profiles of diurnal oscillations in the zonal and meridional winds at Gadanki.
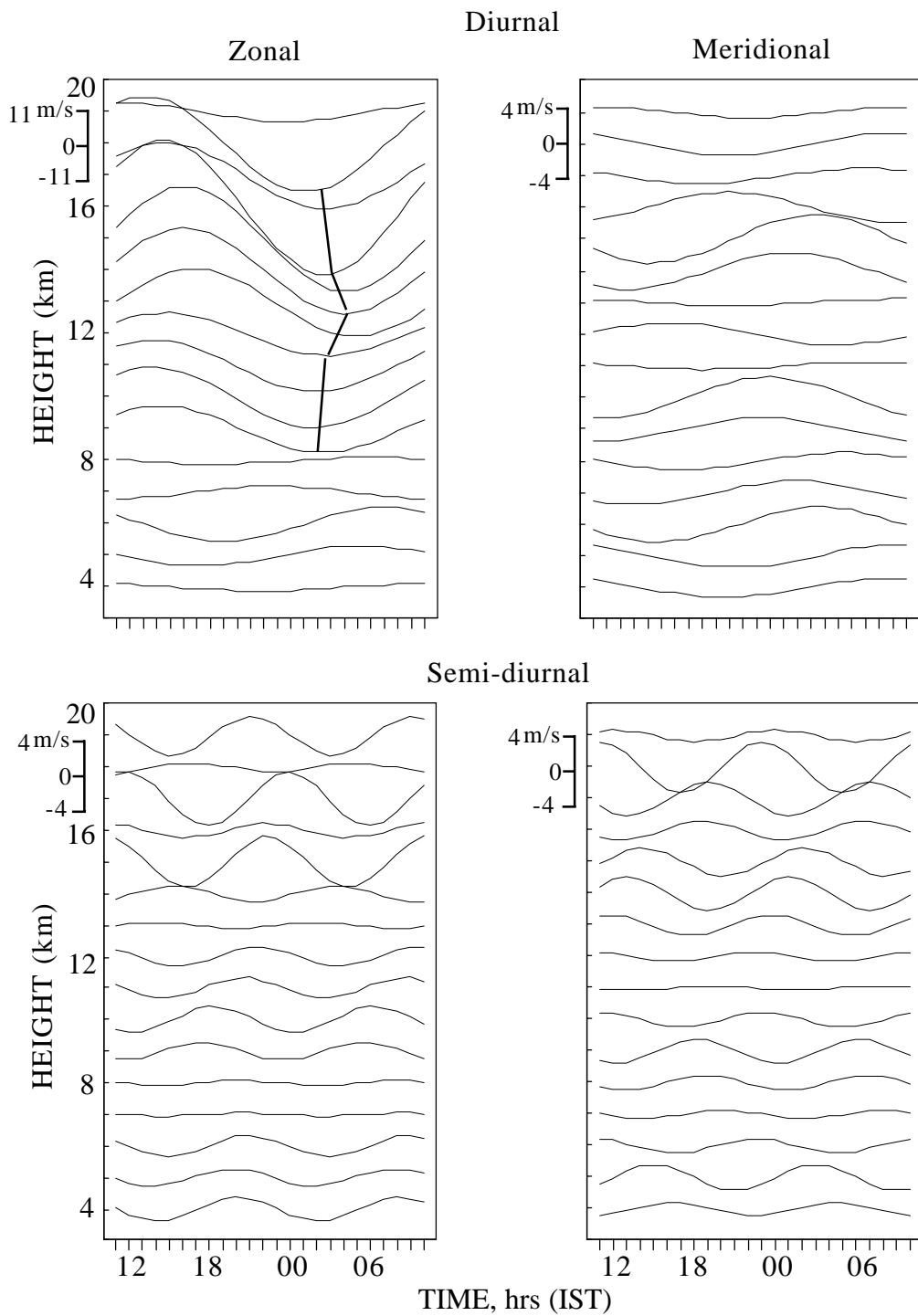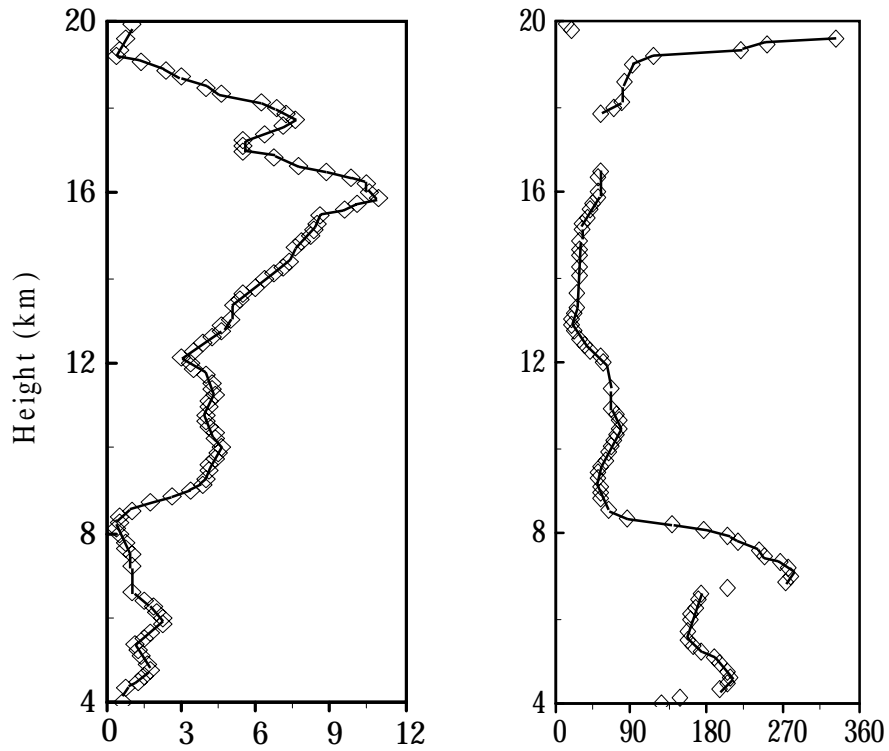
Fig.3.13: Temporal variation of harmonic components(diurnal and semidiurnal) of the tidal oscillations observed in the zonal and meridional winds.
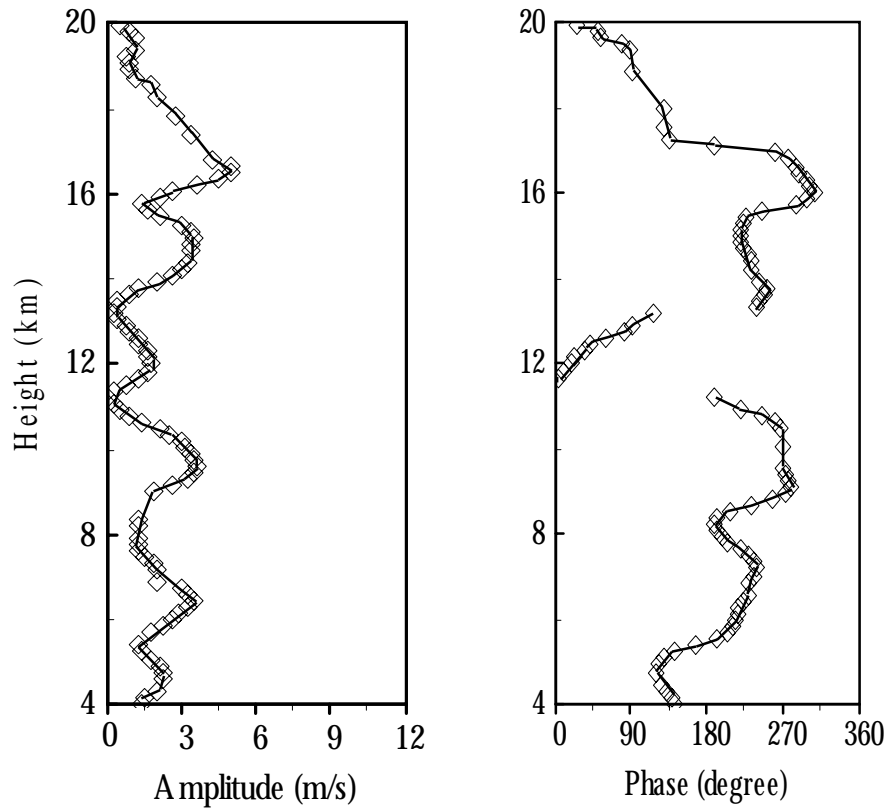
6-7 August1996

Zonal

Meridional
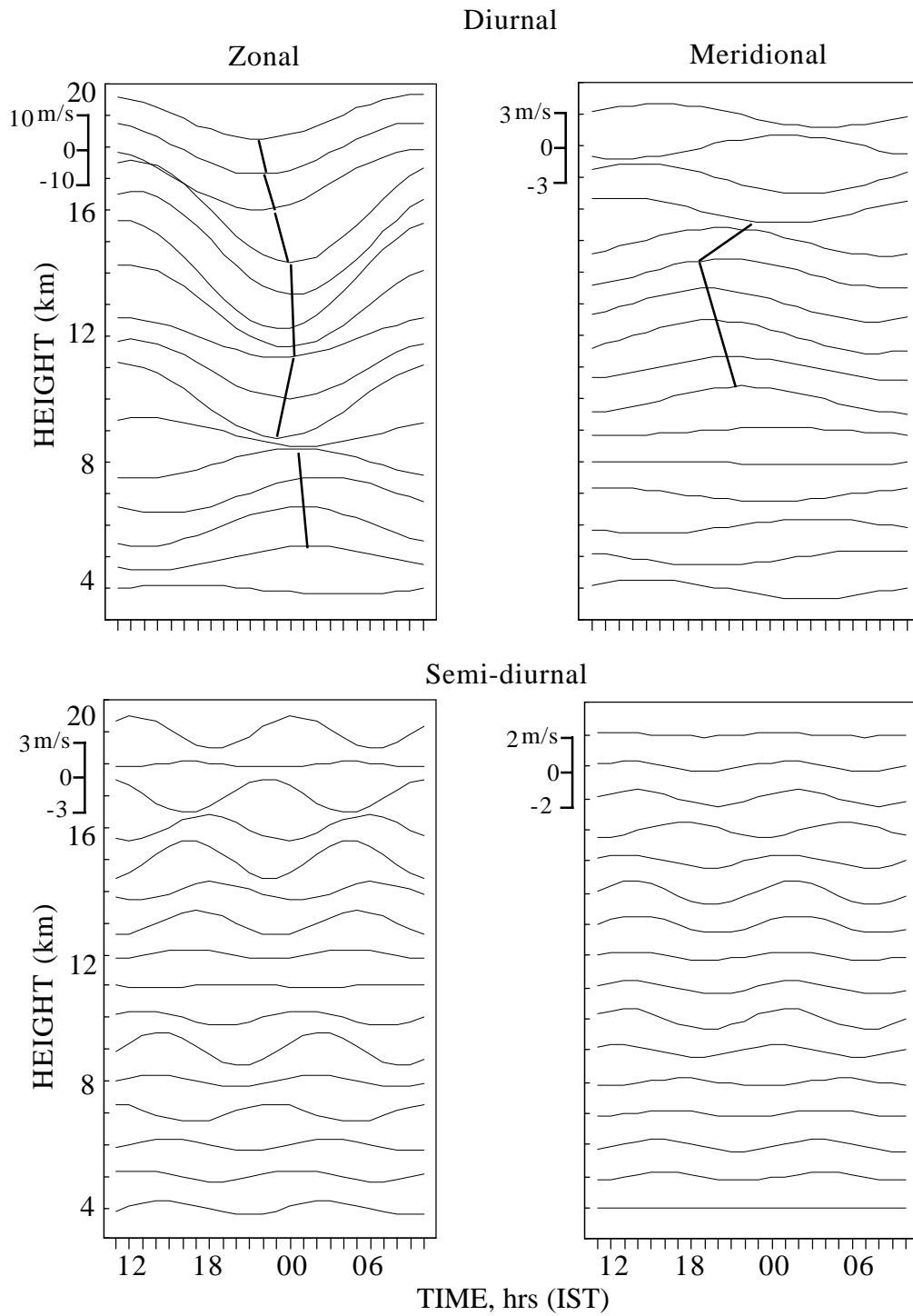

Amplitude (m/s)

Phase (degree)

Fig. 3.14 : Amplitude and phase profiles of diurnal oscillations in the zonal and meridional winds at Gadanki.

The fluctuations in the amplitude profiles due to interference between weak migrating tides and strong non-migrating tides with characteristic wavelength of 2-4 km of non-migrating tides is very clear in the meridional component. Furthermore the peak at about 16 km in the phase profile in zonal wind with upward (downward) energy propagation above (below) 16 km is a clear indication of a source of tidal energy at about 16 km. Probably associated with deep convective activity and latent heat release from cloud tops at that altitude in the monsoon season (Williams and Avery, 1996).

Figure 3.15 shows temporal variation of diurnal and semidiurnal components in the zonal and meridional winds on 3-4 September 1996 (monsoon) derived from the harmonic analysis. The amplitude of the diurnal component ranges ± 10 ms^{-1} and ± 3 ms^{-1} for semidiurnal component in the zonal wind. While it ranges ± 3 ms^{-1} for diurnal and ± 2 ms^{-1} for semidiurnal component in the meridional wind. Phase reversals are observed at ~ 9 km for diurnal component and between 16 km and 20 km for semidiurnal in the zonal wind oscillation. For meridional wind phase reversal are seen at ~ 7 km for diurnal component and between 15 and 18 km for semidiurnal component. The amplitude and phases of the diurnal component in zonal and meridional winds observed during 3-4 September is shown in figure 3.16. The diurnal oscillations attains large value of ~ 8-9 ms^{-1} between 14-17 km in the zonal wind. In meridional wind amplitude of diurnal component is very less (2-3 ms^{-1}) compare to zonal wind and small peaks are seen at different heights. The vertical separation between these two peaks and rate of phase propagation at that particular region (10 to 14 km) again suggest the vertical wavelength is ~ 4 km above 10 km. The phase is more or less steady for diurnal component in the zonal wind while it fluctuating below 8 km and show downward phase propagation between 15 and 20 km for diurnal component in the meridional wind. The downward phase progression with height indicates upward energy propagation.

Figure 3.17 shows temporal variation of diurnal and semidiurnal components of the zonal and meridional winds observed during 13-14 September1995 (monsoon) derived from the harmonic analysis. The amplitude of the the diurnal component ranges ± 4 ms^{-1} and for semidiurnal component it ranges ± 2 ms^{-1} in the zonal wind. While it ranges $\pm 2-3$ ms^{-1} for diurnal and semidiurnal component in the meridional wind. Phase reversal is observed at ~12 km for diurnal component and between 6 and 10 km for semidiurnal component in the zonal wind. For meridional wind phase reversal is seen at ~ 14 km for diurnal component. Figure 3.18 shows the amplitude and phase of diurnal oscillation in the zonal and meridional winds observed during 13-14 September. The diurnal amplitude of both zonal and meridional wind components fluctuates with height. Small scale vertical (~ 3 to 4 km) structures are observed in phase value for zonal winds between 4 to 12 km

3-4 September1996

Diurnal

Fig.3.15: Temporal variation of harmonic components(diurnal and semidiurnal) of the tidal oscillations observed in the zonal and meridional winds.

3-4 September1996
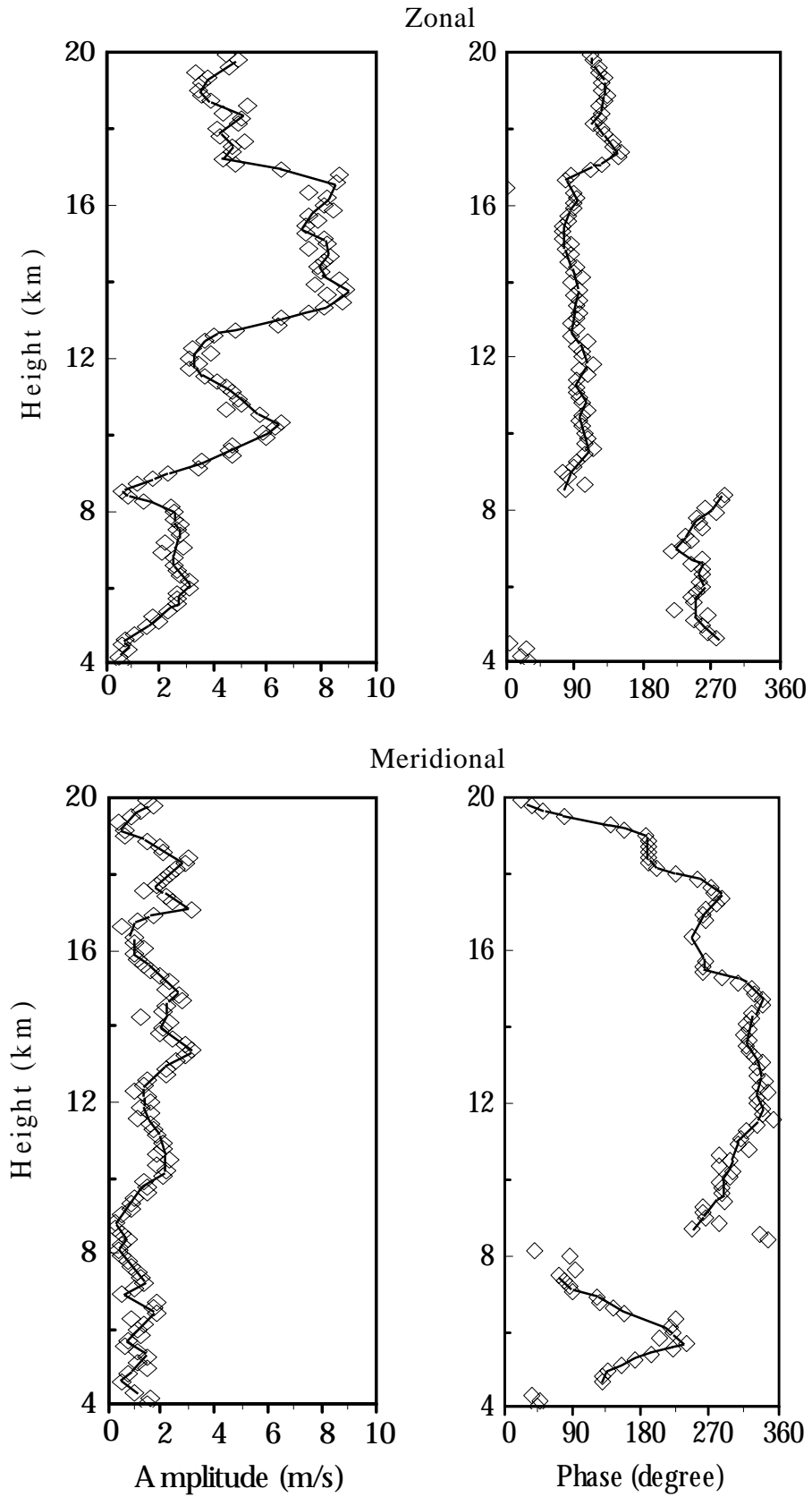
Zonal

Meridional

Fig. 3.16 : Amplitude and phase profiles of diurnal oscillations
in the zonal and meridional winds at Gadanki.

13-14 September 1995

Diurnal
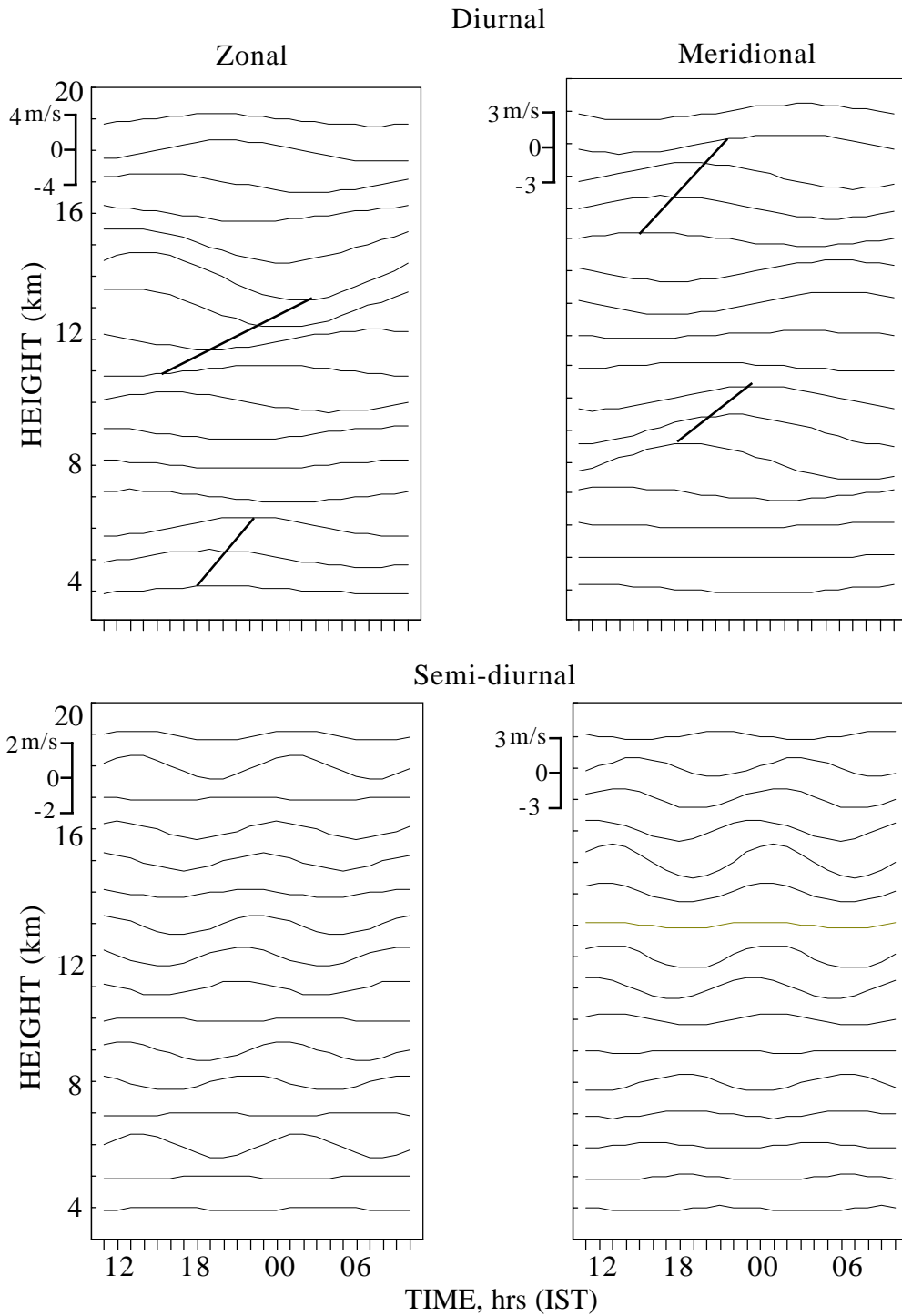

Semi-diurnal

TIME, hrs (IST)
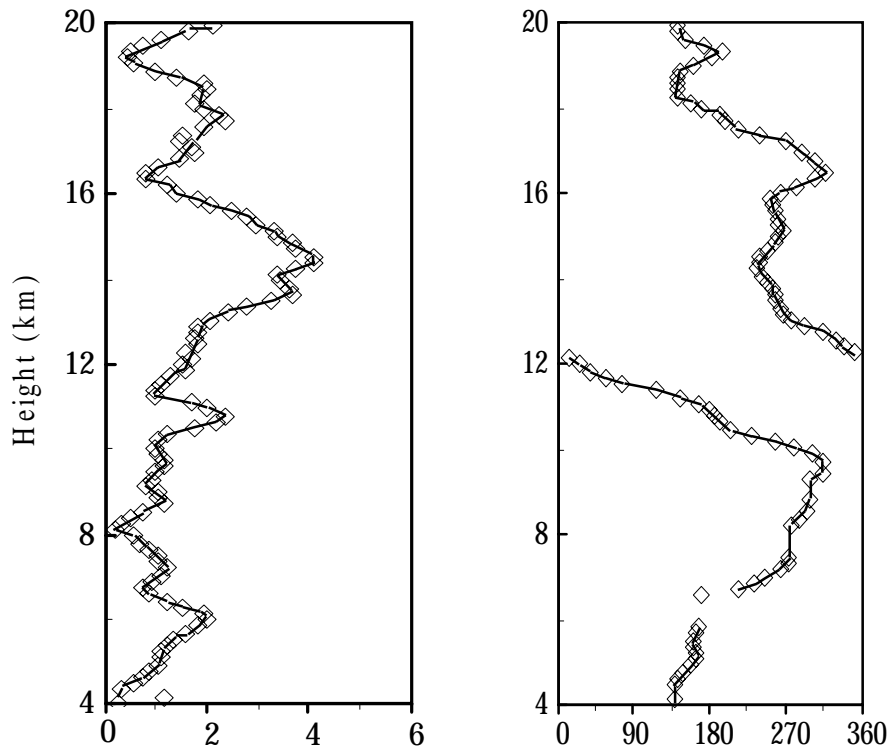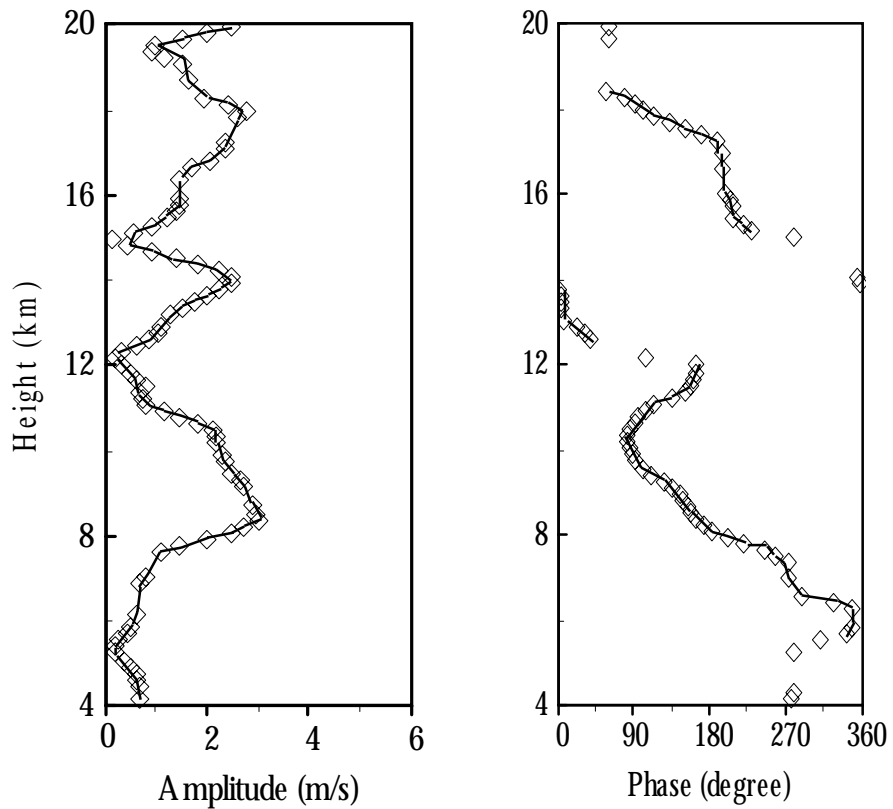
Fig.3.17: Temporal variation of harmonic components(diurnal and semidiurnal) of the tidal oscillations observed in the zonal and meridional winds.

13-14 September1995

Zonal

Meridional

Amplitude (m/s)　　　　　Phase (degree)

Fig. 3.18 : Amplitude and phase profiles of diurnal oscillations
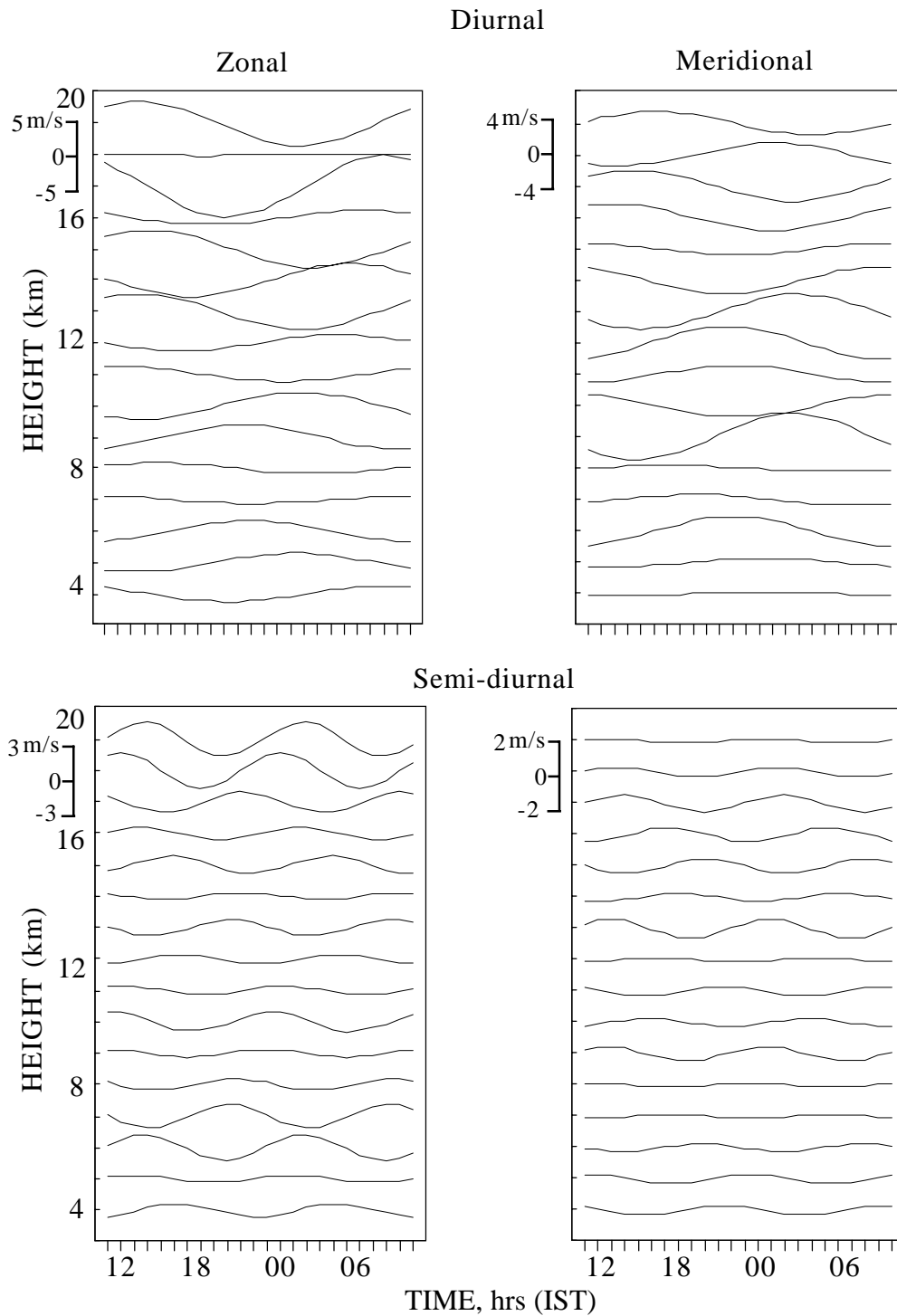in the zonal and meridional winds at Gadanki.

height region and, similar small scale vertical (~ 2 to 3 km) structures are clearly visible in the amplitude profile also in the same height region.

There is upward phase progression between 4 and 10 km in the zonal wind suggest down ward energy propagation and above 10 km down ward phase progression suggest upward energy propagation. A clear downward phase progression is seen in meridional wind from lower troposphere (i.e. at ~ 6 km) to upper troposphere (i.e. at ~ 16 Km) and is indecative of upward energy propagation. These height structures of amplitudes and phases suggest that they are probably produced by the interference of weak global migrating diurnal tidal modes and the locally generated strong non-migrating tidal modes.

Figure 3.19 shows temporal variation of diurnal and semidiurnal components in the zonal and meridional winds observed on 18-19 September1996 (monsoon) derived from the harmonic analysis. The amplitude of the the diurnal component ranges ± 5 ms^{-1} and for semidiurnal component it ranges ± 3 ms^{-1} in the zonal wind. While it ranges ± 4 ms^{-1} for diurnal and ± 2 ms^{-1} semidiurnal component in the merdidional wind. Phase progression for diurnal component in the zonal and meridional winds shows random propagation with altitude above ~ 10 km. The amplitude and phases of the diurnal oscillation in zonal and meridional winds observed during 18-19 September 1996 is shown in Figure 3.20. The diurnal amplitudes of zonal and meridional winds fluctuate with height creating a complex height structure. The observed phase value for zonal winds shows the small vertical scale (~ 2 to 3 km) structures below 12 km height region. There is a similar small scale vertical (~ 2 to 3 km) structure in the amplitude profile in the meridional wind also for same height region. The vertical separation between amplitude peaks again shows vertical wavelength is ~ 2-3 km in below 10 km and 3-4 km above 10 km in the meridional wind. Again a clear down phase propagation is seen between 10 and 16 km for the meridional wind oscialltion. The downward phase progression with height indicates upward energy propagation. Wallace and Tadd (1974) suggested that these type of oscillations are representative of tidal winds and they are excited either at ground or in the boundary layer.

Figures 3.21 and 3.22 shows temporal variation of diurnal and semidiurnal components in the zonal and meridional winds on 3-4 October1996 and 31October 1November 1996 (equniox). The amplitude of the the diurnal component ranges ± 6 ms^{-1} and for semidiurnal component it ranges ± 4 ms^{-1} in the zonal wind on 3-4 October. Phase reversal is seen at ~ 13 km for diurnal component in the zonal wind. On 31October 1November the amplitudes of the the diurnal component ranges ± 4 ms^{-1} and for semidiurnal component it ranges ± 3 ms^{-1} in the zonal wind. While it ranges ± 5 ms^{-1} for diurnal and ± 2 ms^{-1} semidiurnal component in the merdidional wind.

Fig.3.19: Temporal variation of harmonic components(diurnal and semidiurnal) of the tidal oscillations observed in the zonal and meridional winds.

18-19 September 1996

Zonal

Meridional

Amplitude (m/s)   Phase (degree)

Fig. 3.20 : Amplitude and phase profiles of diurnal oscillations in the zonal and meridional winds at Gadanki.

3-4 October1996
Diurnal

Fig.3.21: Temporal variation of harmonic components(diurnal and semidiurnal) of the tidal oscillations observed in the zonal and meridional winds.

31October-1November1996
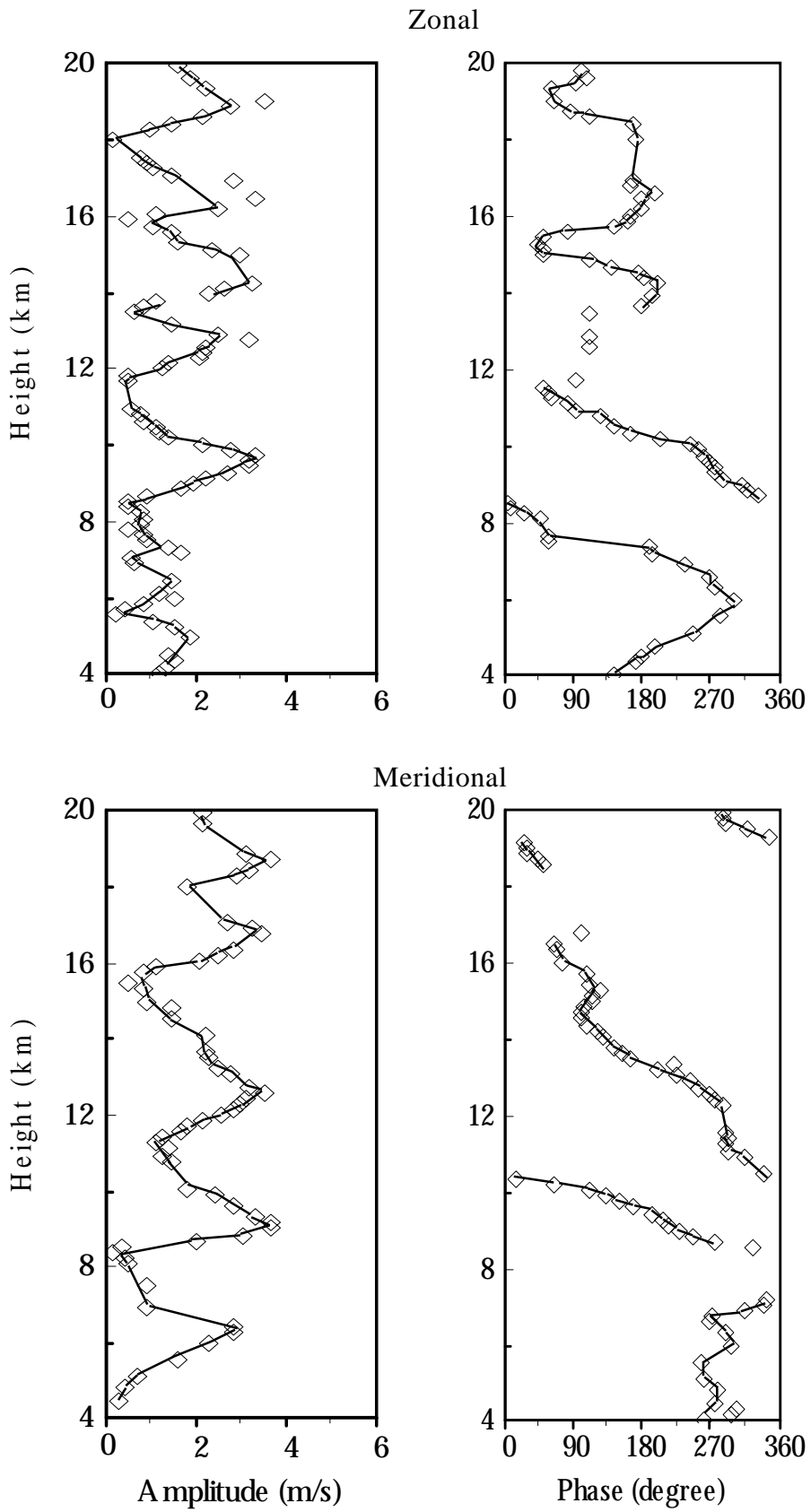
Diurnal

Fig.3.22: Temporal variation of harmonic components(diurnal and semidiurnal) of the tidal oscillations observed in the zonal and meridional winds.
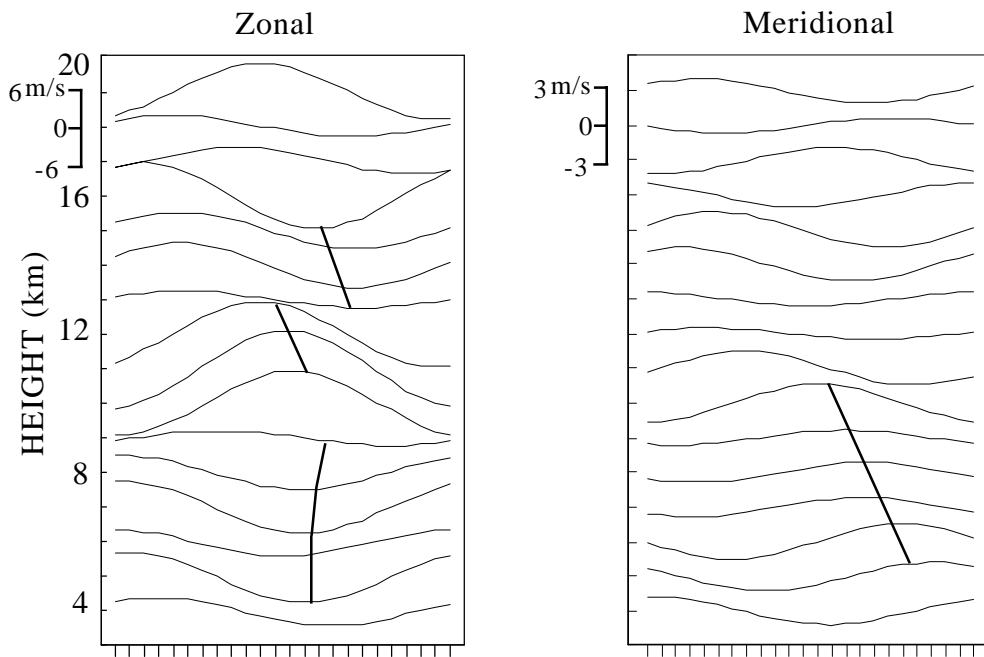
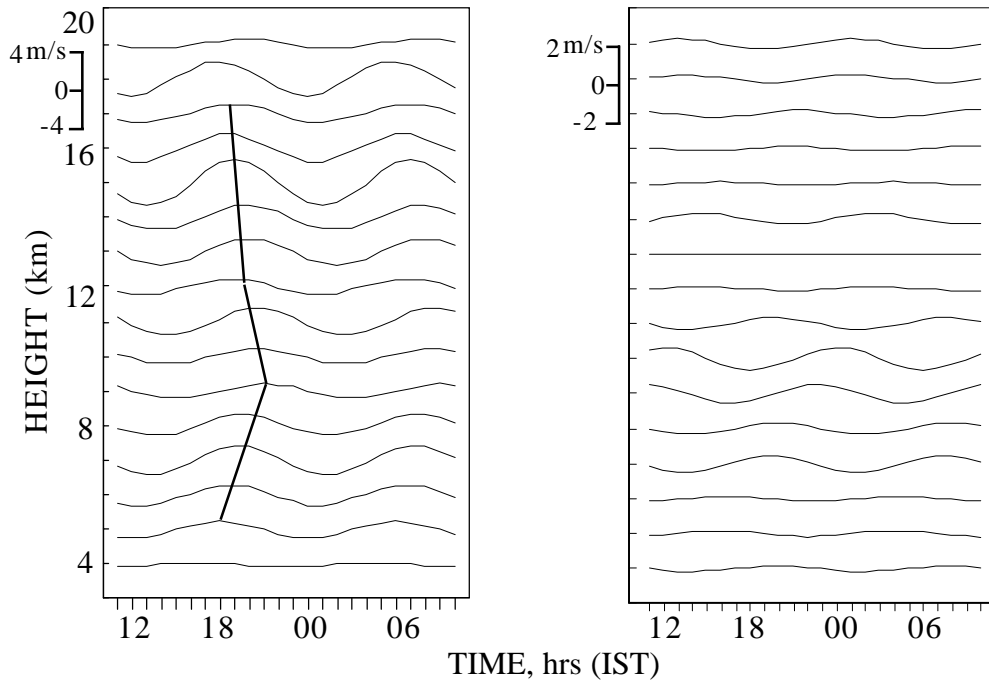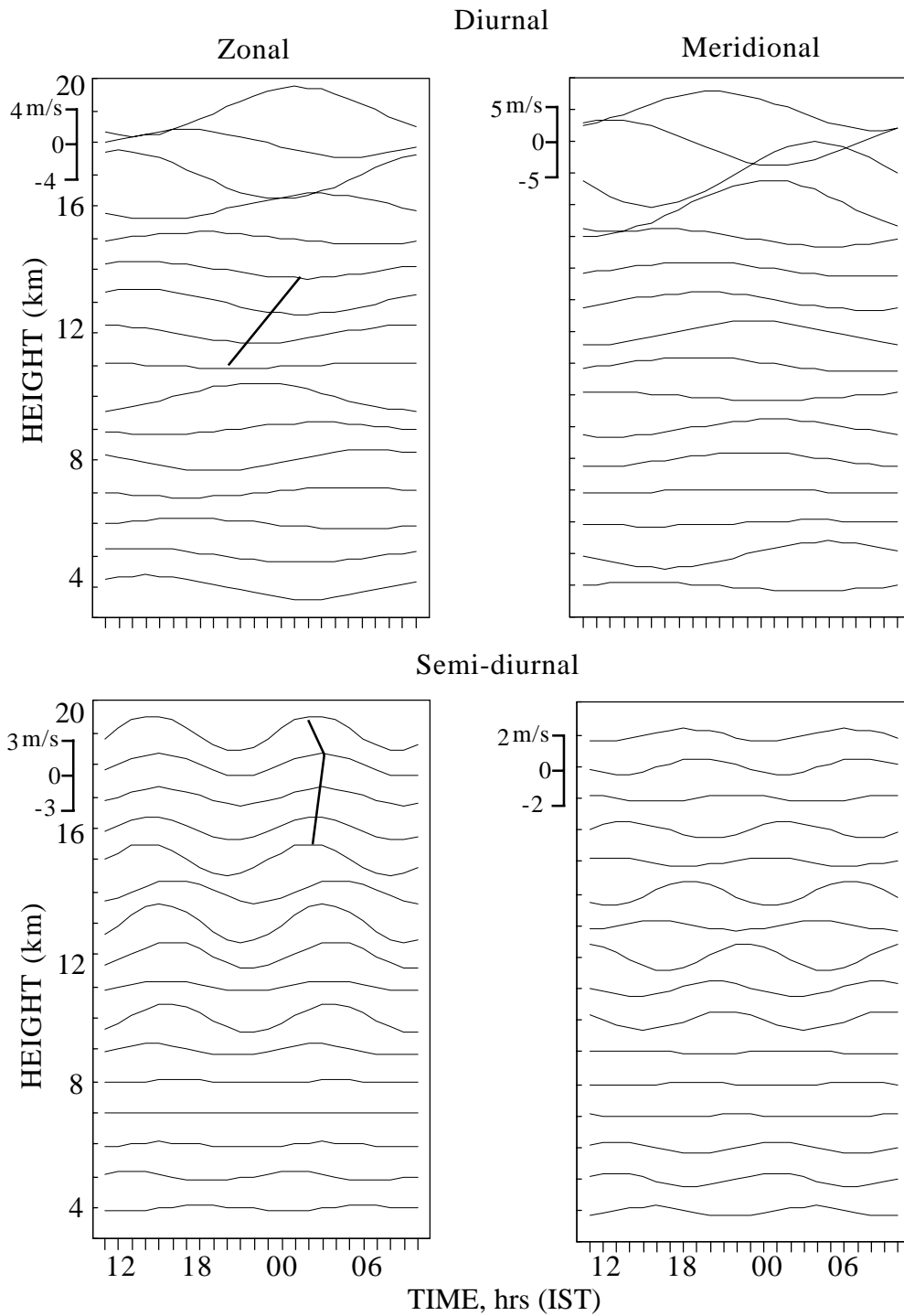Phase reversal are seen at ~ 11 km and ~17 km for diurnal component in the zonal wind and at 18 km for diurnal component and between 12 and 16 km for semidiurnal component in the meridional wind.
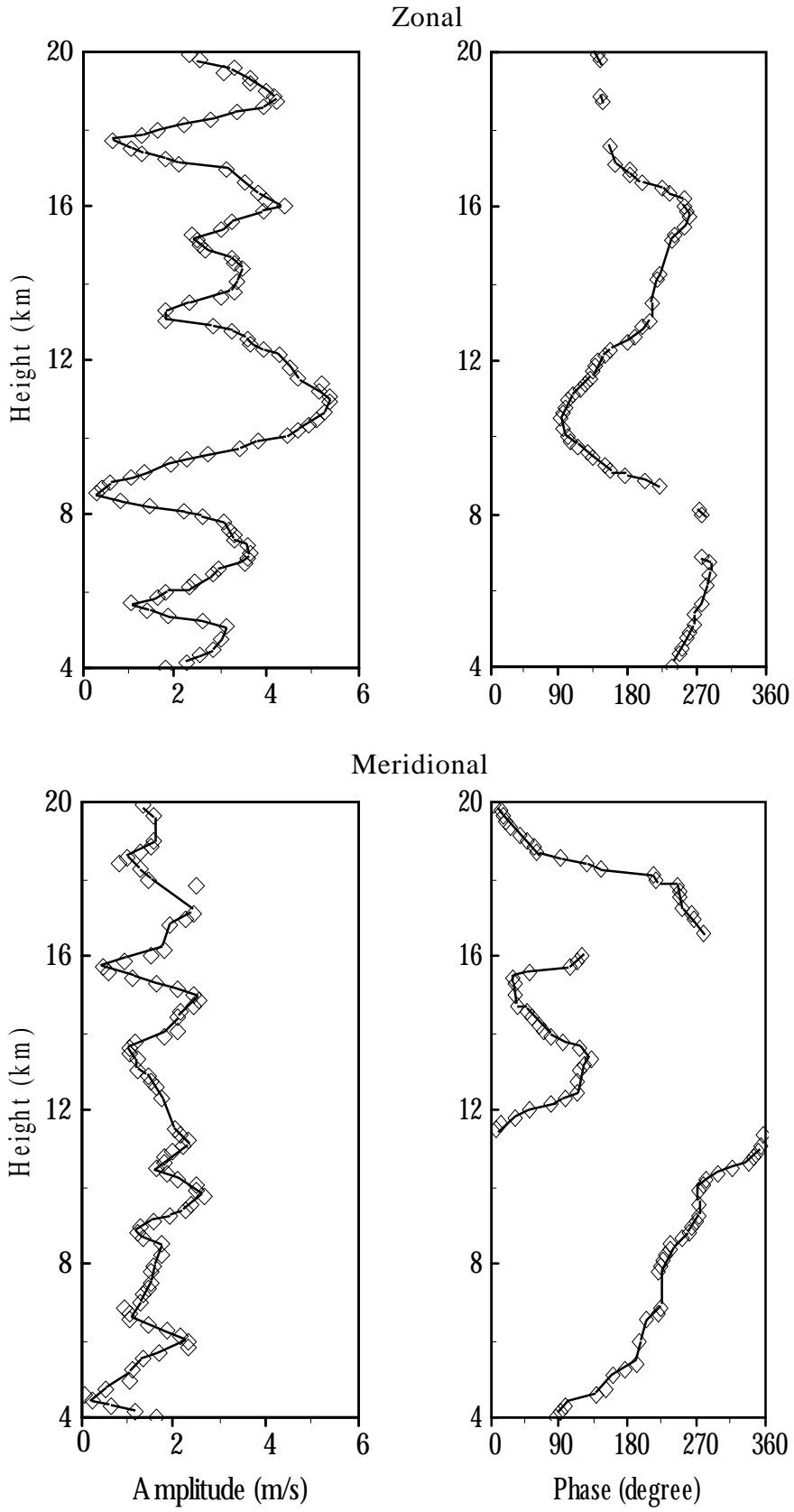
The amplitude and phases of the diurnal oscillation in zonal and meridional winds observed during 3-4 October1996 is shown in Figure 3.23. It is seen from Figure 3.23 that the diurnal amplitudes of zonal wind fluctuate with height and attain large value (5-6 ms^{-1}) at ~ 11 km, while atmplitude is very less in meridional wind oscillation (2-3 ms^{-1}). The phase is fluctuating with height for the zonal wind. While it shows upward phase propagation between 4 and 10 km and it fluctuates between 12 and 15 km and shows downward phase progression between 16 and 20 km in the meridional wind.

Figure 3.24 shows the height profile stcture of the amplitudes and phases for zonal and meridional winds observed on 31October 1November 1996 derived from the harmonic analysis. The amplitude attains large value of 6 ms^{-1} at ~ 17 km in both the winds. The downward phase progrssion is seen between 15 and 20 km for both the wind oscillations, it suggests upward energy proapagation in the lower stratosphere.

The results shown in previous diagrams (height profiles of amplitudes and phases) clearly indicate diurnal tidal propagation characteristics with amplitude 2-3 ms^{-1} and vertical wavelength of ~ 3 km below 10 km and with ampltidue 5-6 ms^{-1} and vertical wavelength ~ 5 km above 10 km. To investigate the vertical propagation of the tidal oscillations further, hodographs of the tidal perturbation velocity (horizontal) were constructed using the time series of zonal and meridional components obtained from the tidal amplitudes and phases at different heights. Such hodographs are shown in Figure 3.25 (for different days) for two height regions at the local times shown therein. It is seen that the perturbation wind vector rotates clock wise with height, indicating upward energy propagation. It again shows the dominance of short vertical wavelength at lower region and larger vertical wavelength at upper height region.

The perturbation wind vector rotates anti-clock wise with height on 3-4 October 1996 (Fig.3.26) and is indicative of down-ward energy propagation. The vertical wavelength inferred from the hodographs are ~ 3 to 4 km and ~ 5 to 7 km for lower and upper height regions, respectively. These values are somewhat consistent with those calculated from the successive amplitude maxima/ minima and rate of phase propagation in different height regions and also consistent with previously observed by Sasi et al.,(1998) for equinox season using Indian MST radar. Observed diurnal tidal amplitudes are, in general larger than predicated by the theoretical values (Forbes and Gillette, 1982). The theoretical vertical wavelength for dominant migrating diurnal tide is 25-30 km, whereas the observed ones inferred from the phase profiles are much shorter with values 3-6 km.

3-4 October 1996

Zonal

Meridional

Amplitude (m/s)

Phase (degree)

Fig. 3.23 : Amplitude and phase profiles of diurnal oscillations
in the zonal and meridional winds at Gadanki.

31October 1November1996
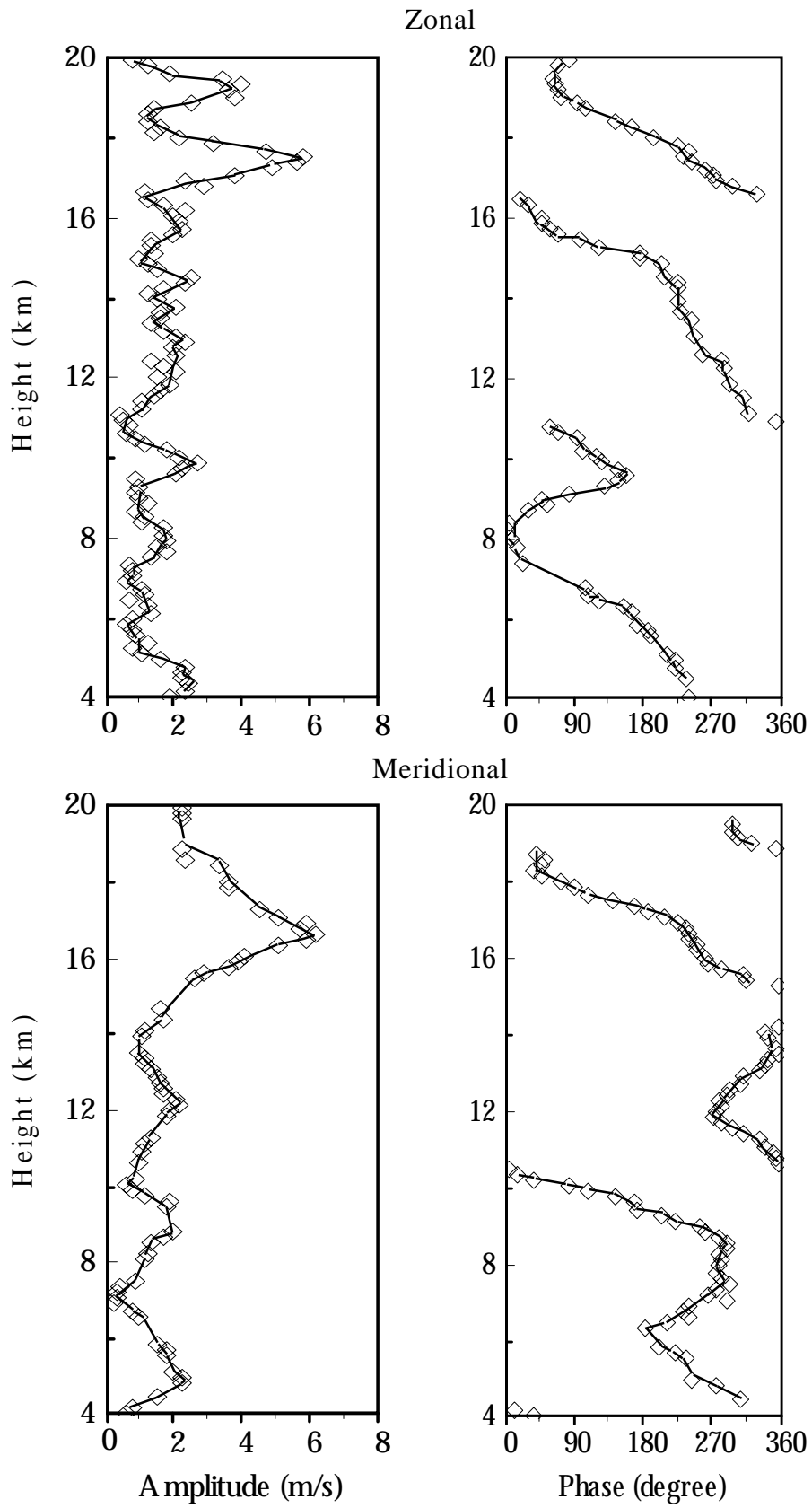
Zonal

Meridional

Amplitude (m/s)

Phase (degree)

Fig. 3.24 : Amplitude and phase profiles of diurnal oscillations in the zonal and meridional winds at Gadanki.

(a)

(b)

(c)

(d)
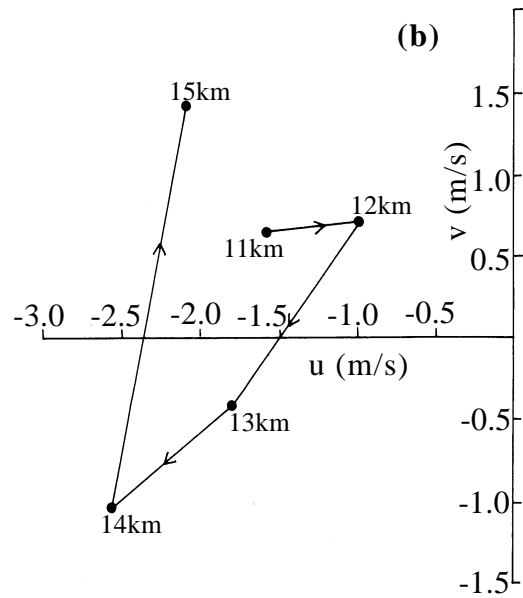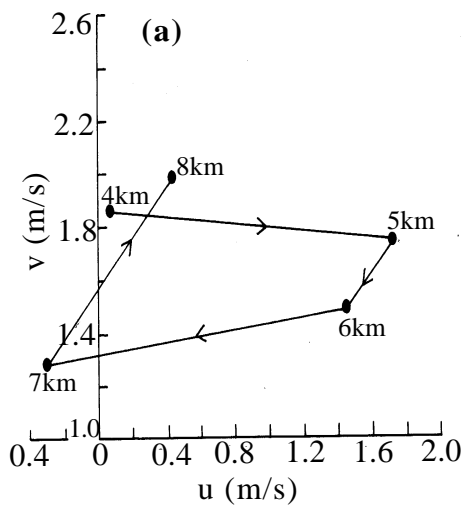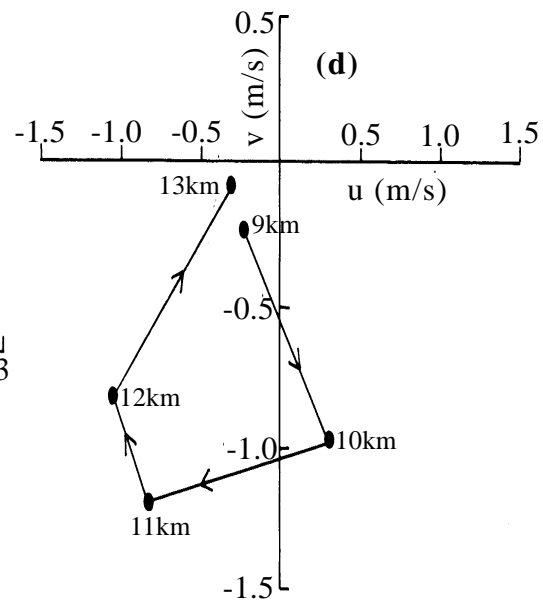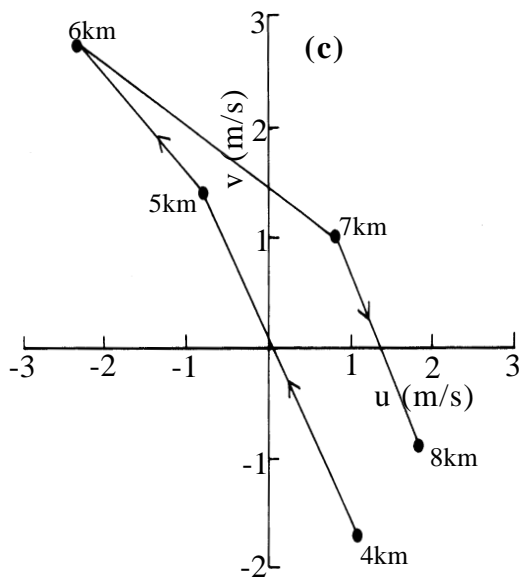
Fig.3.25 : Hodographs of diurnal winds for selected times (0500 and 2200 hours LT) at height from ~ 4 to ~ 20 km. (The direction of rotation with increasing height is shown by arrows; (a) and (b) at 0500 hrs LT and (c) and (d) at 2200 hrs LT).

(a)

(b)
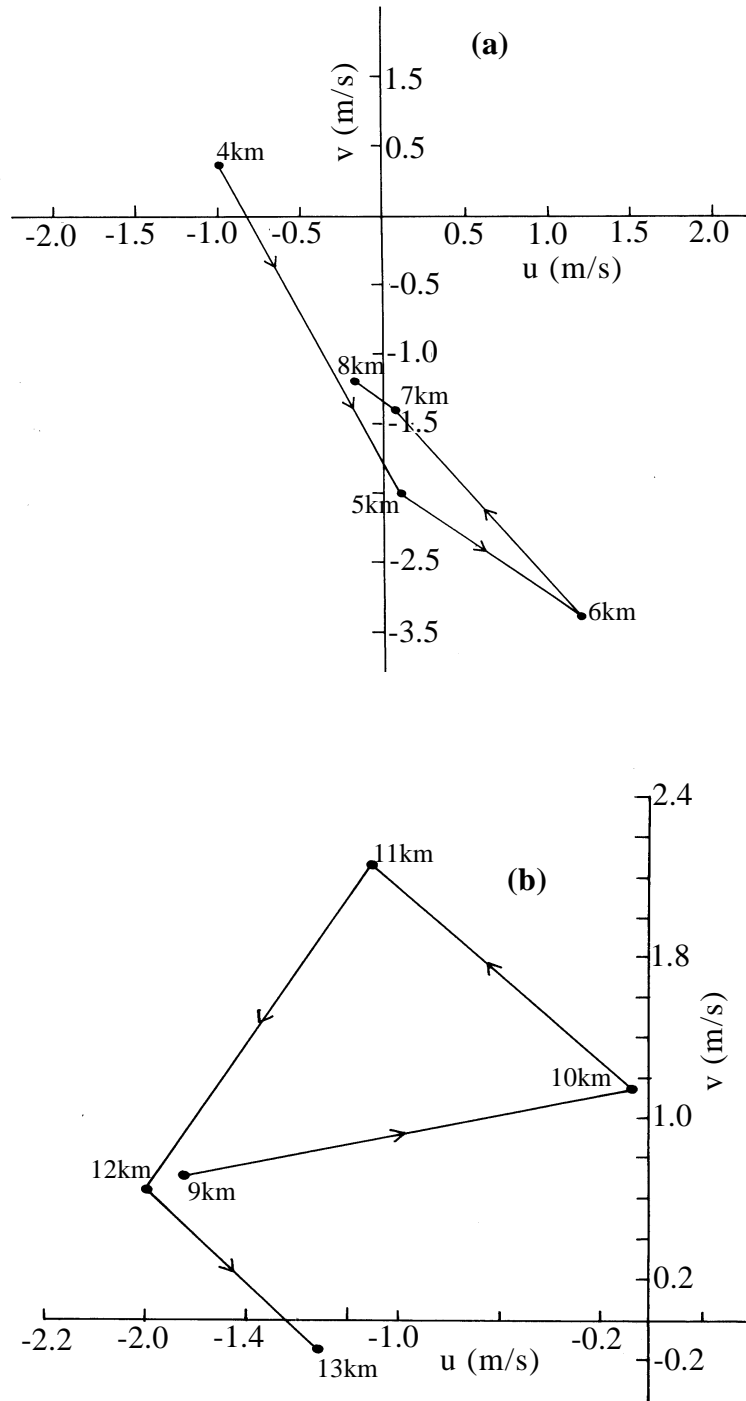
Fig.3.26 : Hodographs of diurnal winds for time 0500 hours LT
(The direction of rotation with increasing height
is shown by arrows; (a) 4-8 km (b) 9-13 km).

The numerical simulation of non-migrating diurnal tides by Tsuda and Kato (1989) shows that similar large diurnal wind amplitudes and short vertical wavelengths can be expected in the tropical troposphere and lower stratosphere which are produced by diurnally varying upward heat fluxes in the planetary boundary layer (PBL) over land. The present observations at Gadanki are also consistent with radar observations of diurnal tidal characteristics at Arecibo (Fukao et al., 1980). Thus the observed diurnal tidal oscillation at Gadanki can be mainly due to the dominance of non-migrating tides.

It is often found from the height profiles of amplitude that the amplitude attain significantly high value near tropopause (i.e. between 14-17 km) for all the seasons in zonal wind and meridional winds. It is now known that air ascends from the upper troposphere into the stratosphere at very low latitudes and returns from the stratosphere to the troposphere at high and middle latitudes. If such a circulation of air does take place, then air in the stratosphere would all have to pass though the very cold region at the top of the troposphere near the equator. While passing through this very cold region, with a temperature of about -80°C, most of the water vapour would condense and may form the extensive layers of thin cirro-stratus and which is one of the source of energy from where energy may propagate upward or downward.

If energy propagate downward then there will be a possibility of mixing of this energy with energy propagating upward from ground level and cause a turbulence like structure between the height region about 14 to17 km and gives maximum amplitude. Williams and Avery (1996) have suggested a probable source near 14 km where the largest meridional wind amplitude is observed and the phase appears constant with altitude. A very similar amplitude and phase structure of meridional winds is seen over Gandanki during 16-17 January and 31January 1February 1996 (Figs.3.3 and 3.4). Williams and Avery (1996) also suggested the solar radiative heating of cloud tops and thin cirrus clouds distributed by deep convection in the tropics as a possible source. In the equatorial region, non-migrating tides seem to be dominant in the troposphere, but are unable to propagate deeply into the stratosphere, unless they are excited by an elevated source such as identified in this work.

However further height coverage incorporating the colocated LIDAR observations and a method of experimentally identifying the elevated source (satellite cloud imaeges for example) would be needed to confirm this point. The forcing for the diurnal tide is provided by a global distribution of solar insolation heating, latent heating, dry convection heating and eddy conduction heating obtained from the Kyushu University general circulation model (Miyahara et al., 1993). Their results for low latitudes show small amplitude (i.e < 1 ms^{-1}) at upper troposphere and lower stratosphere altitudes and vertical wavelength of 7-10 km.

In many numerical studies of the non-migrating diurnal tides it is found that the numerical models, though taking into account significant tidal heat sources such as solar heating, sensible heating in the planetary boundary layer (PBL), and tropospheric latent heat release, are unable to account for all the observed features of diurnal tides (e.g., Lieberman and Leovy, 1995; Ekanayake et al., 1997). The heating rates due to diurnal heating of water vapour and latent heat release of convective clouds extended throughtout the troposphere and will be mainly exciting tidal modes with longer vertical wavelength. Short vertical wavelength modes also be excited, but they will undergo destructive interference within the source region resulting in very small amplitudes. However, it is also probable that the short vetical wavelength in the lower troposphere are associated with the eddy heat flux in the PBL and long vertical wavelength in the upper troposphere associated with some other independent diurnal hear source located in that region. One possibility is the efficient generation of longer vertical wavelength modes by diurnal heating due to latent heat release in troposphere. It is known that vertical extent of this heat source is depper (~14km) in comparision with that in the PBL (Mapes, 1993; Williams, 1994).

3.6 SUMMARY AND CONCLUSIONS

The results of the analysis show that in different seasons the tropical region is dominated by diurnal tides with amplitudes varying from 2-3 ms^{-1}(at lower height) to 8-10 ms^{-1} (upper height) and vertical wavelengths from ~ 3 to 4 km in the lower troposphere and from ~ 5 to 7 km in the upper troposphere. Hodographs of diurnal tidal perturbation in horizontal velocity show that the perturbation wind vector rotates clockwise in the lower troposphere and upper troposphere though with different vertical wavelengths. This indicates the upward propagation of energy in both the height regions. The seasonal variation of amplitudes of the zonal and meridional winds are given in the tables - 2 and 3 respectively.

The comparison of amplitudes of the zonal wind (table-2) for different seasons (i.e. winter, summer, monsoon and equinox) shows that the amplitude peak (maxima) occure at different heights in different seasons and is often occur near tropause height (i.e at ~ 15-16 km). The amplitude values are somewhat similar in winter and summer (i.e. 3-5 ms^{-1}), while it increases significantly during monsoon (8-11 ms^{-1}), particularly very high value of ~ 11 ms^{-1} is observed on 6-7 August 1996 (Fig.3.14). This indicates that during monsoon the tidal activity is enhanced due to latent heat release at cloud top which is a possible source of energy, particularly, in tropics.

From the table-3 it is seen that the amplitude of the diurnal component in the meridional wind is very less compare to the amplitude of the diurnal component in the zonal wind (table-2).

Table -2 (ZONAL WIND)				
Sr. No	Diurnal cycle (zonal wind)	Season	Amplitue(max)	Altitude
1.	16-17 Jan.1996		5-6 ms^{-1}	~14 km
2.	31Jan.1Feb.1996	Winter	3-4 ms^{-1}	~15 km
3.	15-16 Feb.1996		7-8 ms^{-1}	~10 km
4.	10-11 June1996	Summer	3-4ms^{-1}	~18 km
5.	22-23 July1997		5-6 ms^{-1}	~13 km
6.	6-7 August1996		10-11ms^{-1}	~16 km
7.	3-4 Sept.1996	Monsoon	9-10 ms^{-1}	~14 km
8.	3-14 Sept.1995		3-4 ms^{-1}	~15 km
9.	18-19 Sept.1996		4-5 ms^{-1}	**
10.	3-4 Oct.1996	Equinox	5-6 ms^{-1}	~ 11 km
11.	31Oct.1Nov.1996		4-5ms^{-1}	~17 km
** multiple peaks at different heights				

The the amplitude peak (maxima) occure at different heights in different seasons and it occur near tropause height (i.e at ~ 15-16 km), particularly in winter. The multiple amplitude peaks are observed during monsoon and equinox. The amplitude values are varies from 2-3 ms^{-1} to 5-6 ms^{-1} in different seasons. The constant phase propagation in the height region of about at ~ 10-16 km in all season (particularly in meridional component in monsoon) suggests the possibility of two energy sources produce a stationary wave type of pattern, one may be at ground level and the other in the height range 14-17 km.

Possibility of a source at about 16 km altitude and energy propagating above and below this level is very clear in the case for monsoon season. Diurnal heating due to solar radiation absorption by cloud tops and cirrus clouds produced by the deep convection could also be responsible for the diurnal tidal oscillation in the upper troposphere in the tropics. Ramanathan et al.,(1995) and Cess et al., (1995) suggest that heating of clouds (cloud tops and/or cirrus clouds) in the upper troposphere by solar shortwave radiation is a potential source for the generation of non-migrating diurnal tides.

Table -3 (MERIDIONAL WIND)				
Sr. No	Diurnal cycle (meridional wind)	Season	Amplitue(max)	Altitude
1.	16-17 Jan.1996	*Winter*	5-6 ms^{-1}	~15 km
2.	31Jan.1Feb.1996		3-4 ms^{-1}	~16 km
3.	15-16 Feb.1996		3-4 ms^{-1}	~12 km
4.	10-11 June1996	*Summer*	3-4ms^{-1}	**
5.	22-23 July1997	*Monsoon*	4-5 ms^{-1}	##
6.	6-7 August1996		4-5ms^{-1}	***
7.	3-4 Sept.1996		2-3 ms^{-1}	***
8.	13-14 Sept.1995		3-4 ms^{-1}	***
9.	18-19 Sept.1996		3-4 ms^{-1}	***
10.	3-4 Oct.1996	*Equinox*	2-3ms^{-1}	***
11.	31Oct.1Nov.1996		5-6ms^{-1}	~16 km
** two peaks about at ~ 15 and ~19 km ## two peaks about at ~ 8 and ~17 km *** multiple peaks at different heights				

From the observation of persistence of subvisible cirrus clouds in the upper troposphere in the tropics for several days and zonal asymmetry of these clouds Jenson et al.,(1996) reinforce the idea that the heating of these clouds along with cloud tops could act as a diurnal heat sources for the generation of non-migrating diurnal tidal modes. Thus it may be concluded that during different seasons (i.e winter, summer monsoon, and equinox) the obseved non-migrating diurnal tides in the lower troposphere and upper troposphere over Gandanki (13.5^{o}N, 79.2^{o}E) are generated by the diurnally varying heat flux in the planetary boundary layer and by latent heat release in deep convective clouds. Hence, to extract significant difference from season to season more detailed study of seasonal variation is needed. Further detailed study of more diurnal cycles of each season with extended height coverage is also necessary , which leads to feature work.

CHAPTER - 4

STUDY OF MOMENTUM FLUX IN THE TROPOSPHERE AND LOWER STRATOSPHERE

4.1   INTRODUCTION

4.2   OBSERVATIONS AND NUMERICAL MODELS

4.3   DATA AND ANALYSIS

4.4   RESULT AND DISCUSSION

4.5   SUMMARY AND CONCLUSIONS

4.1 INTRODUCTION

It is generally regarded that atmospheric zonal motions are composed of a longitudinally averaged part (zonal mean) plus deviations from the average (perturbations) superimposed on the zonal mean. The divergence of momentum flux as well as heat flux associated with the perturbations are important sources for the mean zonal flow. These flows are parameterized as linear functions of the zonal mean, and implemented in a linear model for the zonal mean circulation. The divergence of momentum flux (or Reynolds stress) gives friction (acceleration or deceleration) to synoptic or planetary-scale atmospheric motions (Holton, 1972). Particularly important is the vertical convergence of the horizontal flux that causes the net acceleration of the general mean circulation. It has been suggested that internal gravity waves play an essential role in transporting momentum flux from the lower atmosphere upward into mesosphere (Lindzen,1981; Holton,1982; Matsuno,1982).

Topographically generated internal gravity waves can transport significant momentum vertically in the atmosphere. The nondissipative nature of internal gravity waves (Elisassen and Palm 1960) may allow the wave stress at the ground surface to be transferred far into the upper atmosphere where the density is small. Wave stress divergence associated with wave breaking acts as a drag on the mean flow at the wave braking level. The impact of gravity wave drag is known to especially important for large-scale motions on time scales longer than one week over continental areas during wintertime. Spectral analysis show that the mesoscale variances are climatologically much larger over mountainous areas than over flat land surfaces or the ocean, and the observed differences are mostly due to gravity wave activity in the atmosphere.

Momentum transfer by gravity waves can be locally important on smaller time scales above significant topography. In the upper troposphere and lower stratospheric region the vertical flux of horizontal momentum is generated primarily by the longer-period fluctuations. In this height range, the long-period momentum flux is due primarily to synoptic-scale or mesoscale disturbances, while the shorter period flux is due primarily to intense vertical air motion. For the lower stratosphere and troposphere, there have been many studies conducted which correlate high frequency motions with the presence of known gravity wave sources, including convection, fronts and orographic forcing. The frequency range of the gravity waves that can propagate upward should be fairly wide, because wave trapping is not significant owing to the low inertial frequency near the equator. Since gravity waves with small vertical scales can easily be saturated, they can effectively produce turbulence in the stratosphere and further act to enhance the eddy diffusion, which seems to have an important effect on the transportation of minor constituents in the equatorial middle atmosphere.

4.2 OBSERVATIONS AND NUMERICAL MODELS

The detailed structure of wind velocity and temperature fluctuation in the equatorial region was observed by means of high-resolution in situ measurements with balloons (Cadet and Teitelbaum,1979). Pfister et al.(1986) employed a stratospheric aircraft for observations of small-scale perturbations in the tropical region and further discussed their role in mixing of minor constituents. However, there was no direct method for the measurement of momentum flux until Vincent and Reid (1983) developed a method using Doppler radars. Direct measurements of wave momentum fluxes were performed over Adelaide, Australia(35°S), using a multiple beam configuration of an MF radar (Vincent and Reid 1983; Fritts and Vincent, 1987; Reid and Vincent, 1987). Fukao et al. (1988) measured momentum flux with three and four-beam methods and reported that the vertical transport of momentum is mainly by the longer-period fluctuations. Fritts et al. (1990) observed fluxes of u'w' $\gg$ -0.1 to -1.0 m^{2}s^{-2}, with a mean of -0.2 m^{2}s^{-2}, in the upper troposphere and lower stratosphere with the MU radar. A zonal drag of 1-2 ms^{-1}d^{-1} was also observed, which is sufficient to balance the momentum in large-scale models.

Representation of the wave breaking process in the frame of linear gravity wave theory plays a central role in the parameterization of gravity wave drag. Lindzen (1981) introduces the wave-stress saturation hypothesis assuming that the maximum amplitude of a gravity wave is limited by the onset of hydrodynamic instability. This wave stress saturation condition has been successfully employed in large-scale modeling studies . However, Smith (1987) and Lindzen (1988) suggest that some degree of convective instability can be maintained in wave breaking regions. Theoretical and observational studies have emphasized that upward propagating gravity waves carry energy and momentum flux from lower atmosphere to middle atmosphere and play an important role in maintaining the general circulation by providing dynamical stress due to braking of gravity waves (e.g. Lindzen, 1981; Holton, 1982; Matsuno, 1982, Tsuda et al.,1990).

Generation mechanisms of gravity waves were also studied by means of observation made with aircraft, radio-sondes, rocket-sondes, MST radars, and Rayleigh lidars. The MST radar at Jicamarca (12^{0}S), Peru, was used for observations of gravity waves in the middle atmosphere, detecting profiles of wave-induced momentum fluxes (Hitchman et al.,1992; Fritts et al.,1992).

The Indian MST radar provides excellent opportunity to study momentum flux with high time and height resolution particularly in the Troposphere and Lower stratosphere. The present observation is made from a fixed ground station. The wind variation is not the spatial variation from the mean value, but instead it is defined as the temporal variation from the mean value calculating by averaging over the entire observational period. Thus, the mean momentum flux observed by this technique is a time mean value obtained from a fixed station.

4.3 DATA AND METHOD OF ANALYSIS

The vertical flux of zonal and meridional momentum is calculated from the winds measured by the MST radar. For the momentum flux (u'w' and v'w') computation, a direct approach where time series of the perturbation components of u, v, and w are obtained. Then products u'w' and v'w' are formed and averaged over a suitable length of time. Vincent and Reid (1983) developed a method for radar measured winds. In this method two oppositely directed off-vertical symmetrical beams in the East-West or North-South planes are used to obtain line-of-sight (LOS) winds. Then the time series of the two LOS winds are filtered to study a particular frequency band and momentum flux (u'w' and v'w') is calculated from the difference between the average variances of two filtered time series. Here the basic assumption is that the statical properties of the atmosphere at one height are spatially invariant in a horizontal plane.

Since the introduction of this dual beam method by Vincent and Reid (1983), numerous studies of gravity wave momentum fluxes in troposphere, stratosphere and mesosphere have been carried out using radar data. However, when the vertical wind velocity can be obtained directly from the radar vertical beam data together with horizontal wind components (from oblique beam data) it is preferable to use direct method (Sasi et al.1999). It is also noted here that the direct method make use of u,v and w obtained from the six LOS wind values, where as the Vincent and Reid (1983) method makes use of only two symmetrical oblique beams.

The 24-hour data set used for the momentum flux estimation (using direct method) is given in table -1.

		Table-1	
Sr. No	Season	Diurnal cycle	altitude region
1.	Winter	(i) 16-17 Jan.,1996	
		(ii) 31Jan.-1Feb.,1996	
		(iii) 15-16 Feb.,1996	
2.	Equinox	(i) 3-4 Oct.1996	4 - 20 km
		(ii) 31Oct.-1Nov.1996	
3.	Monsoon	(i) 22-23 July,1997	
		(ii) 6-7 Aug.1996	
		(iii) 13-14 Sept.1996	

Observation of the winds in the 4-20 km height region for the period given in table-1 was done using the Indian MST radar at Gandanki. For this observation the following radar configuration was used : pulse repetition frequency = 1000 s^{-1}: Pulse width = 16 μs coded with baud of 1 μs: number of coherent integration =128;

number of FFT points = 128; number of beams = 6 (two zenith beams and four 10° off zenith in the North, East, South and West directions); number of incoherent integrations = 4. The Doppler spectra corresponding to the six beams, with a vertical resolution of 150 m, were first converted to line-of-sight (LOS) wind profiles. From these vertical profiles of LOS corresponding to the six beams, the zonal (u), meridional (v) and vertical components of the winds were derived using a least-squares technique assuming a vertical wind contribution to the LOS winds obtained for the oblique beam (Sato, 1989).

Once the vertical profiles (resolution 150 m) of u,v and w are obtained, these are subjected to a 5 point running mean in height with weights 0.125, 0.125, 0.5, 0.125 and 0.125 (Sasi et al. 1998). This smoothing procedure will reduce the small scale wind fluctuations with height which may be due to random fluctuations or real atmospheric phenomena. The ensemble average is done in the height domain over six consecutive heights of these smoothed time series of u,v and w (available at every 150 m), further reduce any random error. Then the perturbation components of u,v and w are obtained and products u'w' (v'w') are formed and averaged over a suitable length of time. The density weighted zonal and meridional momentum flux (for selected days only) is evaluated by the use of atmospheric density calculated from climatological values of pressure and temperature of rawinsonde observation at near by station Madras. Total 8 diurnal cycles of different seasons have been utilized for the momentum flux study.

4.4 RESULTS AND DISCUSSION

The mean values of zonal (u), meridional (v), and vertical (w) velocities, observed during winter (16-17 January,1996, 31 January-1 February,1996, 15-16 February,1996), monsoon (22-23 July,1997, 6-7 August.1996, 13-14 September,1995) and equinox (3-4 October,1996, 31 October-1 November,1996) are shown in figures 4.1, 4.2, and 4.3 respectively. The mean zonal wind is mostly eastward during winter (Fig.4.1), reaching maximum value of 12 ms^{-1} at a height of about ~ 10 km, while it is eastward below 6 km and reverses above this altitude (i.e. westward) during monsoon and equinox (Figs. 4.2, 4.3) with maximum value of ~ -30 ms^{-1} around 15 km during monsoon (Fig.4.2). The mean meridional wind is mostly southward below 9 km, during winter (except on 16-17 January where it is northward below 9 km (Fig.4.1)). It is southward below 9 km and northward above it on 22-23 July, while on 6-7 August it is largely southward with a few northward excursions and on 13-14 September it is mostly northward with a few southward excursions (Fig.4.2), and is northward during equinox for given altitude range (Fig.4.3). During monsoon the zonal wind is significantly high, while meridional wind is low in comparison with any other seasons.

It may be noted here, July and August are the months of south-west monsoon
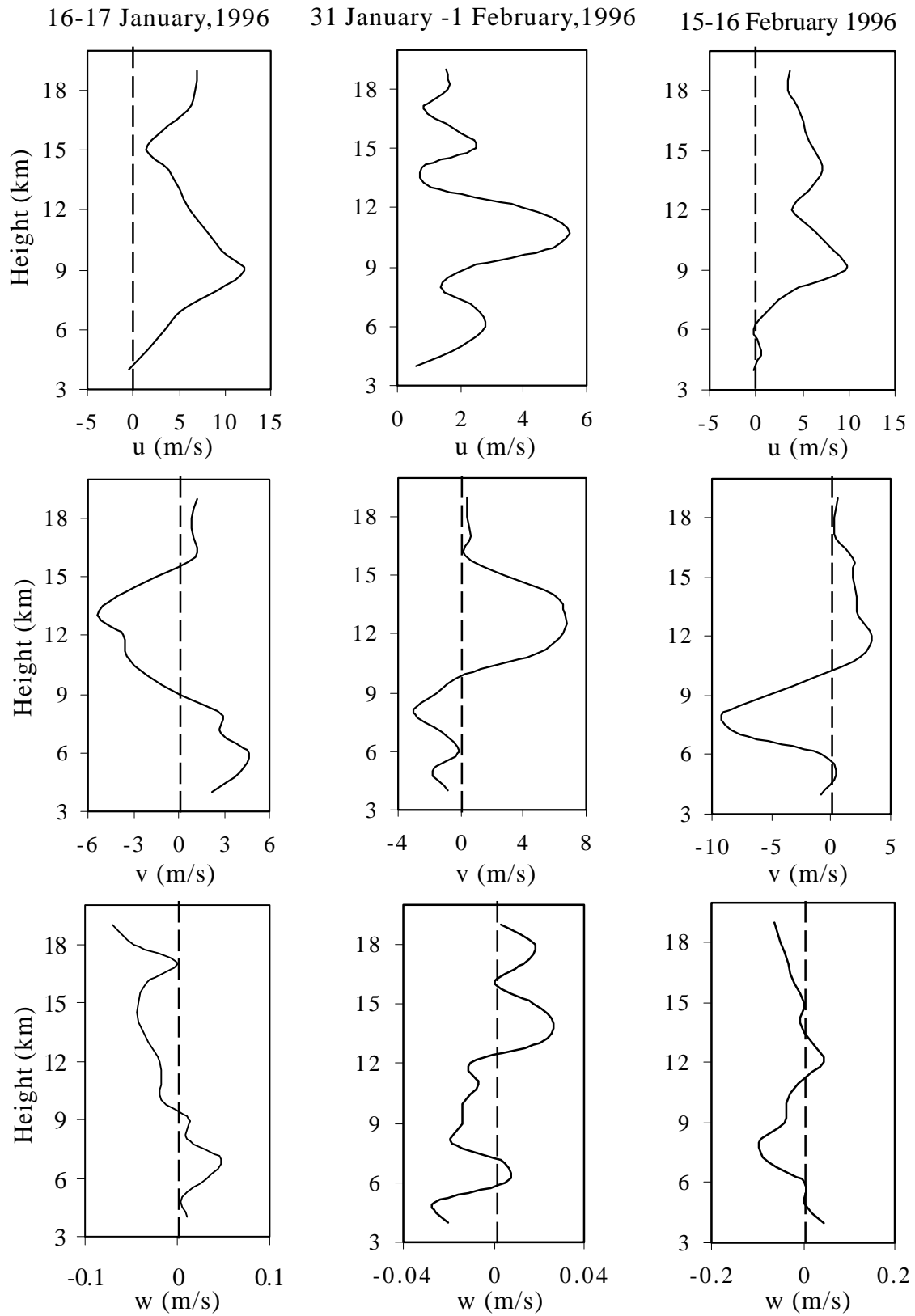
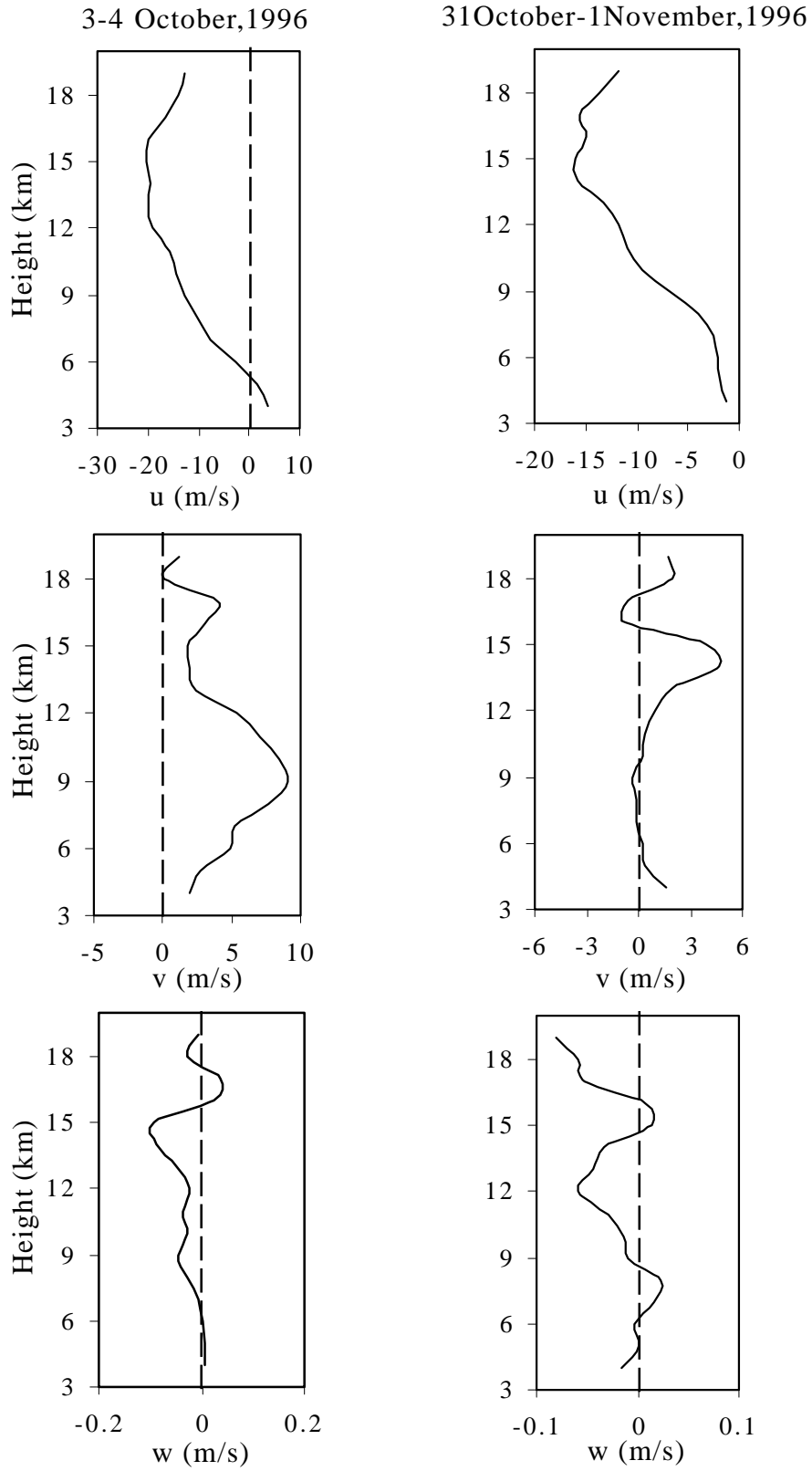**Fig.4.1 :** Mean profiles of zonal (u), meridional (v), and vertical (w) velocities.
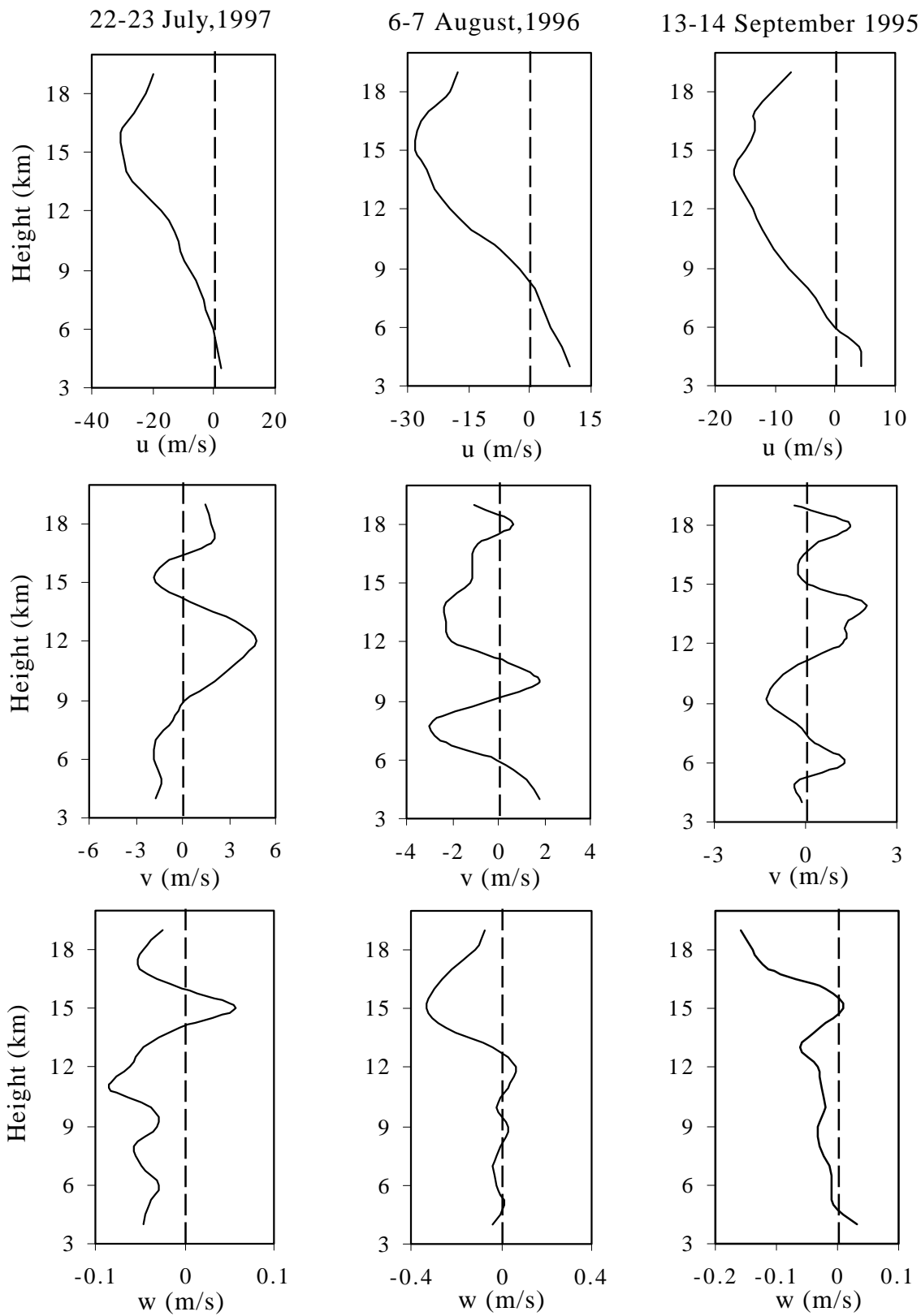
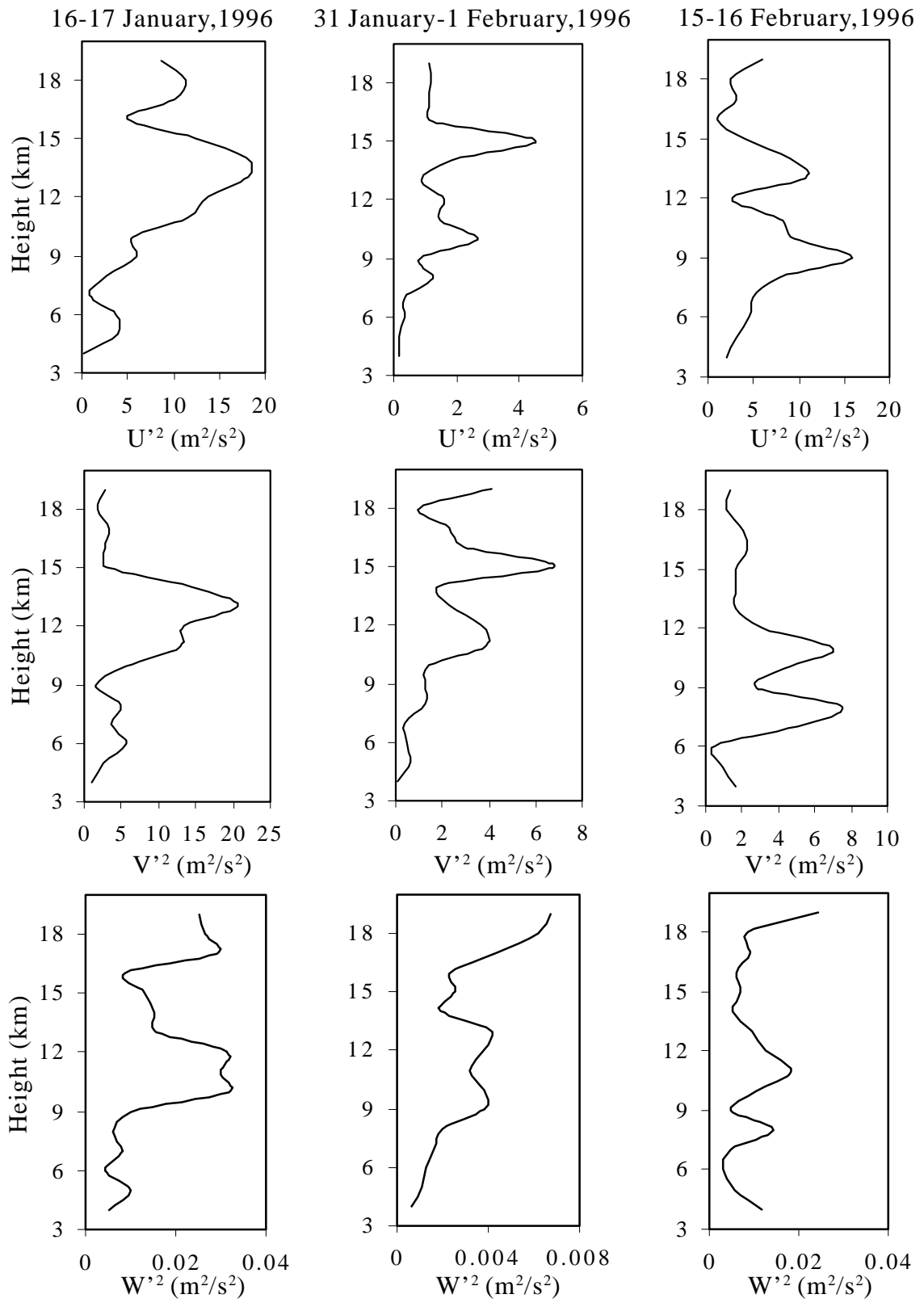**Fig.4.2 :** Mean profiles of zonal (u), meridional (v), and vertical (w) velocities.

Fig.4.3 : Mean profiles of zonal (u), meridional (v), and vertical (w) velocities
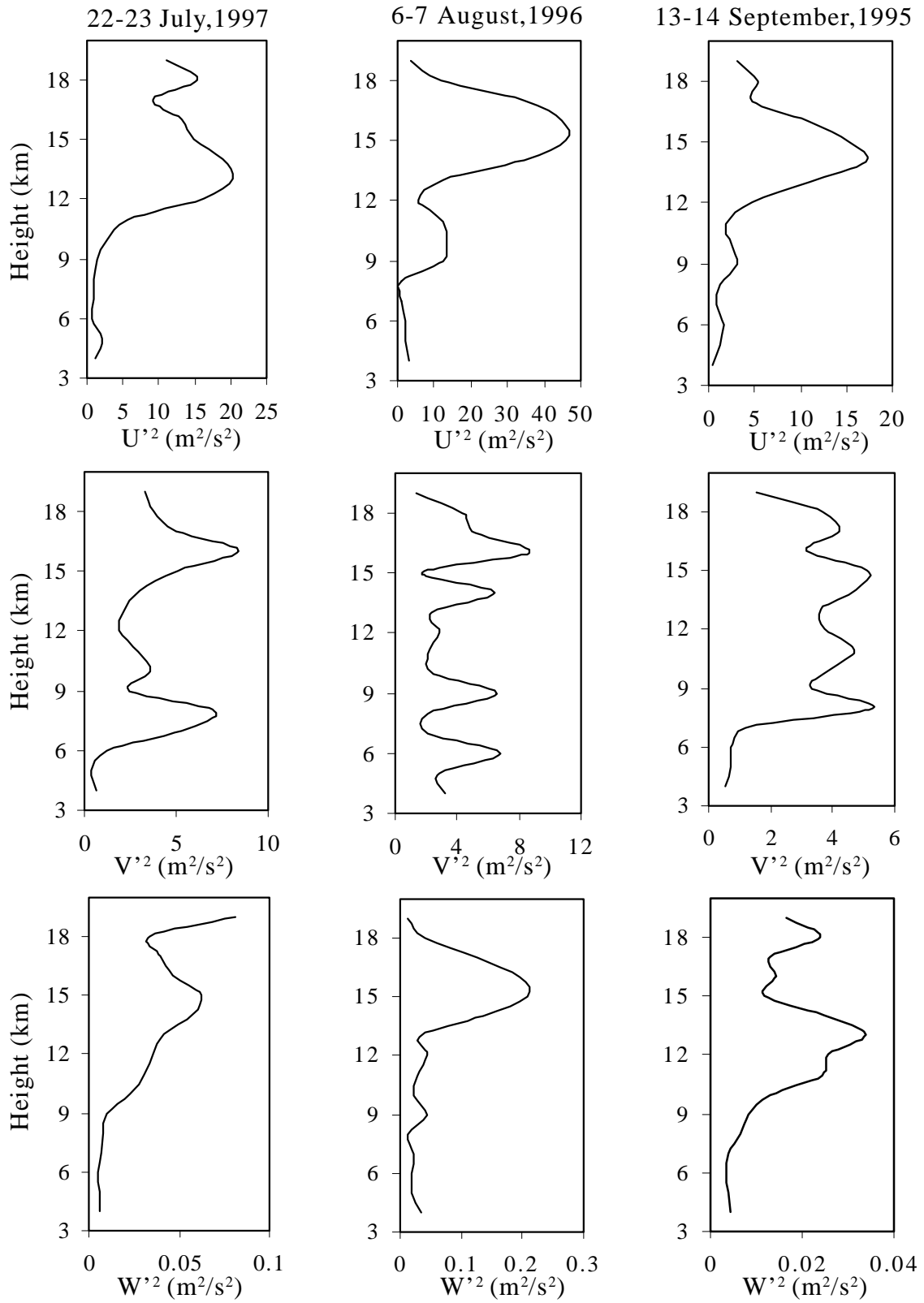
when the winds will be southwesterly-northward and eastward with significant zonal wind and low meridional wind. It is suggested that the Inter-Tropical Convergence Zone (ITCZ) signature of westward wind is suppressed by the strong eastward monsoonal winds giving rise to no clear reversal of zonal wind at lower levels due the passage of ITCZ (Krishna Murthy et al. (2000)). The mean vertical velocities varies from ~ 0.2 to -0.2 ms^{-1} and having maximum value during monsoon, particularly on 6-7 August,1996 (Fig.4.2). The vertical velocities are evaluated with the two vertical beams by noting the importance of vertical wind fluctuations in the calculation of momentum flux, and the average of these two vertical velocities are used for momentum flux estimations.

In order to quantify the strength of fluctuations, the variance (S) of zonal, meridional , and vertical wind in the altitude range under consideration are obtained at interval of 1 km. The mean variances of zonal (U'^{2}), meridional (V'^{2}) and vertical (W'^{2}) component are plotted as a function of altitude for all three seasons and shown in Figures 4.4 (winter), 4.5 (monsoon) and 4.6 (equinox). The prominent peaks are seen at different heights for all three components in the given seasons. As mentioned earlier, variance (S) represents the strength of the fluctuating signal, the prominent peaks of S in the altitude range under consideration indicate the presence of fluctuating component with no propagation in the vertical direction. If there is vertical propagation, then S would show no altitude dependence in the altitude range of propagation. This, of course assumes that the fluctuations do not suffer any significant attenuation in the altitude range. A peak in S is seen between 12 to 15 km for zonal wind mostly in all season and having maximum value observed during monsoon, particularly on 6-7 August,1996 it reaches maximum value of 50 m^{2}s^{-2} at around 15 km (Fig.4.5). The multiple peaks in S are seen for meridional wind in given altitude range, almost for all season.

The vertical flux of mean momentum, both zonal ($\overline{u'w'}$) and meridional ($\overline{v'w'}$) is shown in Figures 4.7 (winter), 4.8 (monsoon), and 4.9 (equinox). There are significant fluxes of westward and northward momentum at most of the heights of observation. The momentum flux values are found to be large at heights where the velocity variances are large. Zonal momentum flux varies from ~ 0.2 to -0.2 m^{2}s^{-2} during winter (Fig.4.7), while it is varies between 0.6 to -0.3 m^{2}s^{-2} during monsoon and equinox (Figs, 4.8 and 4.9), except on 6-7 August,1996 it shows very high value of -2.8 m^{2}s^{-2}. The meridional momentum flux varies from ~ 0.2 to -0.2 m^{2}s^{-2} for all the season except on 6-7 August,1996 where it varies between ~ 0.6 to -0.2 m^{2}s^{-2} (Fig.4.8). These values are comparable (except, only observed on 6-7 Augusut,1996) to the values obtained by Fritts et al (1990) using MU radar and Narayan Rao et al.,(1997) using Indian MST radar. Sato (1990) also used the MU radar to determine the vertical wind disturbances in the troposphere and lower stratosphere. Analyzing eight sets of 2 to 5 days campaign data with the coplanar

Fig.4.4 : Mean profiels of zonal variance (U'^{2}), meridional variance (V'^{2}), and vertical variance (W'^{2}).

Fig.4.5 : Mean profiles of zonal variance (U'^{2}), meridional variance (V'^{2}) and vertical variance (W'^{2}).

Fig.4.6 : Mean profies of zonal variance (U'^{2}), meridional variance (V'^{2}), and vertical variance (W'^{2}).
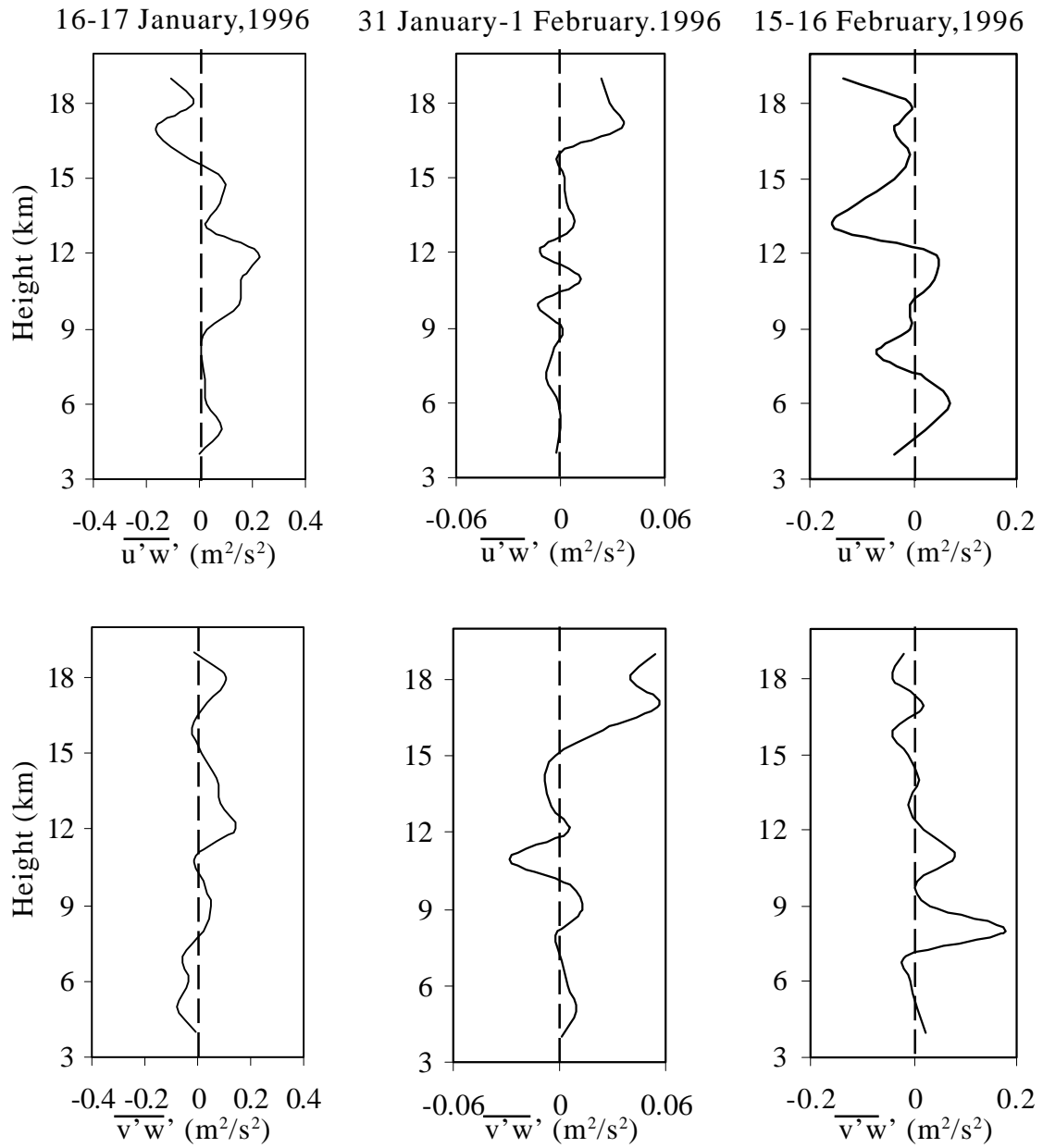
Fig.4.7 : Mean profiles of zonal momentum flux ($\overline{u'w'}$) and meridional momentum flux ($\overline{v'w'}$).
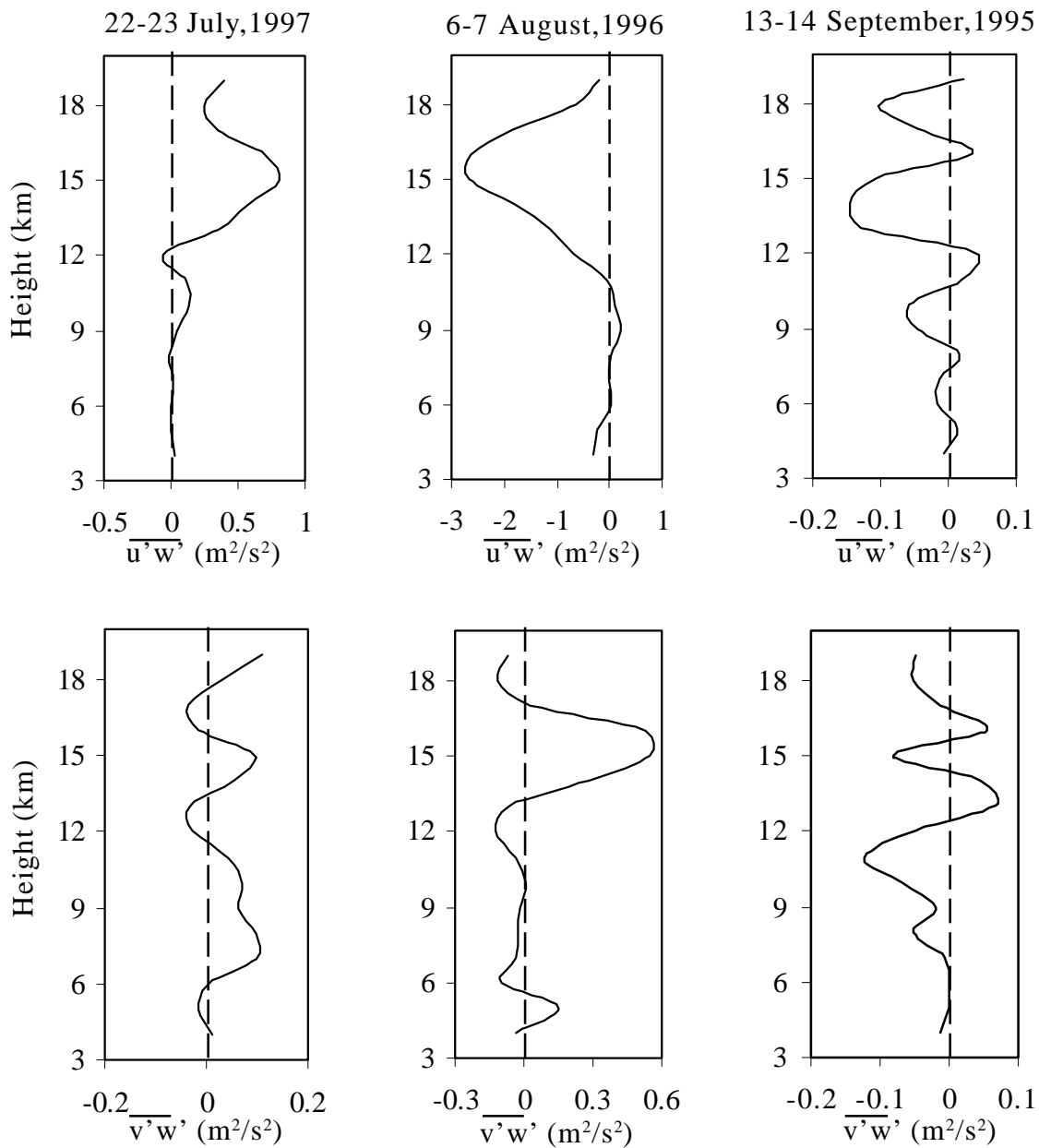
Fig.4.6 : Mean profiles of zonal momentum flux (u'w'), and meridional momentum flux (v'w').
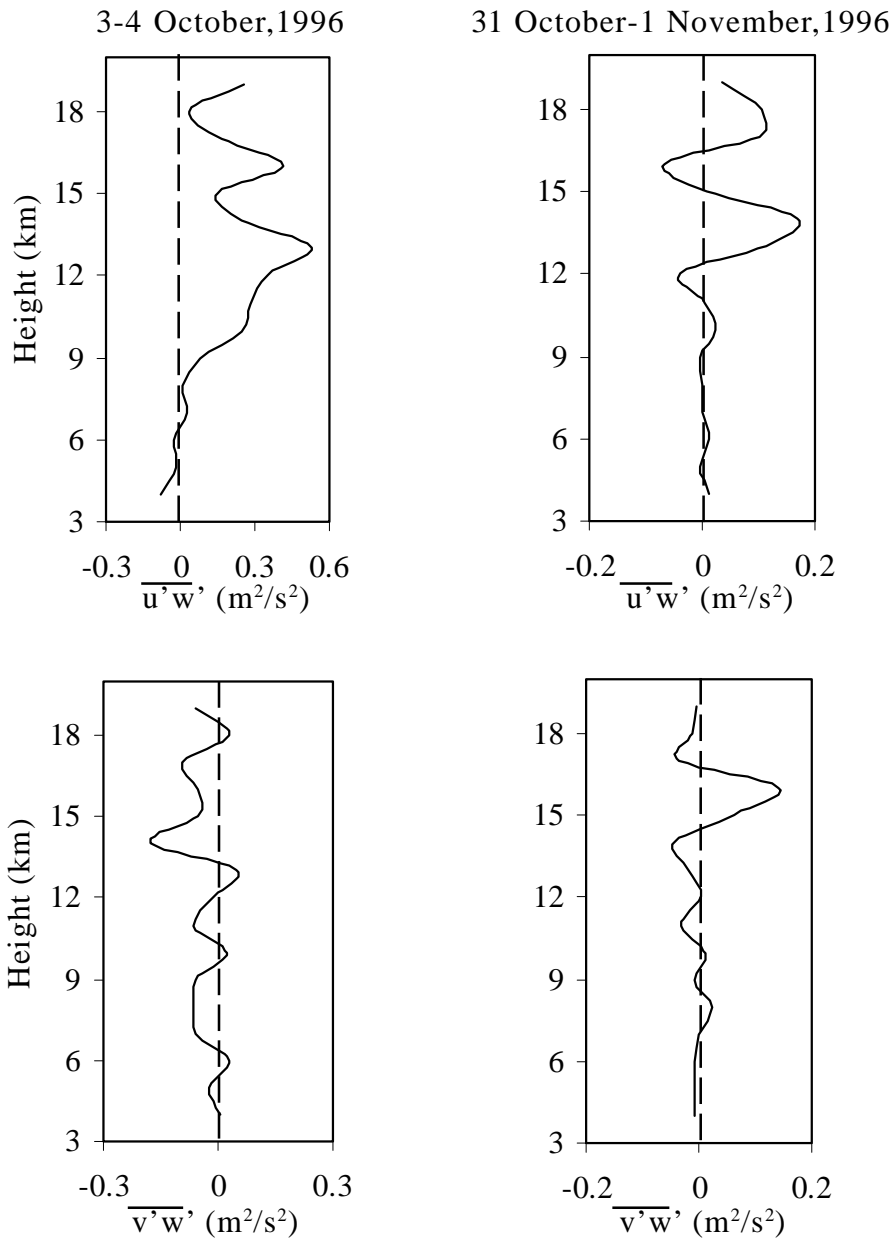
Fig.4.9 : Mean profiles of zonal momentum flux ($\overline{u'w'}$) and meridional momentum flux ($\overline{v'w'}$).

coplanar technique, she compared vertical momentum fluxes calculated for quite and active periods, denoted by large disturbances of the vertical wind, the estimates of the vertical flux per unit mass for the wave period less than 10 hours ranged between $\sim \pm 0.2$ m^{2}s^2 for the lower heights of 5-10 km. Figure 4.10 shows a time -height section of vertical wind, alongwith zonal and meridional momentum flux observed during 22-23 July,1997 and 6-7 August 1996 (monsoon). As shown in this diagram, any wavelike wind changes is, in general, not typical , but the vertical wind variation is fairly coherent in vertical direction over a wide height range up to around 14 km. Considerably large variation is observed in vertical wind and as well as in both zonal and meridional momentum flux below tropopause (i,.e near 15 km). The momentum flux values are found to be quite large during monsoon. This may be due to active cumulus convection during monsoon, because in the equatorial region, where the back ground mean winds are much weaker than at middle latitudes, so that convection in the troposphere can be anticipated to be the chief excitation mechanism there.

The time-height section of the variance of zonal (U'^{2}), meridional (V'^{2}) and vertical (W'^{2}) wind fluctuations observed during 22-23 July 1997 and 6-7 August 1996 is shown in figure 4.11. Fairly large variance value of zonal (U'$^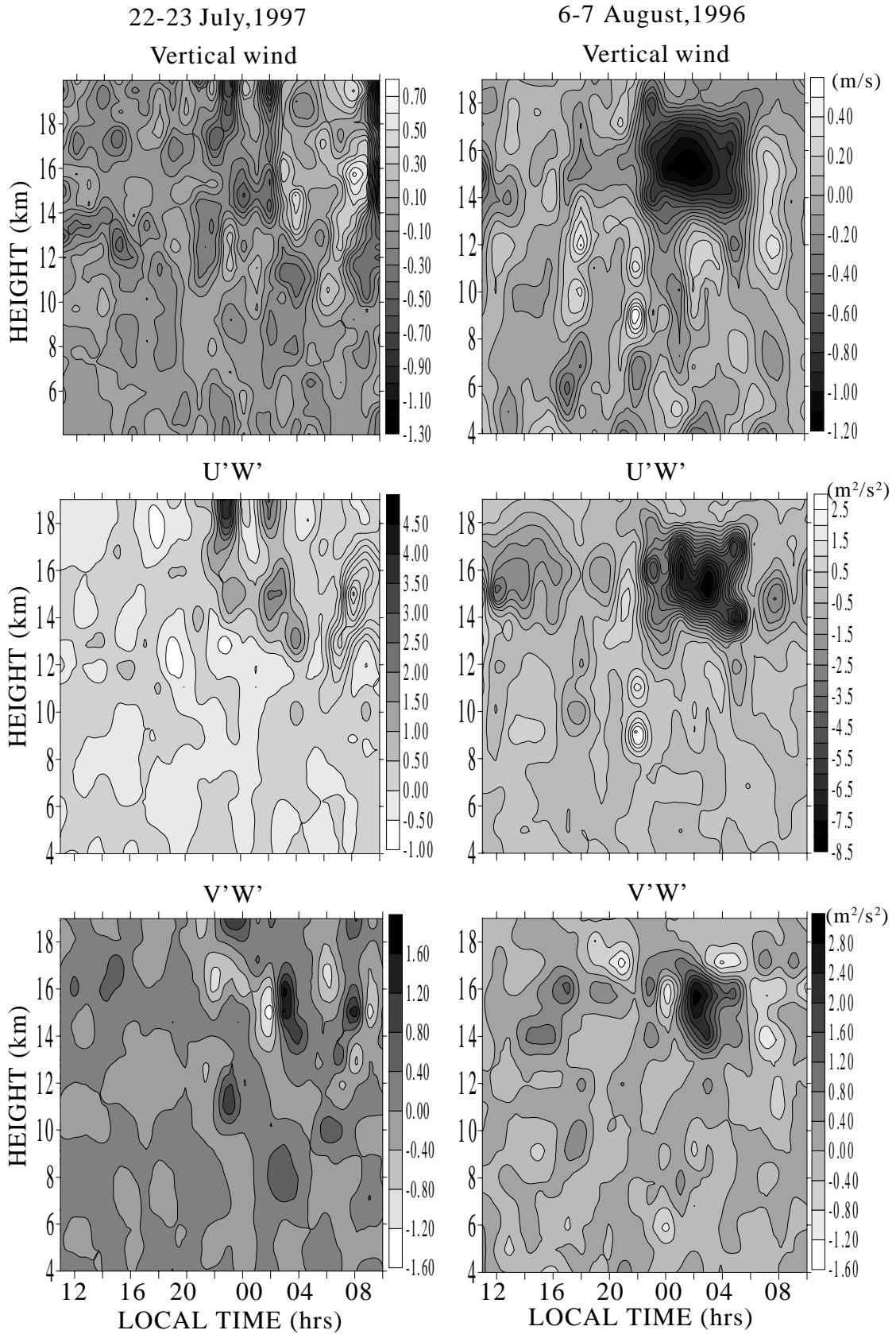2$) and vertical (W'^{2}) wind fluctuations are observed during 6-7 Ausugt,1996 below tropopause (i.e at 15 km). It may be noted here, near tropopause, large value of variance were detected throughout the observation period, (observed by Tsuda et al.(1994), during radiosonde observations over Indonesia). Some columnar structure is seen in vertical wind variance (W'^{2}) during 6-7 August,1996 in a short span of time at, e.g., 2000 h(IST), between 8-14 km, which is considered to be produced by convective air motion. This large columnar structure is not so significant in the similar diagrams for U'^{2} and V'^{2}. Figure 4.12 shows the density-weighted mean momentum flux of zonal ($\overline{ru'w'}$) and meridional ($\overline{rv'w'}$) observed during 22-23 July 1997 and 6-7 August 1996. The values of momentum flux per unit volume ($\overline{ru'w'}$ and $\overline{rv'w'}$) are typically 0.1-0.2 Nm^{-2}, and agrees well with observed by Fukao et al (1988) using MU radar and Narayan Rao et al (1997) using Indian MST radar (except it quite high (-0.8 Nm^{-2}) for zonal wind near tropopause during 6-7 August,1996.

4.5 SUMMARY AND CONCLUSIONS

Overall, results seem reasonable, and the variance and momentum flux estimates appear to agree with those of previous studies. However, very high value of vertical wind, as well as momentum flux is observed during 6-7 Augsut 1996, the mechanism to generate these strong vertical winds in not yet understood. The momentum flux and variance of wind fluctuations are determined from the unfiltered wind data, but to findout the significant contribution of different period waves, more detailed analysis is necessary which leads to feature work..

Vertical wind

Vertical wind

U'W'

U'W'

V'W'

V'W'

LOCAL TIME (hrs)

LOCAL TIME (hrs)

Fig.4.10 : Time-height section of the vartical wind,
zonal momentum flux (U'W') and
meridional momentum fluxes (V'W').
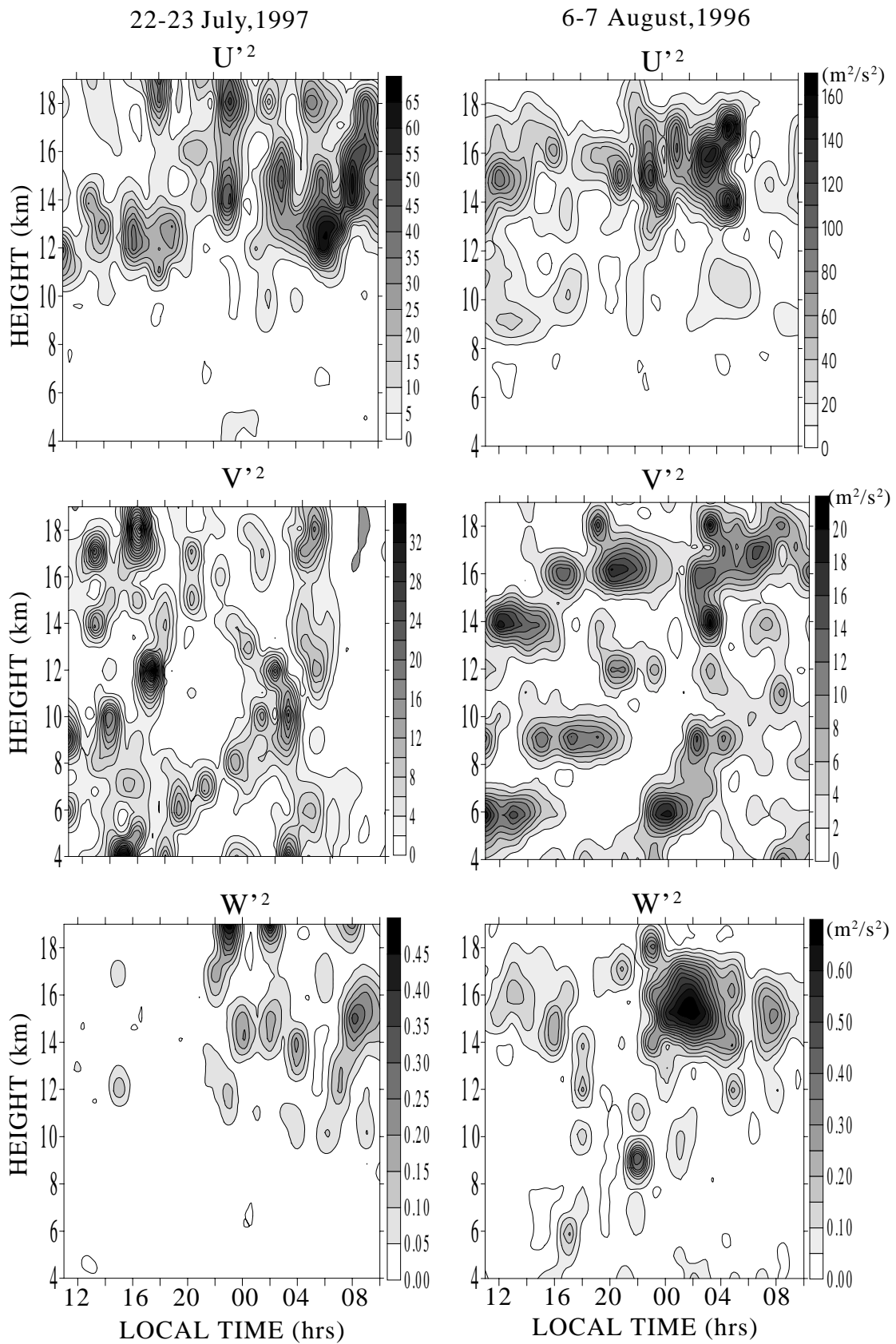
Fig.4.11 : Time-height section of the variance of zonal (U'²),
meridional (V'²), and vertical (W'²) wind fluctuations.

22-23 July 1997

Density wighted zonal flux

Density wighted meridional flux

6-7 August, 1996

Density wighted zonal flux

Density wighted meridional flux
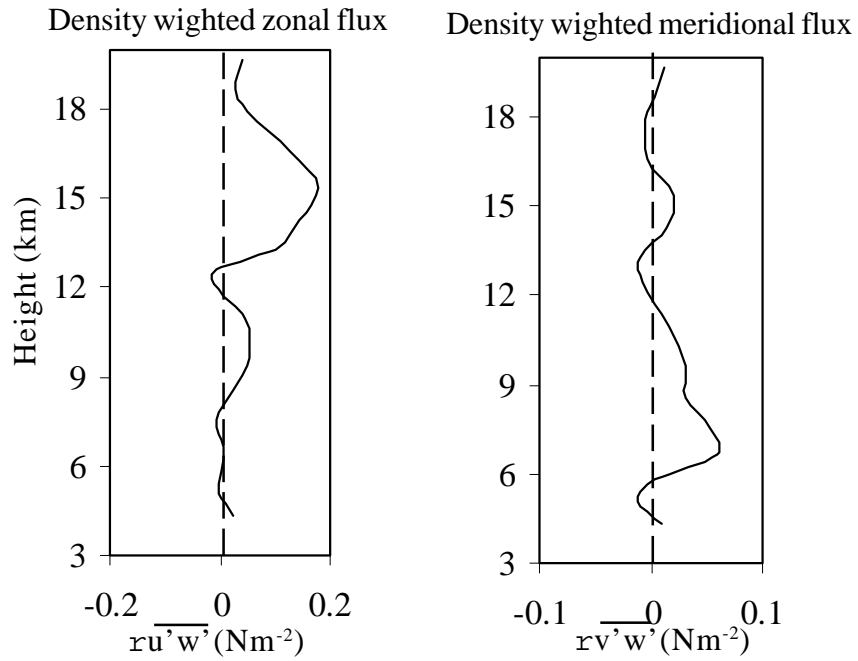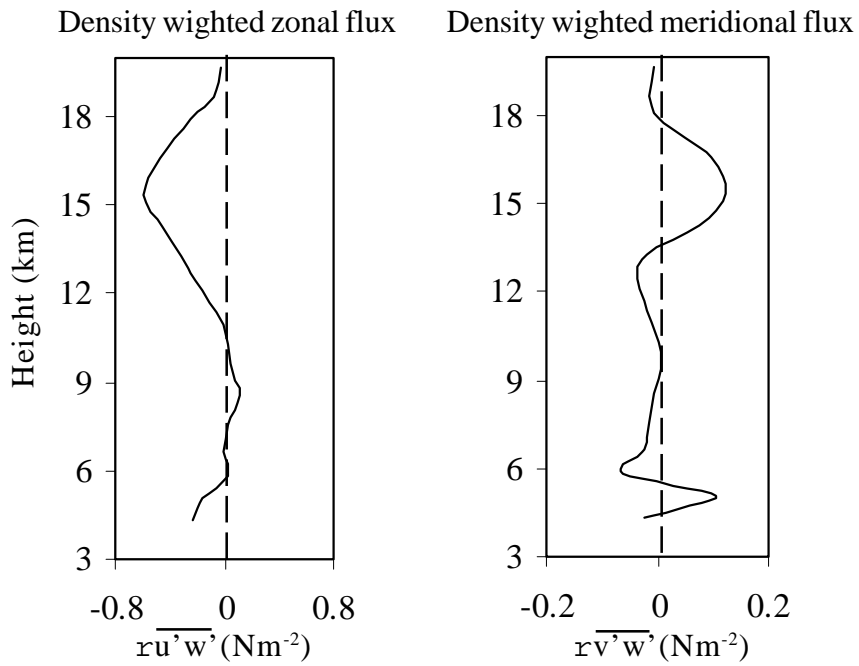
Fig.4.12 : Mean profiles of momentum flux per
unit volume observed in zonal and
meridional planes.

CHAPTER - 5

STUDY OF EQUATORIAL WAVES

5.1 INTRODUCTION

If a sugar cube is dropped into a cup of tea it will generate waves that travel radially out wards; a breeze blowing over a river will produce waves that will move in the direction of the wind on the surface of the river, even if the current flows in some other direction ; and every day at the seashore there is a continuous panorama of incoming waves that become unstable and eventually break against the shore. These are all examples of wave motion in a fluid and they have two properties in common that they share with all other types of waves : firstly, energy is being propagated from one point to another; secondly, the disturbance travels through the medium without giving the medium (as a whole) any permanent displacement. The wave may be considered as perturbation on the steady slowly changing background.

Dynamical processes in the atmosphere are generally considered as being driven by thermal processes, waves can be a major means of energy and momentum transport as well as transport of long-lived trace constituents in the atmosphere. The large difference in the levels of energy absorbed in different regions of the atmosphere results in transport of energy from one region to another. A considerable amount energy is this transported takes place through waves and hence coupling processes, especially through waves has become important subject of study. Thus waves play an important role in coupling between high latitudes to low latitudes and for between troposphere-stratosphere-mesosphere regions.

The atmosphere is capable of sustaining a large number of wave phenomena. Over twenty types of atmospheric waves are listed. Atmospheric waves can be classified into three classes :

Class-I :- Waves that propagate horizontally and are composed of vertical displacements (vertical transverse waves i.g. gravity waves).

Class-II :- Waves that propagate horizontally with horizontal displacements per pendicular to the propagation direction (horizontal transverse waves i.g. Rossby waves).

Class-III Waves whose displacements are in the same direction as the propagation. (longitudinal waves i.g. acoustic waves).
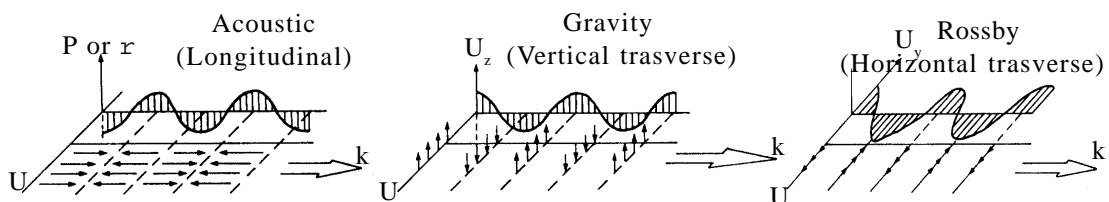
Fig.5.1 : Three principal types of atmospheric waves.

All these waves can exist in the form of very small perturbations on a steady state of the atmosphere, so that the waves will then satisfy linear equations. The best known atmospheric waves are the acoustic waves which play such a vital role in Voice communication. Sound or acoustic waves, are longitudinal waves formed by a balance between compressibility and inertia, which is the resistance to a change of velocity, and is expressed by Newton's second law of motion. In a homogeneous stationary fluid in the absence of an external force (gravitational, magnetic etc.), acoustic waves are the only types of waves that can exist. Acoustic waves include sound waves whose frequency spectrum covers the response range of human hearing.

The earth's atmosphere is a fluid that is continually being acted upon by the force due to the earth's gravity. There is therefore a distinct decrease in density with altitude, which is generally referred to as a density stratification, though in fact it is more likely to be a continuous variation in density than layered one. This density gradient also endows the atmosphere with a stability that is completely lacking in a homogeneous fluid. When the force of the earth's gravity and the magnitude of the stabilizing restoring force introduced by the atmospheric density gradient become comparable with compressibility forces, the resulting waves are some times called acoustic gravity waves. These waves are no longer purely longitudinal (except when they propagate vertically) because gravity has produced a component of the air particle motion that is transverse to propagation direction. Gravity waves occur when the dominant motion in the atmosphere is due to the balance between the gravitational force and stable restoring force of the density gradients.

Shearing waves can occur in the atmosphere. They are very common in a stream of water where there is an interaction between the water waves and the initial sheared flow of the water. The sheared flow arises because the water at the bottom and at the edges of a stream moves substantially slower than the water at the topand the centre. In the atmosphere shearing waves are important at the interface between two adjacent masses of air whose physical properties are different. This interface is called a front and it is along the frontal zones that unstable sheared Rossby waves convert their potential energy into the kinetic energy associated with large travelling storms known as cyclones. There also exist long waves that are influenced by the curvature of the earth and its rotation (the Coriolis effect). The variation of the strength of the Coriolis effect $2W \sin q$ with latitude q (being zero at the equator) acts as an external force field which results in horizontally transverse waves with wavelengths thousands of kilometers long. These waves are knows as Rossby waves or planetary waves; they provide a meteorologically useful theory for the description of the pressure distribution associated with moving wavelike high pressure and low-pressure systems.

The name planetary wave is generic of all waves having periods equal to or

grater than half a day and horizontal wavelengths comparable to the radius of the earth. They can be classified on the basis of their distinct characteristics such as (1) extra tropical modes and equatorially trapped modes, (2) free modes and forced modes, (3) external mode and internal modes and (4) mode that interact with the mean flow through wave transience and those that interact by wave dissipation.

The equatorial atmosphere is characterised by the active generation of atmospheric disturbances due to the large solar heat input, which further generates various atmospheric waves. The equatorial atmospheric dynamics differ significantly from the middle and high latitude atmosphere because of three reasons. (a) The Coriolis parameter '2W sinφ' is very small in the equatorial region. (b) The solar insolation is maximum, resulting in heating of the low latitude atmosphere by the absorption of UV radiation by and ozone and I.R radiation by water vapour.

The distribution of sea and land mass in different longitudes in the equatorial region produces uneven heating and results in East-West circulation along the equator. The release of latent heat in cumulus convection is considered as a primary energy source for the maintenance of the equatorial disturbances. Because of the special nature of the driving force, as well as, the smallness of the Coriolis parameter, the large-scale equatorial atmospheric dynamics have certain distinct characteristic structural features which are quite different from those of the mid-latitude systems.

Detailed theoretical studies, which are borne out to a very large extent by the observational data, show that in the equatorial latitudes there are two gravest forced oscillations, one propagating eastward (Westerly mode) and another westward (Easterly mode). The westerly mode, known as the Kelvin wave is symmetric about the equator. The easterly mode is antisymmetric about the equator and is variously called as, mixed Rossby Wave, or Mixed Rossby Gravity Wave. Both the wave modes are latitudinally trapped, i.e. their propagation which is essentially zonal in the horizontal plane are confined to about $\pm 15^{\circ}$ latitude.

The waves which are of primary importance, because of their role in middle atmospheric dynamics, are forced internal modes which are excited by various processes in the troposphere and propagate vertically into the middle atmosphere The most significant forced vertically propagating extra tropical wave modes are the quasi-stationary Rossby waves, while the most significant forced vertically propagating latitudinally trapped equatorial modes are the Kelvin and Mixed Rossby Gravity waves. The Kelvin and Mixed Rossby Gravity (MRG) waves propagate vertically with relatively short vertical wavelengths and interact with the mean flow via the wave dissipation processes. As a result of this interaction process the Kelvin waves produce westerly acceleration of the mean zonal wind, while, the MRG waves produce easterly acceleration. Chacteristics features of Kelvin wave and Mixed-Rossby-Gravity (MRG) waves in the equatorial lower stratosphere are given in table -1 (After Wallace 1973).

Sr. No	Feature	Kelvin wave	MRG wave
			Table -1

Sr. No	Feature	Kelvin wave	MRG wave
1.	Period	~ 15 day	~ 4.5 day
2.	Horizonatal wavelength	~ 30,000	~ 10,000
3.	Vertical wavelength	~ 8 km	~ 6 km
4.	Zonal wave number	1-2	4
5.	Phase speed	25 ms^{-1}	-23 ms^{-1}
6.	Amplitude		
	(a) Zonal wind (U)	~ 8ms^{-1}	~ 2-3ms^{-1}
	(b) Meridional wind (V)	0 ms^{-1}	~2-3 ms^{-1}
	(c) Vertical wind (W)	~ 0.15 cm.s^{-1}	~ 0.15 cm.s^{-1}
	(d) Geopotential height 'Z'	~ 4 meters	~ 30 meters
	(e)Temperature(T)	~2-3 ^{o}k	~1°k
7.	Direction of Propagation	Westerly (East ward)	Easterly (West ward)
8.	Symmetry about the equator		
	(a) Zonal wind	even	odd
	(b) Meridional wind	-	even
	(c) Geoptential height 'Z'	even	odd
9.	Group velocity	Individual phase travels down wards but the group velocity is upwards	Individual phase travels down wards but the group velocity is upwards
10.	Region of absorption	Penetrates through zone of easterlies but gets absorbed near the level of transition between the easterlies and westerlies	Penetrates through zone of westerlies but gets absorbed in the zone of easterlies

From the physics point of view, the most significant features of the equatorial middle atmosphere are quasi-biennial oscillation (QBO), and semi-annual oscillations (SAO) produced by the equatorial waves.

The observed semi-annual oscillation (SAO) and the qausi-biennial oscillation (QBO) of the zonal wind in the equatorial middle atmosphere have been successfully explained in terms of the wave-mean flow interaction processes. The upward propagating Kelvin waves deposit their eastward momentum into the atmosphere and increase its eastward (westerly) flow velocity; and similarly, the MRG waves and Rossby waves deposit their westward momentum and increase the westward (easterly) flow in the middle atmosphere.

The QBO is the dominant wind component in the 20-35 km altitude range, while the SAO, along with the annual oscillation (AO) of comparable magnitude, is a dominant of the zonal wind in the equatorial upper stratosphere (30-50 km) and the mesosphere (50-90 km). The wave-mean flow interaction processes are also responsible for other important atmospheric phenomena at middle and high latitudes like the Sudden Stratospheric Warming events.

Most of the evidence for the equatorial waves came from the data (rawinsonde and rocket) corresponding to stations located in the Pacific zone. It is quite likely and probable that characteristics of equatorial waves are different in different longitude zones as is the case with SAO and QBO. Particularly, observations pertaining to the Indian zone are lacking in this regard. However a comprehensive experimental programme has been planned as part of the Indian Middle Atmospheric programme (IMAP) and carried out using balloon and rocket experiments to delineate the characteristics of the equatorial waves over the Indian Zone. The generation and propagation of equatorial waves may be expected to have a seasonal dependence, since convective heating in the tropical troposphere may be expected to vary seasonally in response to changes taking place in Sea Surface Temperature (SST) influence of the monsoon circulation and tropical easterly jet on the equatorial waves in the stratosphere. With these in view, it will be of great interest to study the equatorial wave characteristics in different seasons over the Indian zone.

The continuous data, with excellent height and time resolution providing by the Indian MST radar should enable the delineation and detailed study of all the wave motion in the equatorial atmosphere having periods ranging from few hours to few days, and even longer period SAO, AO and QBO. This chapter describes the characteristics of the equatorial waves with periods ranging from 4 to 64 days (i.g. MRG waves, Kelvin waves and long period waves) in different seasons. The zonal and meridional winds measured by the Indian MST radar located at Gadanki (13.47^{o}N, 79.18^{o}E) are used for this study. The results shows that in different seasons this tropical region is dominated by equatorial waves of different types.

5.2 THEORY OF EQUATORIAL WAVES

Theoretically, the vertically propagating wave disturbances in the tropical middle atmosphere can be classified in two kinds. One kind are the free or natural modes which are characteristic of the atmosphere. The second kind are the forced modes having periods dependent on the exciting source function. The forced modes can again be classified as external or vertically trapped oscillations having very large vertical wavelengths, and the internal or vertically propagating oscillations having relatively short vertical wavelength. The internal modes have a vertical component group velocity and can transport energy and momentum vertically. Just like the vertically trapped and vertically propagating waves modes, some of the wave modes are trapped in one of the horizontal directions and propagate horizontally in other direction only. The equatorial waves are trapped horizontally in latitude and propagate both zonally and vertically.

The basic state of the atmosphere is governed by the equations expressing conservation of momentum (force equation) and energy, the continuity equation and the hydrostatic equations. Ignoring sources and sinks, the governing equations of the atmosphere can be written in terms of the perturbations in the velocity and geopotential fields. These equations are then linearised by neglecting the second order terms of products of perturbations. The different modes of atmospheric oscillations are assumed to be wave like and are obtain as eigen solutions of the linearised perturbation equations. General solution to these equations are complex. Solutions work out to be simpler if investigation of midlatitude and low latitude being done separately. These are so called equatorial beta plane and midlatitude beta plane approximations which essentially limit the description of the flow fields in the meridional extent. The sine and cosine functions of latitude (q) are expanded in Taylor series and for equatorial beta plane $\sin(q)$ is taken as equal to y/a where y is the distance in the meridional directions from the equator and a the earth radius. $\text{Cos}(q)$ is approximated as unity.

The linear perturbation equations, after the equatorial beta plane approximation are further simplified by separating the variable, where in , each dependent variable is assumed to depend on the independent variables, and the independent variable are not coupled. In this case each variable is separated into vertical and horizontal parametric equations. The horizontal structure of the field variables of the wave motion is given by the Laplace's tidal wave equation and the vertical structure by the vertical structure equation. Both the equations are dependent on a variable called the separation variable 'h' often referred to as equivalent depth, by analogy to circulation in the oceans for which the theory was developed initially. In the mid-latitudes, for the synoptic scale disturbances the Coriolis force and the pressure gradient force are in approximate balance. The geostrophic balance gives the approximate relation between the pressure field and the horizontal velocity.

The horizontal wind field thus obtained is the geostropic wind, Vg expressed as

$$Vg = iug + jvg \circ k \times (1/rf)Dp \underline{\hspace{3cm}}(1)$$

Where r = Atmospheric density, p = Atmospheric pressure

f = the Coriolis parameter = $2W \sin f$, W = earth's angular velocity

f = latitude

In the presence of horizontal temperature gradients, the wind differs from Vg and the difference is given by the thermal wind equation.

$$\frac{\partial V_g}{\partial (\ln p)} = k \, R \, \frac{DT_p}{f} \underline{\hspace{3cm}}(2)$$

Equation (2) shows that the thermal wind refers to the vector difference between the geostrophic wind at two pressure levels.

While seeking a vertical propagation wave solution of the form

$$G = A \exp(ifz) + B \exp(-ifz)\underline{\hspace{2cm}}(3)$$

here f is given by

$$f^2 = \frac{N^2}{gh} - \frac{N}{r_o^{1/2}} \frac{d^2}{dz^2}\left(\frac{r_o^{1/2}}{N}\right)\underline{\hspace{1cm}}(4)$$

$$\text{Where,} \quad N^2 = \frac{R}{H}\left[\frac{dT_o}{dz} + K\frac{T_o}{H}\right]\underline{\hspace{1cm}}(5)$$

is the square of the Brunt Vaisala frequency

G = The separation variable connecting the vertical and horizontal structure equation of the wave.

H = The scale height of the atmosphere

r_o, T_o = The atmospheric density and temperature respectively

g = The acceleration due to gravity

For the internal wave modes, upward energy propagation corresponds to downward phase propagation. Thus the component has only downward phase propagation is considered. f = 0 corresponds to free or natural oscillation. In this case only a particular value of h = g H (where g is the ratio of specific heats) satisfy the equation.

In the case of forced oscillation the nature of forcing depends on the sign of f^2. For the h < 0, f^2 is less than 0. At heights above the earth's surface, where f^2 is negative, the waves propagating upwards will be reflected and the energy introduced by the forcing is trapped. The value of 'h' is a faction of period of oscillation, and mode. f can be considered as a measure of the vertical wavelength, which when becomes purely imaginary (f^2 < 0), the wave represents a vertically trapped mode. For forced oscillations 'h' can be considered as the eigen value and is obtained by the Laplace's tidal wave equation including the forcing function.

The vertical wavelength l_z of the internal waves is given by

$$l_z = \frac{2p}{\left[\frac{1}{H} \frac{(g-1)}{g} \frac{H}{h} - \frac{1}{N} \right]^{1/2}} \hspace{2cm} (6)$$

only real value of l_z corresponds to vertically propagating wave, which intern is decided by the sign of 'h'.

In terms of 'h', the dispersion equation for the waves under equatorial beta plane approximation can be obtained from the Laplace's tidal equation as

$$\hat{I}^{1/2} = \frac{(n + 1/2) \pm [(n + 1/2)^2 + ss + s^2 s^2]^{1/2}}{s^2} \hspace{1cm} (7)$$

Where n = discrete meridional wavenumber (0, 1, 2, ...) representing the number of nodes of the wave between the equator and the pole.

S = Zoanl wave number of the wave

s = Wave frequency normalised by 2W

$$\hat{I} = 2W \, a \, / \, (g \, h) \hspace{3cm} (8)$$

The value of $\hat{I}$ depends on 'h' obtain from the vertical structure equation. For isothermal atmosphere, h = g H, and with $\hat{I} = \hat{I}_f$ for free mode the dispersion equation can be written as a cubic equation in s

$$\hat{I}_f^{1/2} [\hat{I}_f s^2 - s/s - s^2] = 2n + 1 \hspace{2cm} (9)$$

The type of forced and free wave motions for different meridional wave numbers can be identified from the above two equations (7) and (9). For the forced waves, with meridional wave number n = -1, the dispersion equation gives a wave solution of an equatorially trapped mode for these modes, called Kelvin waves, the pressure and the velocity fields are symmetrical about the equator and propagate eastwards. These waves are analogous to the eastward propagating Kelvin waves in the oceans, propagating parallel to the coast line.

For n grater than zero the dispersion relation gives, three wave solutions and they are distinguished by their angular frequencies. The solutions corresponds to two inertia gravity waves, one propagating eastward and another westward and third , the Rossby wave, propagating westward. The phase speed of Rossby modes are by far small compared to inertia gravity waves. The wind velocity associated with the Rossby waves are geostrophic, in that, the velocity vectors are parallel to the isobars. For inertia gravity waves the velocity vectors are inclined to the isobars. They have vertical wavelength of a few kilometer and escape detection and study using wind data of poor height resolution.

For n = 0 an interesting solution is obtained for waves which have the mixed characteristics of both the Rossby mode and the inertia gravity mode.

For larger zonal wave numbers, the waves show characteristic more similar to inertia gravity waves and for large negative zonal wave numbers the wave solutions are similar to Rossby waves. In between, the wave solutions show wave characteristic similar to inertia gravity waves close to the equator and tend to be more similar to the Rossby waves far away from the equator. These wave solution are called the mixed Rossby gravity wave modes.

5.3 OBSERVATIONS AND NUMERICAL MODELS

Atmospheric waves are characterized by variation in the wind speed, the atmospheric density, the atmospheric pressure and temperature. It is possible to determine the existence of the waves by measuring the small changes in the atmospheric pressure produced during the passage of a wave. This is done by using a barometer that is capable of measuring pressure changes of the order of a few microbars. Within the narrow band of periods between 5 and 10 minutes, uniform sinusoidal oscillation in the pressure variation frequently appear. These are the result of tropospheric gravity waves. Convection and the influence of nearby weather systems produce rather more irregular fluctuations with periodicities of 15 minutes to one hour. The vertical fluctuations in the temperature can also form waveguides within the atmosphere because of which wave system can become ducted and propagate its energy over very large distances.

During the late 1960s, a number of observational studies revealed the presence of vertically propagating planetary-scale wave in the equatorial lower stratosphere. Yanai and Maruyama (1966) and Maruyama (1967) documented fluctuations in the meridional wind with period 4-5 days corresponding to the mixed Rossby-gravity wave (MRGW) predicted by linear theory (Matsuno 1966). The role of large-scale equatorial waves in the QBO has been recognized since the discovery of equatorial Kelvin waves by Wallace and Kousky (1968) and Rossby-gravity (RG) waves by Yanai and Maruyama (1966). Both theoretical (Holton and Lindzen 1972) and experimental (wallace and Kousky, 1968 ; Kousky and Wallace 1971 ; Angell et al. 1973) results indicate that Kelvin waves have a dominant role in driving the westerly phase of the QBO. However Takahashi and Boville (1992), using a 3-dimensional high -resolution model of the stratosphere, found that the observed Kelvin wave activity is apparently not sufficient to completely account for the westerly acceleration of the QBO.

Mak (1969) examined the response of a two-layer model of the tropical atmosphere to stochastic forcing at lateral boundaries (30^oN and 30^oS). He found large response of a model Tropics at wavenumbers and frequencies corresponding to the observed MRGW and a gravest Rossby mode. Lamb (1973) studied the response of a modelled of the tropical atmosphere to midlatitude forcing, including the effect of condensation heating in the Tropics. The model of Chang (1976)

showed that randomly distributed sources most efficiently excite the longest zonal-scale Kelvin waves, and that the preferred vertical wavelength of the excited waves is about twice the vertical scale of the heat source. Strong support for the hypothesis that both Kelvin and RG waves are indeed by tropical convective heating has been provided by Hayashi and Golder (1978) by means of controlled experiments with a sophisticated non-linear General Circulation Model (GCM). Also Boville and Randel (1991) have studied in detail the equatorial wave properties using a GCM.

A detailed study of the vertical and horizontal structure and properties of equatorial Kelvin and RG waves undergoing thermal and mechanical dissipation was done by Plumb and Bell (1982). Wilson and Mak (1984) analysed the response of tropical atmosphere to lateral forcing in a zonally non-uniform basic state and found that the interaction between a steady planetary wave with zonal wavenumber 1 and a forcing wave provides a dynamical mechanism to excite equatorially trapped waves such as MRG waves. Lu (1987) made a detailed analysis of equatorial waves in the upper troposphere during the special observing periods of the first GARP Global Experiment (FGGE) and showed that MRG waves are locally and sporadically excited by midlatitude disturbances. Using Satellite data Salby et al., (1984, 1990) and Randel (1990) found evidence for Kelvin wave activity in temperature and tracer species in the middle atmosphere. Satellite data were used by Coy and Hitchman (1984), Hitchman and Leovy (1988), Hirota et al (1991) and Randel and Gille (1991) to study the relationship between Kelvin wave activity and the mean flow, particularly the role of the kelvin waves in the forcing of SAO.

Hirota (1978) using wind and temperature data showed the existence of disturbances with vertical wavelength 10-20 km and large amplitude during the easterly phase of the SAO in zonal wind. These were identified as Kelvin waves of period 10 days. Salby et al., (1984) analysing the Nimbus-7 LIMS data, have identified the different kelvin wave modes propagating in the tropical stratosphere. The results of Hitchman and Leoves (1988) based on the LIMS data showed that Kelvin waves are apparently too weak to fully drive the westerly phase of SAO. Randel and Gille (1991) using solar backscatter ultraviolet (SBVV) retrievals, obtained 8 year ensemble mean power spectra of the Ozone field at 3 and 0.5 h Pa, which are consistent with the LIMS result. Hamilton and Malhman (1988) using a general circulation model reached similar conclusions. The mechanisms associated with the excitation of Mixed-Rossby Gravity waves in the upper troposphere were studied using wind and outgoing long wave radiation (OLR) by Magana and Yanai (1995). Tsuda et al., (1994) detected Kevin waves with period of about 7 and 20 days in the lower stratosphere using radiosonde data over Indonesia.

Substantial effort has been made over the past two decades to delineate the wave mode present over the Indian tropical region (Devrajan et al., 1985; Kumar and Nagpal, 1985; Krishnamuthy et al.,1986; Nagpal et al.,1994; Dhaka et al.,1995)

using a number of time-series analysis based on radiosonde data. Theoretically, other waves modes can also exist over equatorial latitudes. These include inertia-gravity modes, Rossby modes and higher order Kelvin modes though observational evidence in respect of these wave modes is rather limited. Sensitive VHF Doppler radars are used to study the atmospheric wind field. During the past decade or so, there has been a rapid increase in the measurements of wind field by the MST radar and wind profiler networks.

The Indian MST radar should offer an excellent opportunity for the study of the dynamics of the tropical middle atmosphere, by virtue of its unique location. This chapter describes the seasonal aspects of the generation of the equatorial waves using large data base of Indian MST radar first time. This chapter not only explorer the possibility of using Indian MST radar to detect the equatorial wave but also describes.

5.4 DATA AND METHOD OF ANALYSIS

The Indian MST radar located at Gadanki (13.5^oN, 79.2^oE) is a high power VHF phased array radar operating at ~ 53 MHz in coherent backscatter mode with an average power aperture product of 7×10^8 W m^2 . The total transmitter power is 2.5 MW. The radar beam can be scanned in the North-South and East-West planes. More detailed specifications of the radar system are given by Rao et al. (1995).

Observations of the winds in the 3-20 km height region for the period from 1 December 1995 to 31 March 1996 (winter) and 1 June96 to 31October 1996 (monsoon) was done daily (around 1700 hr) using Indian MST radar at Gandanki. Total more than 300 days daily wind (around 1630 -1700 hrs IST , i.e. half an hour data or around 1630-1730 hrs IST, i.e one hour data) observations of two different seasons is utilised. For this observation the following radar configuration was used: pulse repetition frequency = $1000s^{-1}$; pulse width = 16 ms coded with baud length of 1 ms; number of coherent integration = 128; number of beams = 6 (two zenith beams and four 10° off zenith beams in the North, East, South and West directions); number of incoherent integration = 4. Daily Doppler spectra corresponding to the six beams, with a vertical resolution of 150m, were first converted to line-of-sight (LOS) wind profiles. From these daily vertical profiles of LOS winds corresponding to the six beams, the zonal (u), meridional (v), and vertical (w) components of the daily winds were derived using least -squares technique assuming a vertical wind contribution to the LOS profiles (resolution of 150 m) of u,v and w are obtained.

There exists a few gaps in the time series which are filled by using a cubic spline method. A continuous time series is thus obtained in two different seasons (winter and monsoon). The length of the of the time series in the study of equatorial waves (i.e Kelvin and MRG) is 120 days for winter and 128 days for monsoon.

The data length is sufficient for the study of RG waves (3-5 day period), slow Kelvin waves (10-20 day period) and long period waves(30-45 days). In order to identify the wave periods and their respective amplitudes and phases at different heights, the data are first subjected to a numerical low pass filter which removes periods less than 3-days. The data are then reduced to zero means to eliminate any linear trend. Weights of a Cosine Bell window are applied to first and last 10 % of the individual data sets so that the end regions have smooth transitions to the mean of the measured value, which lessen the effects of discontinuties during spectral estimation (Kumar et al. 1994). The weights are defined by

$$W(x) = \frac{1}{2} \left[1 - \cos\left\{\frac{px}{fL}\right\} \right]; \qquad fL \le x \le L(1-f)$$

$$W(x) = 1; \qquad 0 \le x \le fL$$

$$W(x) = \frac{1}{2} \left[1 - \cos\left\{ p - \frac{L-x}{fL} \right\} \right]; \quad L(1-f) \le x \le L$$

Where L is the length of the data and f is the desire fraction (usually 0.1). The filtered data are then subjected to Fast Fourier Transform (FFT) analysis to obtain different periodic components of the winds at every km. The amplitudes and phases of dominant periodic components are obtained by FFT.

5.5 RESULTS AND DISCUSSION

Figures 5.2 and 5.3 represents the wind data (3-day running average) of the zonal and meridional components in winter (December 1995-March 1996) and monsoon (June-October 1996) seasons respectively. In Figure 5.2 on the x-axis, day number 1 corresponds to 3 December 1995 (winter) and in Figure 5.3 on the x-axis, day number 1 corresponds to 15 June1996 (monsoon). In these Figures the zonal and meridional winds at each height (the number on the right hand side of the curves represent height) are displaced along the Y-axis. The wind magnitude scale is shown alongside. The following are the general features that can be discerned from these figures.

1. Strong wave activity can be noticed in the zonal and meridional wind plots in the entire troposphere region (i.e. between 7-17 km) in both the seasons.
2. The amplitudes of both the components (i.e. zonal and meridional) are comparable in winter, while in monsoon the zonal component shows stronger wave activity than the meridional component.
3. Short (4-6 days), medium (10-16 days) and long period (20-30 days) oscillations are clearly visible in both seasons.

December 1995 - March 1996
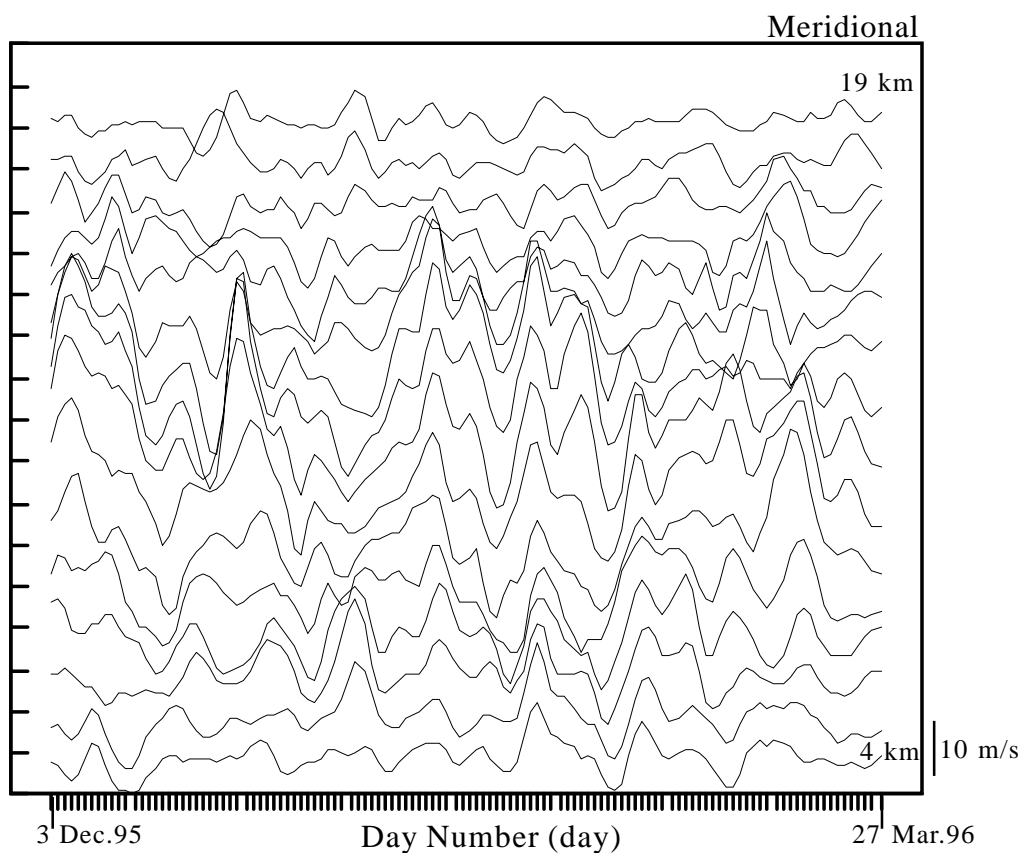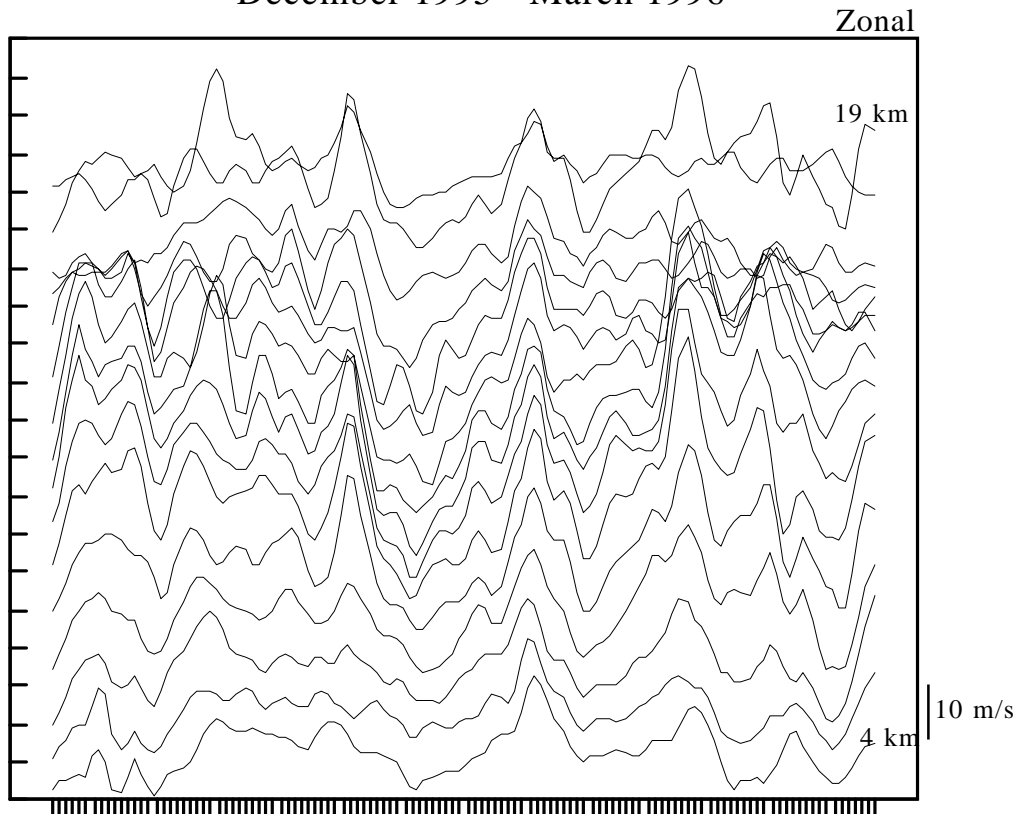
Fig.5.2 : Zonal (Top panel) and meridional (bottom panel) wind plots as a function of
day number, displaced vertically over Gadanki (4-19 km). The wind magnitude
scale is shown at the bottom right handside corener of the figures.
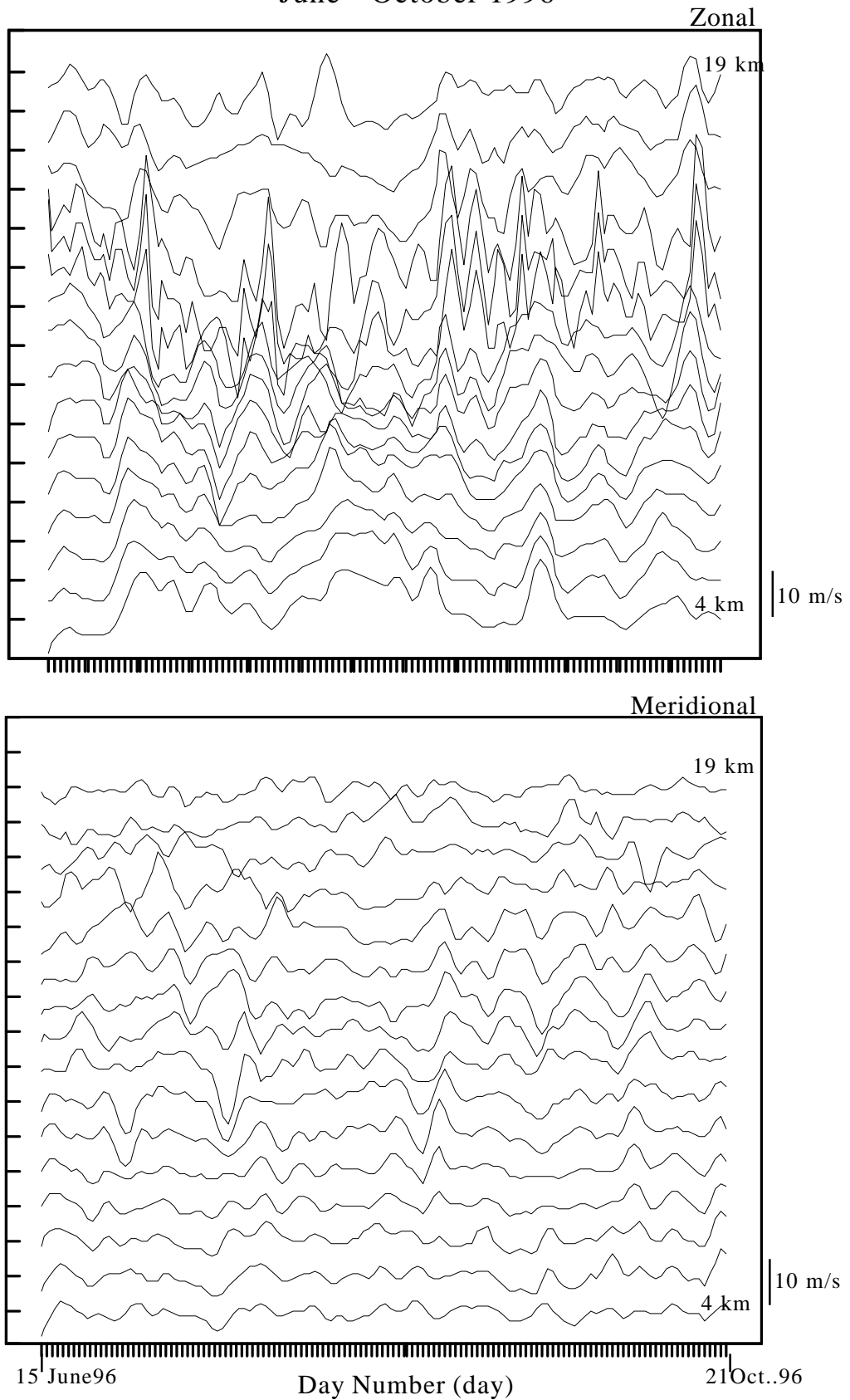
Fig.5.3 : Zonal (Top panel) and meridional (bottom panel) wind plots as a function of day number, displaced vertically over Gadanki (4-19 km). The wind magnitude scale is shown at the bottom right handside corener of the figures.

The mean zonal and meridional wind height profiles for both the seasons are shown in Figure 5.4. Considering first the zonal component (left top panel in Figure-5.4), in winter season westerlies prevail throughout the given altitude range, while during monsoon mean zonal wind (left bottom panel in Figure-5.4) shows weterlies below 7 km and easterlies above 7 km. Examining the mean meridional wind during winter (right top panel in Figure-5.4), it is seen that mean meridional wind is northerly below 8 km and southerly above 8 km. While during monsoon the mean meridional wind (right bottom panel in Figure-5.4) is alternating northerlies and southerlies in given altitude range.
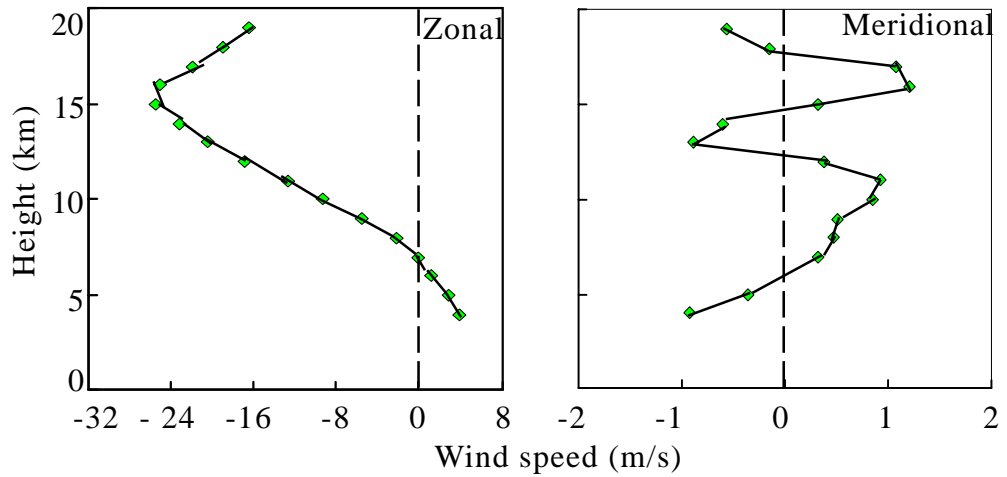
Equatorial waves are believed to originate in the troposphere and their momentum flux may be modulated by monsoonal activity. The Indian summer monsoon sets in over the Kerala coast generally between May 20 and June 10 the most probable occurrence being June1. The zonal winds which are weak easterly/westerly during the preceding winter reverse their direction and become easterly a few days prior to the onset of monsoon. The zonal component in Figure 5.4. (right top panel) shows that strong easterlies prevail at the altitude range 7-15 km. This easterly wind regime is conducive for the propagation of Kelvin waves and hence is easily detectable during this period.

Figures 5.5 and 5.6 shows the contour plots of the spectral amplitudes obtained after FFT in the altitude-period plane for the zonal and meridional winds. In general, the amplitudes of zonal wind oscillations are greater than those of meridional wind oscillation in the entire altitude range as can be seen from Figures 5.5 and 5.6. It is seen from Figure 5.5 (winter) dominant oscillations in the zonal wind (top panel) is seen between ~ 10-14 km altitude region. These oscillation are centered around 8-12, 12-16 and 24-28 days periods. The amplitudes corresponding to these oscillations decrease significantly at about ~17 km altitude region. It can also be noticed that amplitude attenuation is much less for smaller periods such as 8-12 and 12-16 days oscillations as compared to that for longer period oscillations (i.e.24-28 days). While in meridional wind (bottom panel in Figure 5.5) prominent oscillations are seen at ~ 10-12 km altitude region with periods centered around 16-20 days. However, other periods (8-12 and 12-16 days) are also clearly visible at different heights. Figure 5.6 (monsoon) shows that dominant oscillations in the zonal wind (top panel) are seen at lower troposphere (i.e. at ~ 4-6 km) with period 24-28 days, this period is again become significant at lower stratospheric height (i.e. at 18 km). This is indicative of two excitation regions for this wave period. The wave period with ~ 12-16 days is also clearly visible at almost tropopause height (i.e. at ~ 16 km) in the zonal wind. The prominent oscillations centered around 8-12, 16-20 and 24-28 days periods at different altitude are seen in the meridional component during monsoon (bottom panel in Figure5.6).

December 1995 - March 1996 (winter)
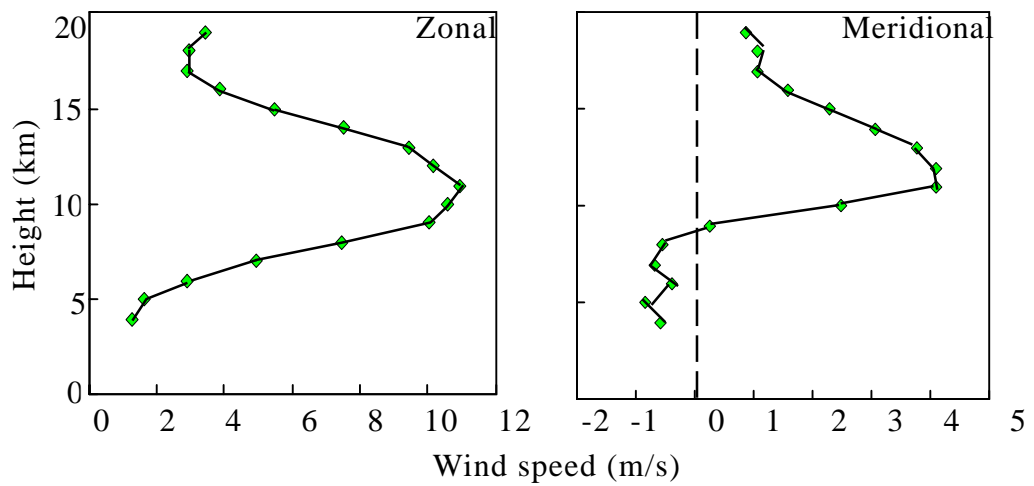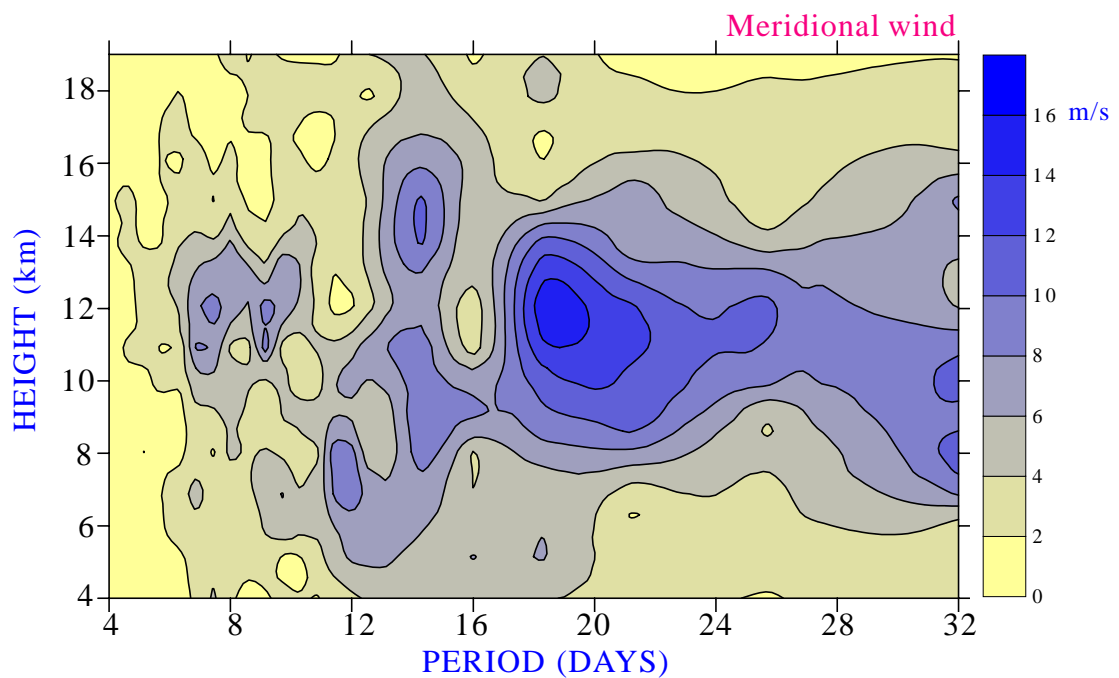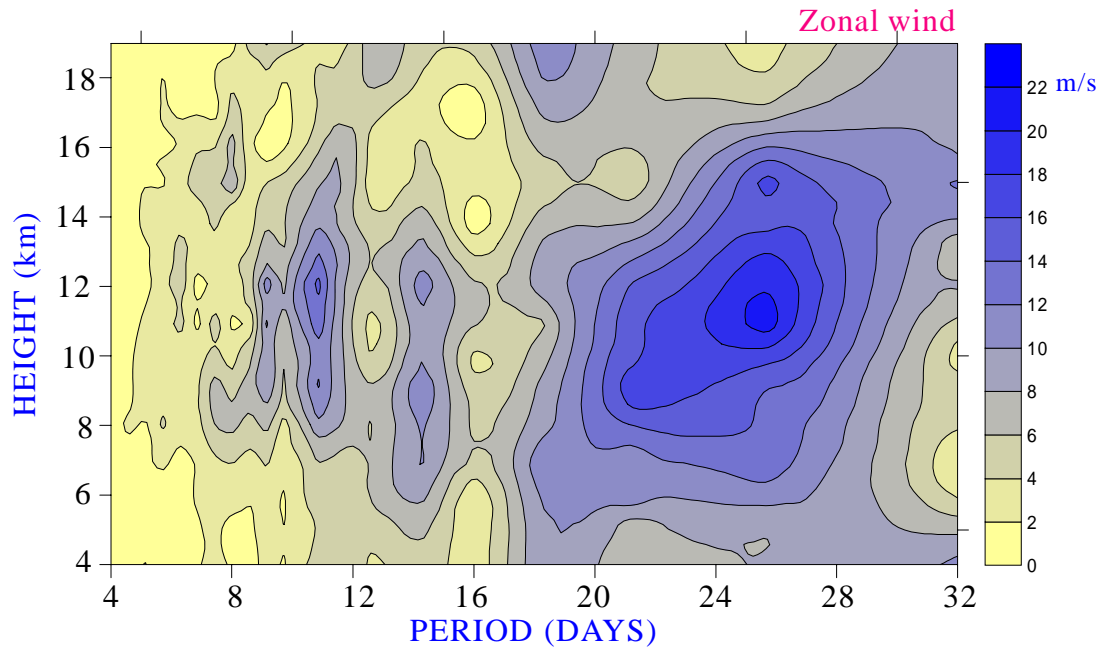
June - October 1996 (monsoon)

Fig.5.4 : Mean zonal and meridional components as a function of altitude.

Fig.5.5 : Amplitude spectrum of zonal (top panel) and meridional (bottom panel) wind oscillations in the 4-20 km altitude range over Gadanki (13.5°N, 79.2°E).
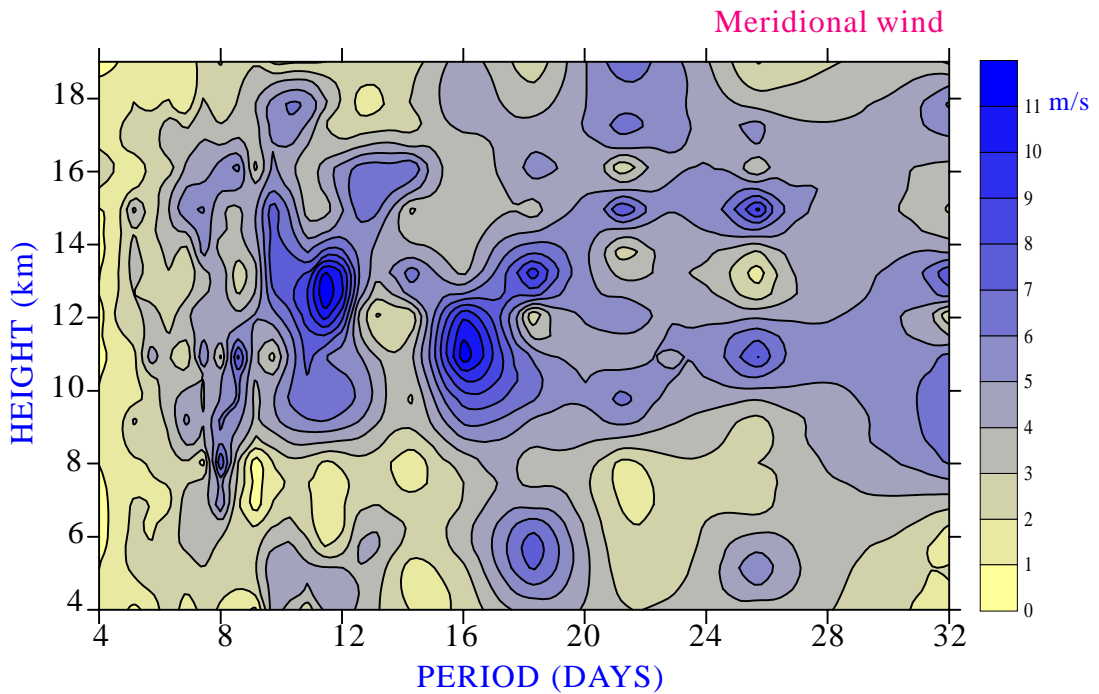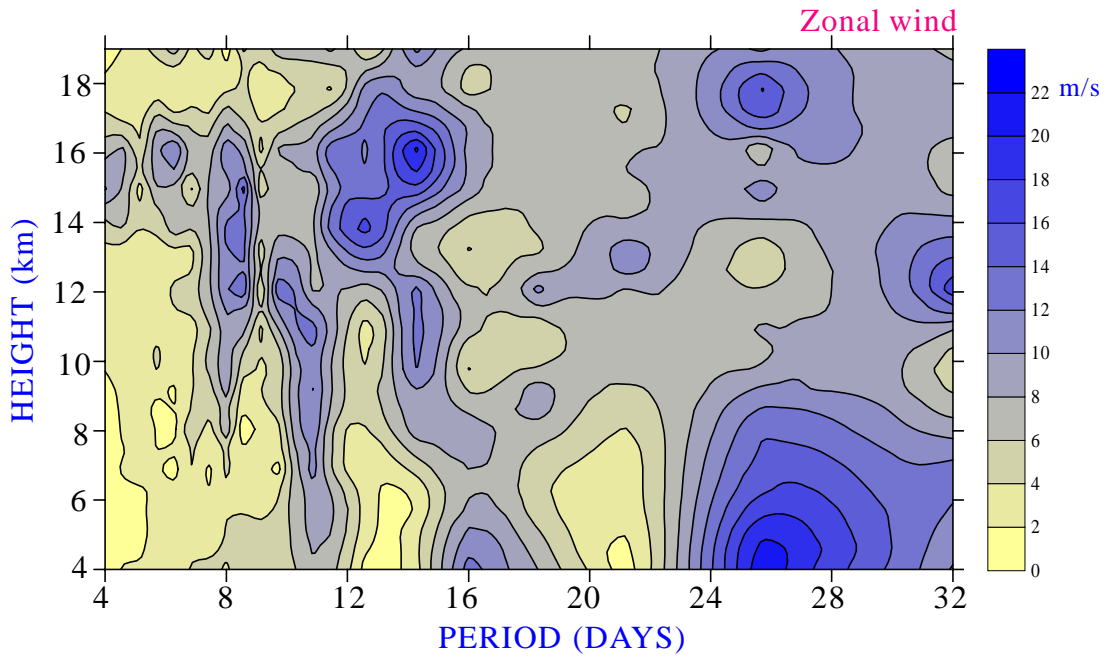
Fig.5.6 : Amplitude spectrum of zonal (top panel) and meridional (bottom panel) wind oscillations in the 4-20 km altitude range over Gadanki (13.5°N, 79.2°E).

In order to see whether the observed oscillation of winds in different periods belongs to the theoretically known equatorial wave modes, the vertical structure of the phases and amplitudes of the oscillations for different periods are examined. Figures 5.7 and 5.8 shows the height structures of the spectral amplitudes and phases of the zonal and meridional components only for selected periods. These periods are 4.4, 5.8, 12.8, 14.2, 21.3 and 25.6 day. From Figure 5.7 it is seen that in the zonal wind, 25.6 and 21.3 day periods (left top panel) are dominant than other periods with almost steady phase progression. This indicates that there is no significant vertical propagation of the disturbances and is quite similar to previously observed by Krishana Murthy et at., (1986) in summer for long period oscillations during Indian Middle Atmosphere Programme (IMAP). The downward phase progression is seen for 5.8 day period between 4-14 km and is indicative of upward energy propagation. In meridional wind (Figure 5.7) during winter 21.3 day period is more dominant and shows downward phase progression below 8 km and remains almost steady above 8 km.

It is seen from Figure 5.8 that the zonal component with period 25.6 day shows very large amplitude at ~ 4 km and decreases with height up to 13 km. The downward phase propagation in this period, between 4-13 km altitude region is seen and indicates upward energy propagation. On examining the amplitude of the zonal component with periods 12-16 day (i.e. 14.2 day and 12.8 day periods) it is seen that, (i) very large amplitude near 15 km without any corresponding significant oscillation in the meridional component and (ii) clear down ward phase propagation in the lower stratosphere in zonal wind.   These characteristics suggest that the observed waves are kelvin waves with period 12-16 days.

 It is interesting to note here that, during monsoon (Figure 5.8) the zonal wind amplitudes corresponding to prominent periods of oscillation reach their maximum amplitudes at altitude near the levels where the prevailing easterlies show a peak (Figure 5.4) and again indicates that the zonal wind oscillations are due to Kelvin mode. It may be noted that Holton (1982a) and Salby and Garcia (1987) showed from simulation studies that vertical wavelengths of the equatorial waves are related to the vertical extent of the heating region responsible for their generation. Thus the origin of the Kelvin waves appears to be from an extended region in the troposphere. Devarajan et al.,(1985) reported rocket observations of Kelvin waves in the upper stratosphere over India based on the data from Trivandrum using M-100 rockets and from Balasore using RH-200 rockets. The zonal wind variance due to these waves was large during the easterly phase of AO and SAO.

The presence of westerlies in the troposphere especially in winter season (Figure 5.4) makes it conducive for the presence of Rossby waves. The Rossby waves originate in the extratropical regions and penetrate deep into the tropics, Webster and Holton (1982) and Webster and Chang (1988) show that Rossby waves
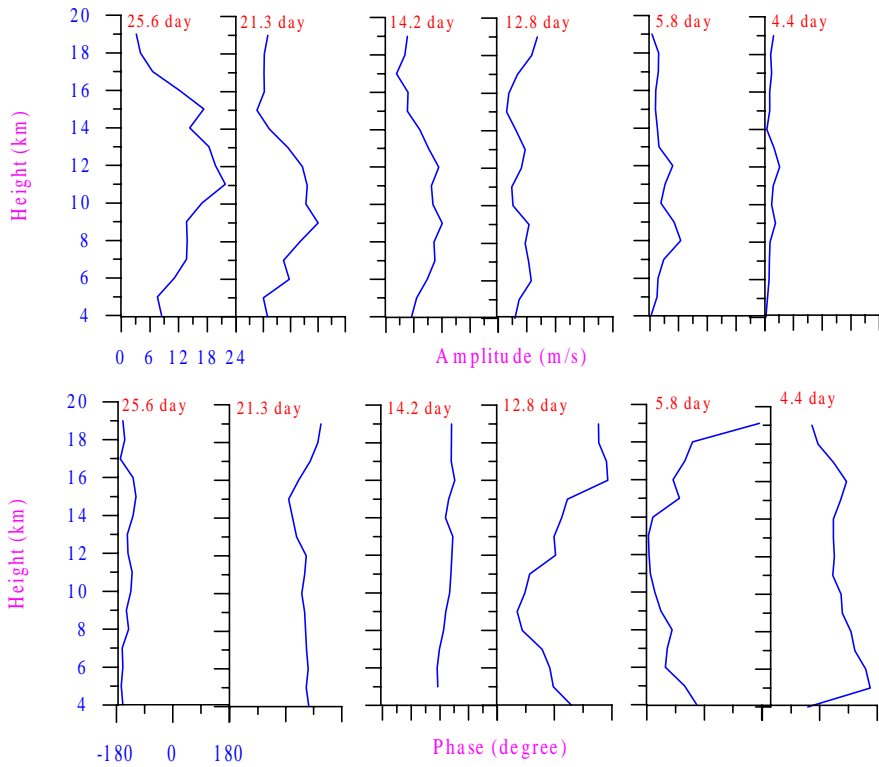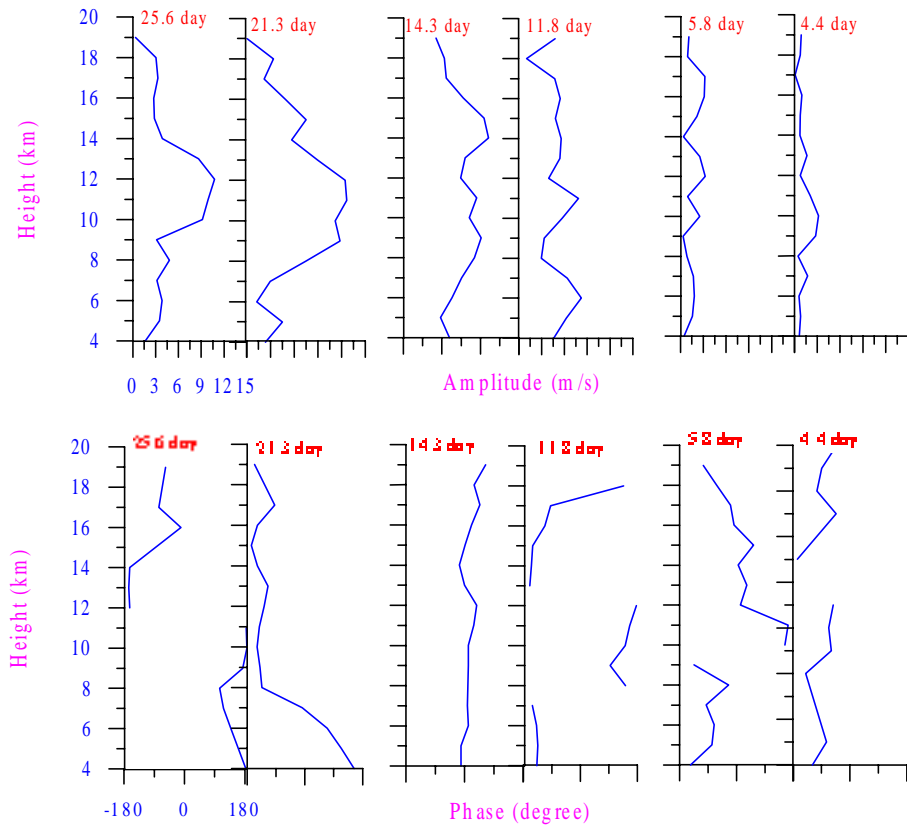
Fig.5.7 : Height profiles of spectral amplitudes and phases for 25.6, 21.3, 14.2, 11.8, 5.8 and 4.4 day periods waves in the zonal and meridional wind over Gadanki.
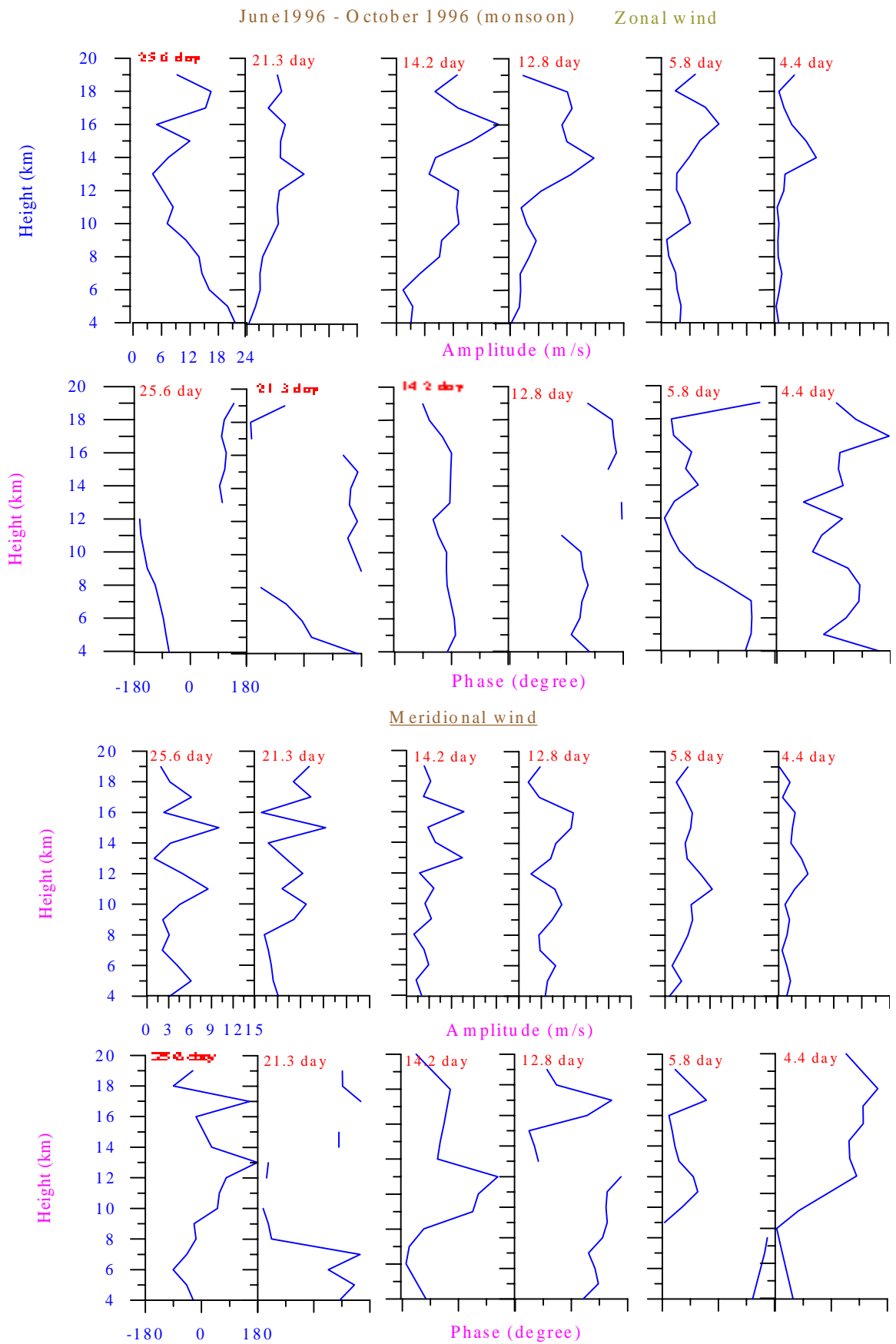
Fig.5.8 : Height profiles of spectral amplitudes and phases for 25.6, 21.3, 14.2, 11.8, 5.8 and 4.4 day periods waves in the zonal and meridional wind over Gadanki.

can indeed propagate from mid-latitudes deep into tropical latitudes as long as the mean zonal wind is westerlies in the troposphere. The kelvin and Rossby -gravity modes are thought to be generated by heating occurring in large-scale convective complexes (cloud clusters) in the equatorial zone. The model of Chang (1976) showed that randomly distributed sources most efficiently excite the longest zonal-scale Kelvin waves, and that the preferred vertical wavelength of the excited waves is about twice the vertical scale of the heat source.

5.6 SUMMARY AND CONCLUSIONS

The results of the analysis shows that in different seasons the Indian tropical region is dominated by equatorial waves of different periods. Result obtained from the analysis of the data leads to the identification of strong wave activity between 12 and 16 km in the troposphere. This feature is seen in Figures 5.2. and 5.3. During winter (December 95- March 96), the entire height region in the zonal wind is dominated by westerly (Figure 5.4) winds, which is conductive to MRG waves. While during monsoon (June-October 96) the altitude region (i.e. 7-19 km) is dominated by easterly winds (Figure 5.5). These background easterly winds are conducive for the propagation of Kelvin wave mode.

In general, in this study of equatorial waves, the waves with periodicities (i) 4-6 days, (ii) 8-12 days, (iii) 12-16 days and (iv) 24-26 days are detected during winter and monsoon over Gadanki. Particularly Kelvin waves with period 12-16 days are detected with some of its properties and excitation region during monsoon. Although, short wave periods like MRG waves and other longer period waves are also detected but no consistent phase pattern is found. Hence to confirm and find out the exact wave period comparison with numerical models and other observed data are needed that may leads to feature work. It is worthwhile to mention here that a major capability of the MST radar is the measurements of vertical wind which enables estimation of wave momentum flux, an important parameter in the characterization of the waves. By making use of the vertical wind data to estimate wave momentum fluxes is also consider as further feature work.

In addition to this, we have found some other interesting features of this study which is explained as below :

1. The equatorial waves can propagate both in vertical and horizontal directions by carrying energy and momentum from source region to other regions, thus playing significant role in dynamical coupling process of different regions of the atmosphere. The vertical propagation of these waves may, sometimes, effect the height of stable regions such as tropopause, which is characterized by the hydrostatic stability. It may mention here that considerable decay in amplitude is seen for long periods (24-28 days) near tropopause (~ at 16 km) in both, zonal and meridional wind during winter (Figure5.7). Also Y Jaya Rao and Jain (2000) reported a rapid

attenuation in the amplitudes for longer periodocities in zonal and meridional oscillations over Gadanki during winter.

2. In low latitudes, there is a region of wind discontinuity with horizontal velocity convergence and upward vertical motion at lower levels of troposphere and horizontal divergence at upper levels. This region is called the Inter-Tropical Convergence Zone (ITCZ). The ITCZ plays a pivotal role in the interhemispheric transport of trace gases and aerosols. From Figure 5.4 it is seen that the mean zonal wind during monsoon (left bottom panel) is east ward (westerly) below 7 km and reverses above this altitude, means no complete reversal to westward (easterly) direction. Which may be a indicative of ITCZ over Gadanki. Recently Krishnamurthy et al., (2000) have also reported , singnature of ITCZ over Gadanki during monsoon season.

SUMMARY & CONCLUSION

Summary and conclusions

The main objective of this thesis is to study tides and equatorial waves in the middle atmosphere. The results are out lines in the three chapters. The detailed discussion are already outlined at the end of each chapters. However some points are listed here for the completion.

Using the 11 diurnal cycles spread over the different seasons are used to study the tidal oscillations and its characteristics. On general it is observed that the amplitude is always grater than the theoretically estimated. During monsoon season the amplitude of tidal oscillations is observed to be larger than that in winter and summer. The downward/upward phase (upward/downward energy) propagation from lower atmosphere (i.e. at 4 km) and from troposphere is found and is indicative of two sources, i.e. one at ground level and one may in the troposphere.

For the study of momentum flux total 8 diurnal cycles of different seasons are utilized To find density weighted momentum flux, the atmospheric density is derived from the meteorological data obtained from near by station Madras. Significant momentumflux is observed during monsoon, while during other seasons momentum flux shows more or less similar values.

The equatorial waves play dominant role in mean zonal flow and QBO and SAO. The MST radar observations from December 1995 to March 1996 and June to October 1996 used to study detect and characterized the equatorial waves. The waves ranging in the period from 4-6 day to 26 days are detected during the monsoon and winter seasons over Gadanki. During monsoon season the entire region of altitude about 20 km is dominated by Kelvin waves with a period 12-16 days. While in winter both the MRG waves (4-5 days) and Kelvin waves have comparable amplitudes. The downward progression of these waves is indicative of upward energy propagation. It is interesting to note here that during monsoon the zonal wind amplitudes corresponding to prominent period of oscillations reach their maximum amplitudes at altitude near the levels where prevailing easterly show a peak and again indicates that the zonal wind oscillations are due to Kelvin waves. The present of westerlies in the troposphere specially in the winter season make it conducive for the present of Rossby waves.

In low latitudes, there is a region of wind discontinuity with horizontal velocity convergence and upward vertical motion at lower levels of troposphere and horizontal divergence at upper levels. This region is called the Inter-Tropical Convergence Zone (ITCZ). The ITCZ plays a pivotal role in the interhemispheric transport of trace gases and aerosols.

From Figure 5.4 it is seen that the mean zonal wind during monsoon (left bottom panel) is east ward (westerly) below 7 km and reverses above this altitude, means no complete reversal to westward (easterly) direction. Which may be a indicative of ITCZ over Gadanki. Recently Krishnamurthy et al., (2000) have also reported , singnature of ITCZ over Gadanki during monsoon season.

Once the equatorial waves with different period are detected, the energy carried upwards by these waves can be estimated. This will lead to better understanding of the dynamics of the middle atmosphere through coupling processes. This is proposed for the extension of the present thesis.

The study on the tidal oscillation, momentum flux and the equatorial waves presented in the thesis shows the capability the Indian MST radar. The limitations of the conventional experiments are superseded by the MST radar with its high time and height resolutions. The radar provides continuous observations, where as the same with other technique is nonfeasible. Particularly if one wants to study the equatorial waves, the MST radar is perhaps only tool.

REFERENCES

Authors	Year	Journal
Anadaan, V. K.	1997	Technical and user refereence. manual, NMRF, Triupti.
Angell, J. K., Cotton, G. F. and Korshover. J.	1973	J. Atmos. Sci., **30**, 13.
Balsley, B. B. and Farley, D. T.	1976	Geophys. Res. Lett., **3**, 525.
Balsley, B. B. and Gage, K. S.	1980	J. Pure Appl. Geophys., **118**, 452.
Basley, B. B. and K. S. Gage	1982	Bull. Amer. Meteor. Soc., **63**, 1009.
Battan, L. J.,	1973	The university of Chicago press, Chicago, **l,** 324pp.
Boville, B. A. and Randel, W. J.	1991	J. Atmos. Sci., **49**, 785.
Bowles, K. L.	1958	Phys. Rev. Lett., **1**, 454.
Brasseur, G. Derudder, A., Keating, G. M. and Pitts, M. C.	1978	J. Geophys. Res., **92**, 876.
Briggs, B. H.	1980	J. Atmos. Terr. Phys., **42**, 823.
Cadet,D. and Teiltelbaum. H.	1979	J. Atmos. Sci., **36**, 892.
Cess, R. D. et. al.	1995	Science, **267**, 496.
Chang, C.	1976	J. Atmos. Sci., **35**, 740.
Chapman, S. and Lindzen, R. S.	1970	D. Reidel, 200.
Coy, L. and Hitchman, M.	1984	J. Atmos. Sci., **41**, 1875.
Crane. R. K.	1980	Radio Sci., **15**, 177.
Devarajn, M., Reddy, C. A., and Reddy, R.	1985	J. Atmos. Sci., **42**, 1873.
Dhaka, S. K., Krishna Murthy, B.V., Nagpal, O. P., Raghava Rao, R., Sasi, M. N. and Sundaresan, S.	1995	J.Atmos. Terr. Phys., **57**, 1189.

Doviak, R. J., Zrnic, D.S. and Sirmans, D. S.	1979	Proc. TEEE, **67**, 1522.
Eliassen, A., and Palm, E.	1960	Geofysiske publikasjoner (oslo), **22**, 23.
Ekanayake E. M. P., ASO, T.	1997	J. Atmos. Sol. Terr. Phys., **59**, 401.
Farely, D. T. Balsley, B. B., Swartz, W. E. , and LaHoz, C.	1979	J. Appl. Meteorol., **18**, 227.
Flock, W. L. and Balsely, B. B.	1967	J. Geophys. Res., **72**, 5537.
Forbes, J. M., and Goves, G. V.	1987	J. Atmos, Terr. Phys., **49**, 153.
Forbes, J. M., and Gillette, D. F.	1982	Rep. AFGL - TR - 82 -173 (i) Airforce Geophys. Lab, Hanscom AFB, Mass.
Forbes, J. M. and Garett., H. B.	1979	Rev. Geophys. Space Phys., **17**, 1951.
Forbes, J. M.	1985	Map Handbook, **16**, 278.
Fritts, D. C. and Vincent R. A.	1987	J. Atmos. Sci., **44**, 605.
Fritts, D. C., Tsada, T. Vanzandt, T. E., Smith, S. A., Sato, T., Fakao, S., and Kato, S.	1990	J. Atmos. Sci., **47**, 51.
Fritts, D. C., Yuan, L., Hitchman, M. H., Coy, L., Kudeki, E., and Woodman, R. F.	1992	J. Atmos, Sci., **49**, 2353.
Fukao, S., Kato, S., Yokoi, S., Harper. R. M., Woodman, R. F., Gordon, W. E.	1978	J. Atmos. Terr. Phys., **40**, 1331.
Fukao, S., Sato, T. Yamasaki, N., Harper, R. M., and Kato, S.	1980	J. Atmos. Sci., **37**, 2540.
Fukao, S. Sato,T., Tsuda, T., and Kato, S.	1988	J. Atmos and Oceanc Techn. **5**, 57.
Fukao S., Aoki K., Wakasugi, K., Tauda, T., Kato, S., and Fleisch, D. A.	1981	J. Atmos. Terr. Phys., **43**, 649.
Gage, K. S. and Balsey, B. B.	1978	Bull. Amer. Meteor. Soc., **59**, 1074.
Gage, K. S. and Balsley, B. B.	1980	Radio Sci., **15**, 243.

Gage, K. S. and Vanzandt, T. E.   1981   J. Geophys. Res., **86**, 9591.

Gage, K. S. and W. L. Clark   1978   Radio Sci., **13**, 991.

Gage, K. S.   1979   J. Atmos. Sci., **36**, 1950.

Groves, G. V.   1980   Philos. Trans. R. Soc. London, Ser. A., **296**, 19.

Hamilton, K., and Mahlman, J. D.   1988   J. Atmos. Sci., **45**, 3213.

Harper, R. M. and Garden, W.E.   1980   Radio Sci., **15**, 195.

Haurwitz, B.   1965   Archiv. Meteor, Geophys. Biokl, A14, 361.

Hayashi, Y., and Golder, D. G.   1978   J. Atmos. Sci., **35**, 2068.

Hildebrand, P. H. and
    Sekhon R. H.   1974   J. Appl. Meteorol, **13**, 808.

Hitchman, M. H., Bywaters,
    K. W., Fritts, D. C.
    Coy, L. Kudeki, E., Surucu, F.,
    and Woodman, R. F.   1992   J. Atmos. Sci., **49**, 2372.

Hitchman, M. H. and Leovy, C. B.   1988   J. Atmos. Sci., **45**, 1462.

Hirota, I.   1978   J. Atmos. Sci., **35**, 714.

Hirota, I. Shiotani, M. Sakurai,
    T., and Gille, J. C.   1991   J. Meteorol. Soc., Jpn., **69**, 179.

Hocking W. K.   1985   Radio Sci., **20**, 1403.

Hogg, D. C. Decker, M. T.
    Guiraud, F. O., Earnshaw, K. B.,
    Merritt, D. A., Moxan, K. P.,
    Sweezj, W. B., Strauch, R. G.,
    Weswater, F. R., and Little, C. G.   1983   J. Climate Appl. Meteor., **22**, 807.

Holton, J. R.   1975   Meteorol. Monogr. 37, Ams. Boston 218.

Holton, J. R.   1982   J. Atmos. Sci., **39**, 791.

Holton, J. R. and Lindzen R. S.   1972   J. Atmos. Sci., **29**, 1076.

Holton, J. R.   1982a   D, Reidel, Norwell, Mass. 1982.

Holton, J. R.   1972   J. Atmos. Sci., **29**, 368.

Hong, S. S. and Lindzen, R. S.   1976   J. Atmos. Sci., **33**, 135.

Hood   1978   J. Geophys. Res., **92**, 839.

Iyer, K. N. Joshi, H. P. and Jivrajani, R. D.	1994	Ind. J. Radio and Space Phys. **23**, 52.
Jain, A. R. Jaya Rao, Y. Rao, P. B., Anandan, V. K., Damle S. H., Balamusalldhar, P. Kalkarni Anil and Viswarnthan, G.	1995	Radio Sci., **30**, 1139.
James, P. K.	1980	Radio Sci., **15**, 151.
Jani, Y. N. Joshi, H. P. and Iyer, K. N.	2000	Ind. J. Radio and Space Phys., **29**, 210.
Jivrajani R. D. Iyer, K. N. and Joshi, H. P.	1997	Ind. J. Radio and Space Phys., **26**, 141.
Jaya Rao, Y. and Jain, A. R.	2000	Ind. J. Radio and Space Phys., **29**, 203.
Jenson, E. J. Toon, O. B. Selkirk, H. B., Spinhirne, J. D., and Schoeberi, M. R.	1996	J. Geophys. Res., **101**, 21361.
Kato, S. Tsuda, T., and Watanabe, F.	1982	J. Atmos, Terr. Phys., **44**, 131.
Klostermeyer, J.	1981	Nature **292**, 107.
Kousky, V. E. and Wallace, J. M.	1971	J. Atmos. Sci., **28**, 162.
Krishna Murhy B. V., Prabhakaran Nayar, S. R. Revathy, K. Mridula, G., Satheesan, K., and Jain, A. R.	2000	Ind. J. Radio and Space Phys., **29**, 199.
Krishna Murthy, B. V., Indukumar, S., Reddi, C. R., Raghava Rao, R., and Rama, G. V.	1986	Ind. J. Radio and Space Phys. **15**, 125.
Kumar, K. and Jain A. R.	1994	J. Atmos. Terr. Phys. **56**, 1135.
Kumar S. and Nagpal, O. P.	1985	Scientific Rept. ISRO - IMAP - SR- 25, ISRO HQ Bangalore.
Lamb, V. R.	1973	Ph. D. thesis, University of Calfornia, Los Angeles, 151pp.
Larsen, M. F. and J. Rotteger	1982	Bull. Amer. Mateor. Soc., **63**, 996.
Larsen, M. F.	1983a	Workshop on Techn. Aspects of MST radar 23-27 may 1983 Univ. of Illionois, Urbana,

Larsen, M. F. 1983b Workshop on Techn. Aspects of Mst Radar 23-27 May 1938, Univ. of Illionis, Urbana.

Larsen, M. F., Kelley, C. M., and Gage K. S. 1982 J. Atmos. Sci., **39**, 1035.

Lhermitte, R. M., and Atlas, D. 1963 Proc, 10th Weather Radar Conference Washington, D. C. AMS, Boston, 297.

Lhermitte, R. M. 1979 Rev. Geophys. Space Phys., **17**, 1833.

Liberman, R. S. and Leovy, C. B. 1995 J. Atmos. Sci., **52**, 389.

Lindzen, R. S. 1981 J. Geophys. Res., **86**, 9707.

Lindzen, R. S. 1978 Mon. Wea. Rev., **106**, 526.

Lu, M. M. 1987 Ph. D. thesis University of California, Los Angeles, 328pp.

Magana, V., and Yanai, M. 1995 J. Atmos. Sci., **52**, 1473

Mak, M. K. 1969 J. Atmos. Sci., **26**, 41.

Mapes, B. E. 1993 J. Atmos. Sci., **50**, 2026.

Maruyama, T. 1967 J. Meteor. Soc. Jpn., **45**, 391.

Matsuno, T. 1982 J. Meteorol, Soc. Jpn., **60**, 215.

Matsuno, T. 1966 J. Meteorol. Soc. Jpn., **44**, 25

Mckenzie,D. 1968 Ph. D. thesis Univ. of Wash., Seattle,

Miyahara. S., Yoshida, Y., and Miyoshi, Y. 1993 J. Atmos. Terr. Phys., **55**, 1039.

Nagpal, O. P., Dhaka, S. K. and Srivastav, S. K. 1994 J. Atmos. Terr. Phys., **56**, 1117.

Narayan Rao, D., Kishore, P., Narayan Rao, T., Vijaya Bhaskara Rao, Krishna Reddy, K. Yarraih, M. and Hareesh, M. 1997 Radio Sci., **32**, 1375.

Nastrom, G.D. and Belmont, A. D. 1976 J. Atmos. Sci., **33**, 315.

Pfister, L., Starr, W. Craig, R. and Lowenstein, M. 1986 J. Atmos. Sci., **43**, 3210.

Plumb, R. A. and Bell, R. C. 1982 Quart. J. Roy. Meteroal, Soc., **108**, 313.

Ramanathan, V., Subasilar, B., Zhang, G. J. Conant, W., Cess, R. D., Kiehl, J. T., Grassl, H., and Shi, L. 1995 Science, **267**, 499.

Randel, W. J. and Gille J. C. 1991 J. Atmos. Sci., **48**, 2336.

Randel, W. J. 1990 J. Geophys. Res. Sci., **95**, 18641.

Rao, P. B., Jain, A. R., Viswanathan, G. and Damle, S. H. 1994 Ind. J. Radio and Space Phys., **23**, 1.

Rao, P. B., Jain, A. R. Kishore, P. Balamuralidhar, P., Damle, S. H.,and Viswanathan, G. 1995 Radio Sci., **30**, 1125.

Rastogi, P. K. 1981 J. Atmos. Terr. Phys. **43**, 511.

Reid, I. M., and Vincent R. A. 1987 J. Atmos. Terr. Phys., **49**, 443.

Roble, R. G. Richmond, A. D., Oliver, W. L. and Harper, R. M. 1978 J. Geophys. Res. **83**, 999.

Rottger, J. and vincent, R. A. 1978 Geophys. Res. Lett. **5**, 917.

Rottger, J. 1980 Radio Sci., **15**, 259.

Rottger, J. 1980a J. Pure Appl. Geophys. **118**, 494.

Salby, M. L., Hartmann, D. L. Bailey, P. L. and Gille, J. C. 1984 J. Atmos. Sci., **41**, 220.

Salby, M. L., Callaghan, P., Solomon, S. and Garcia, R. R. 1990 J. Geophys. Res., **95**, 20491.

Salby, M. L., and Garcia, R. R. 1987 J. Atmos. Sci., **44**, 458.

Sasi, M. N. Geetha R., and Deepa V. 1998 J. Geophy Res., **103**, 19485.

Sasi, M. N., Lekshmi Vijayan, Deepa, V. and Krishna Murthy, B. V. 1999 J. Atmos, Terr. Solar Phys., **61**, 377.

Sasi, M. N., and Krishna Murthy, B. V. 1990 J. Atmos. Sci., **47**, 2101.

Sasi, M. N., and Krishna Murthy B. V. 1993 J. Geomagn. Geoelectr. **45**, 547.

Sato, K. 1990 J. Atmos. Sci., **47**, 2803.

Sato, T., and Woodman R. F. 1982 J. Atmos. Sci., **394**, 2539.

Sato. T. 1989 MAP Hand book, **30**, 19.

Smith, S. A., Fritts, D. C. and Vanzandt, T. E.	1987	J. Atmos. Sci., **44**, 1404.
Strauch, R. G.	1981	20th Conterence on Radar meteorology (Boston) AMS, Boston, 430.
Takahashi, M., and Boville, B. A.	1992	J. Atmos. Sci., **49**, 1020.
Tokioka, T. and Yagai, I.	1987	J. Meteorol. Soc. Jpn., **65**, 423.
Tsuda, T., Kato, S., Yokoi, T. and Tnoue, T.	1990	Radio Sci., **25**, 1005.
Tsuda, T., and Kato, S.	1989	J. Meteorol. Soc. Jpn., **67**, 43.

Tsuda, T., Murayama, Y.,
  Wiryosumatro, H.,
  Harijono, S.W.B. and Kato, S.
	1994	J. Geophys. Res., **99**, 10491.

Tsuda, T., Mangern, Y.,
  Wiryosumatro, H., Kato, S.,
  Harijono, S.-W.B., Fukao,
  S., Karmini, M., Mngan., C. M.,
  Saraspriya, S., and Suripto, A.
	1992	J. Geomagn. Geoelectr. **44**, 1041.

Vilal, F.	1986	J. Geophys. Res., **91**, 8955.
Vincent, R. A. and Rottger, J.	1980	The Austraian Physicist, **19**, 70.
Vincent, R. A. and Reid I. M.	1983	J. Atmos. Sci., **40**, 1321.
Wallace, J. M. and Tadd., R. F.	1974	Mon. Wea. Rev., **102**, 795.
Wallace, J. M. and Hartranft, F. R.	1969	Mon. Wea. Rev., **97**, 446.
Wallace, J. M. and Kousky V. E.	1968	J. Atmos. Sci., **25**, 900.
Walker, J. C. G.	1979	Science, **206**, 180.
Webester, P. J. and Chang, H. R.	1988	J. Atmos. Sci., **45**, 803.
Webseter P. J. and Holton, J. R.	1982	J. Meteor. Soc., Jpn., **44**, 291.
Williams, C. R.	1994	NOAA Tech. Memo., ERL AL - 13.
Williams, C. R. and Avery, S. K.	1996	J. Geophys. Res., **101**, 15051.
Wilson, D. A. and Miller L. J.	1972	NOAA, Washington D. C.
Wilson, J., Carbone, R., Bayrton, H., and Serafin, R.	1980	Bull. Amer. Meteor Soc., **61**, 1154.
Wilson, J. D., and Mak, M.	1984	J. Atmos. Sci., **41**, 1187.

Woodman, R. F. and Guillen, A.	1974	J. Atmos. Sci., **31**, 493.
Woodman, R. F.	1981	Handbook for MAP, Vol. **2**, 293.
Woodman, R. F., Rastogi, P. K. and Sato, T.	1981	Handbook for MAP 363-369 Uni. of Illinois, Urabana.
Yanai, M., and Marujama, T.	1966	J. Meteor. Soc., Jpn., **44**, 291.